THESIS FOR THE DEGREE OF DOCTOR OF PHILOSOPHY

Filtration of Microcrystalline and Microfibrillated Cellulose

The impact of ions and electric field

ANNA HJORTH

Department of Chemistry and Chemical Engineering

CHALMERS UNIVERSITY OF TECHNOLOGY

Gothenburg, Sweden 2023

Filtration of Microcrystalline and Microfibrillated Cellulose
The impact of ions and electric field
ANNA HJORTH
ISBN 978-91-7905-900-2

Doktorsavhandlingar vid Chalmers tekniska högskola
Ny serie nr 5366
ISSN 0346-718X

Department of Chemistry and Chemical Engineering
Chalmers University of Technology
SE-412 96 Gothenburg
Sweden
Telephone + 46 (0)31-772 1000

Front cover
Cover art by Isa Bengzon, artistic interpretation of the filtration set-up
Quote
"This is what I want to be: researcher in Lund or Mölndal" – the author, 2004
Dedication
This thesis is dedicated to my mum: *blundar jag är vi tillsammans igen*
Back cover
Photograph by Oscar Hjorth

Printed by Chalmers Digitaltryck
Gothenburg, Sweden 2023

Filtration of Microcrystalline and Microfibrillated Cellulose
The impact of ions and electric field

ANNA HJORTH
Department of Chemistry and Chemical Engineering
Chalmers University of Technology

ABSTRACT

Dewatering plays an essential role in the processing of microcrystalline cellulose (MCC) and microfibrillated cellulose (MFC), as their commercial attractiveness in many applications is limited by the high water content of the products. Filtration is the most common mechanical dewatering technique, but the filtration of these materials results in filter cakes with high filtration resistance. Therefore, the process needs to be modified to make a viable option; this thesis presents two types of such modifications.

In one study, the electrostatic repulsive interactions between MCC particles were altered by the addition of NaCl (0.1-1.0 g/L) during dead-end filtration. The addition of ions resulted in the agglomeration of MCC, which was confirmed by focused beam reflectance measurements, and a reduction in the average as well as local filtration resistance.

Electro-assisted filtration, in which an electric field is applied across part of the filter chamber, was used to dewater two types of MFC: one produced via 2,2,6,6-tetramethylpiperidinyl-1-oxyl (TEMPO)-mediated oxidation of dissolving pulp and one commercially available. Regardless of the MFC type, a clear improvement in the dewatering rate was observed when pressure and electric field were combined. This was also observed with molecular dynamic (MD) simulations, which related it to the electro-osmotic flow of water and the electrophoresis of the negatively charged MFC towards the anode.

Filter cakes with a channelled structure were formed, which may have contributed to the accelerated dewatering rate. This structure was especially pronounced for the TEMPO-oxidised MFC, and it was found that the microfibrils were partially oriented in the direction of the electric field by studying the structures using X-ray scattering and scanning electron microscopy.

After dewatering, a slight reduction in the water retention value and viscoelastic properties of the MFC was observed. This may be attributed to a reduction in the total surface area, plausibly due to aggregation of the microfibrils and/or reshaping of the microfibrils/fibril bundles.

Keywords: *filtration, electro-assisted, ions, microfibrillated cellulose, microcrystalline cellulose*

Detta vill jag bli: Forskare

i Lund eller Mölndal

Anna, 2004

Foreword

In this section, the author addresses the subject of "how it really happened" and, more importantly, presents the main outcome of her years of doctoral studies.

More than four and a half years ago, I joined the Division of Forest Products and Chemical Engineering (SIKT) at Chalmers University of Technology when I wrote my Master's thesis. I ended up at SIKT thanks to inspiring courses given by Associate Prof. Merima Hasani and Prof. Hans Theliander on the wonders of biorefineries, pulp and cellulose technology.

After extensive Kraft cooking and acid hydrolysis of the pulp produced ("klasoning") during my time as a thesis worker, I was eager to learn more. As luck would have it, Prof. Hans Theliander was looking for a Ph.D. student to work on something entirely different: filtration of cellulose materials. For some inexplicable reason, he thought of me, even though I had not expressed any passion at that time for flow through porous beds or the nature of compressible filter cakes.

Whilst writing this thesis, almost four years has passed by, filled with filtration of various types of cellulose materials. Little did I know, when embarking on this journey, that it would also include the exploration of techniques such as X-ray scattering and rheology and – most surprisingly – how to make the most of working from home during the Covid pandemic. Ultimately, it is not only this but also the many hours spent analysing confusing data and the inescapable struggle with various equipment that shaped me into a researcher.

I have found great pleasure in presenting my work in different formats; frankly, this has often been what I enjoyed the most, and I have been fortunate enough to do so at several conferences. Moreover, I also truly enjoyed teaching transport phenomena, and it made me realise how demanding I myself must have been as an undergraduate student.

I will end this section with the following quote, which is from the thesis of my greatest source of inspiration when it comes to life in academia. It has provided me with a well-needed perspective during my final months as a Ph.D. student:

"I believe that most Ph.D. students, especially those students who tend to do well on the exams, expect their theses to be far more outstanding than what they actually turn out to be. I am certainly no exception to this rule."[1]

[1] G. Lidén, On-line Monitoring Techniques for the Study of Yeast Physiology – Some studies on the Yeast *Pichia stipites* and *Saccharomyces cerevisiae*, Chalmers University of Technology, 1993

List of Publications

Please note that the maiden name of Anna Hjorth was Anna Lidén.

This thesis is based on the following appended papers:

Paper I **Dewatering microcrystalline cellulose: The influence of ionic strength**
Anna Lidén, Nabin Kumar Karna, Tuve Mattsson & Hans Theliander

Separation and Purification Technology 264 (June).
doi:10.1016/j.seppur.2020.118245

Paper II **Electroassisted Filtration of Microfibrillated Cellulose: Insights Gained from Experimental and Simulation Studies**
Nabin Kumar Karna*, Anna Lidén*, Jakob Wohlert & Hans Theliander

Industrial & Engineering Chemistry Research 60 (48): 17663–76.
doi:10.1021/acs.iecr.1c03749

Paper III **Structure of Filter Cakes During the Electroassisted Filtration of Microfibrillated Cellulose**
Anna Lidén, Polina Naidjonoka, Nabin Kumar Karna & Hans Theliander

Industrial and Engineering Chemistry Research 61 (43): 16247-16256–16256.
doi:10.1021/acs.iecr.2c03216.

Paper IV **Electroassisted Filtration of Microfibrillated Cellulose: The Impact of the Degree of Fibrillation**
Anna Hjorth, Anna Vøllo Christiansen, Hans Henrik Øvrebø & Hans Theliander

Submitted

** Shared first authorship*

Publications not included:

Paper A **Wettability of Cellulose Surfaces under the Influence of an External Electric Field**
Nabin Kumar Karna, Jakob Wohlert, Anna Lidén, Tuve Mattsson & Hans Theliander

Journal of Colloid and Interface Science 589 (May): 347–55.
doi:10.1016/j.jcis.2021.01.003.

Paper B **Capillary Forces Exerted by a Water Bridge on Cellulose Nanocrystals: The Effect of an External Electric Field**
Nabin Kumar Karna, Jakob Wohlert, Anna Hjorth & Hans Theliander

Physical chemistry chemical physics: PCCP (February 2023).
doi:10.1039/d2cp05563e

Contribution Report

Paper I **First author.** AH planned and performed the filtration experiments together with NK, and was mainly responsible for the characterisation of the materials. TM contributed with expertise regarding the filtration set-up. The data was analysed together with the co-authors, and the manuscript prepared.

Paper II **Shared first authorship** with NK. The main responsibility of AH was to plan and conduct the experimental work, whilst that of NK was the molecular dynamic simulations. The results were evaluated with the co-authors. The manuscript was prepared and revised together with the co-authors.

Paper III **First author**. AH conceptualised the study and performed the experimental work; the results were evaluated in collaboration with the co-authors. WAXS and SAXS data was discussed with PN. AH was mainly responsible for the preparation of the manuscript, which was revised together with the co-authors.

Paper IV **First author**. AH conceptualised the study, performed the experimental work and prepared the manuscript, which was revised with the co-authors. The results were discussed and analysed together with the co-authors.

Conferences

The work has also been presented by the author at the following conferences:

I. *Efficient dewatering of microfibrillated cellulose: the use of electro-assisted filtration*
A. Lidén, N.K. Karna, H. Theliander
7th International Polysaccharide Conference
Nantes, France, October 2021
(Poster)

II. *Dewatering Microfibrillated Cellulose: the use of electro-assisted filtration*
A. Lidén, N.K. Karna, J. Wohlert, H. Theliander
Ekmandagarna 2022
Stockholm, Sweden, January 2022
(Oral presentation in Pecha Kucha format)

III. *Electro-assisted Filtration of Microfibrillated Cellulose: insights gained from experiments and molecular dynamic simulations*
N.K. Karna, A. Lidén, J. Wohlert, H. Theliander
Filtech 2022
Cologne, Germany, March 2022
(Oral presentation)

IV. *Dewatering of microfibrillated cellulose: the use of electro-assisted filtration*
A. Lidén, N.K. Karna, H. Theliander
16th European Workshop on Lignocellulosics and Pulp
Gothenburg, Sweden, June 2022
(Poster)

V. *Exploring electro-assisted filtration of microfibrillated cellulose*
A. Lidén, P. Naidjonoka, N.K. Karna, H. Theliander
18th Nordic Filtration Symposium
Gothenburg, Sweden, August 2022
(Oral presentation)

VI. *Dewatering Microfibrillated Cellulose: the use of electro-assisted filtration*
A. Lidén, N.K. Karna, H. Theliander
13th World Filtration Congress
San Diego, U.S.A, October 2022
(Oral presentation and poster)

Nomenclature and abbreviations

Greek letters

α	Local filtration resistance [m/kg]
α_0	Model parameter [m/kg]
α_{av}	Average filtration resistance [m/kg]
β	Model parameter [-]
ε	Porosity [-]
ε_0	Permittivity of vacuum [F/m]
ε_r	Relative dielectric constant of the fluid [F/m]
ΔP	Pressure drop across the filter cake and filter medium [Pa]
η_γ	Number of counts [-]
$\eta_{\gamma 0}$	Number of counts in empty filter cell [-]
μ	Dynamic viscosity [Pa s]
$\mu_{\gamma,l}$	Attenuation factor liquid phase [1/m]
$\mu_{\gamma,s}$	Attenuation factor solid phase [1/m]
ρ	Density of liquid phase [kg/m^3]
ρ_s	Density of solid phase [kg/m^3]
φ	Local solidosity [-]
φ_0	Model parameter [-]
ζ	Zeta potential [V]

Latin letters

A	Area of filter cell [m^2]
c	Mass of solids to volume of filtrate [kg/m^3]
d_γ	Average path length of γ-radiation [m]
E	Electric field strength [V/m]
K	Permeability [m^2]
n	Model parameter [-]
P_s	Solid pressure [Pa]
P_l	Hydrostatic pressure [Pa]
P_0	Model parameter [Pa]
R_m	Average resistance of filter medium [1/m]
t	Time [s]
v	Superficial velocity [m/s]
v_{solid}	Superficial velocity of the solids [m/s]
V	Volume of filtrate [m^3]
z	Distance from filter medium [m]

Abbreviations

ASL	Acid soluble lignin
ATR-FTIR	Attenuated total reflectance-Fourier transform infrared spectroscopy
B.E.T.	Brunauer-Emmet-Teller
CNC	Nanocrystalline cellulose
CNF	Nanofibrillated cellulose
EDL	Electrolytic double layer
FBRM	Focused beam reflectance measurement
HPAEC-PAD	High performance anion exchange chromatography with pulsed amperometry detection
KL	Klason lignin
LVE	Linear viscoelastic regime
MCC	Microcrystalline cellulose
MD	Molecular Dynamics
MFC	Microfibrillated cellulose
PES	Polyethersulfone
SEM	Scanning electron microscopy
TEMPO	2,2,6,6-tetramethylpiperidinyl-1-oxyl
TOC	TEMPO-oxidised cellulose oligomers (modelled)
WRV	Water retention value

Table of Contents

1

INTRODUCTION

This chapter begins by uncovering the motivation of the thesis and the objectives and ends with a presentation of the outline.

The emerging shift from a finite fossil-based to a bio-based industry has led to a rapidly growing demand for renewable and bio-based resources. One bio-based resource with the absolute potential for replacing fossil-based resources is cellulose. Readily available in nature (e.g. in grass, tunicates and wood) and renewable, the hierarchical structure of cellulose makes it suitable for a wide range of applications. It is therefore of fundamental importance to explore the cellulose fibre so that all the structures may be used efficiently.

Cellulose has been used by mankind for centuries in traditional applications such as paper and packaging, viscose textiles and specialty chemicals (e.g. hydroxypropyl methylcellulose). The potential of cellulose lies nevertheless beyond the scope of these traditional applications. For the past decade, this has led to a fascination of the nanoscale structures isolated from the cellulose fibrils, commonly referred to as “nanocelluloses”. This is not only because they are derived from cellulose, but also the fact that they possess valuable features owing to their low density and particularly large surface area to volume ratio, along with superior mechanical strength: together, these allow for the engineering of new materials.

Nanocellulose is typically divided into two subclasses, namely crystalline and fibrillated, with inherently different morphologies. The former has a higher degree of crystallinity and is composed of shorter, stiffer fractions (resembling grains of rice in shape) than the latter, which are longer and flexible (resembling spaghetti in shape). Achieving complete isolation to nanoscale is both challenging and expensive, so various qualities of the intermediate structures are therefore produced. For example, microcrystalline cellulose (MCC) is coarser and contains a higher fraction of amorphous parts compared to the nanocrystalline cellulose (CNC), and the microfibrillated cellulose (MFC) contains larger bundles of nanofibrillated cellulose (CNF) and presents a wide size distribution.

A broad spectrum of potential applications of micro/nanocelluloses is continuously being expressed in research articles and reviews (e.g. [1–3]), but the big commercial success has yet to transpire. At present, a handful of companies produce different qualities of nanocellulose, albeit in relatively small quantities. One hinder in the commercial attractiveness of these materials is the bottleneck in their production: water and, more specifically, its removal. These types of materials are produced in dilute conditions (typically >95% of water [4], but it can be as much as 99%) and, consequently, the costs associated with its storage and transportation are steep. Moreover, certain applications do not allow for such high contents of water.

Water removal can be achieved through various form of drying [5] and/or dewatering. The high energy demand of thermal drying, however, quickly makes this option economically unfeasible. In addition, drying is associated with difficulties related to the re-dispersibility of the material, and thereby places limitations on product applications [6]. One alternative for reducing the total energy demand is to add a preceding mechanical dewatering step, as this requires much less energy than thermal drying. Filtration is the most common method used for mechanical dewatering but, owing to the large surface area of these materials, there is excessive drag and hence high filtration resistance. This, in turn, results in the need for long operation times and/or large filter area, which could be problematic from an economical perspective. In other words, the filtration process needs to be modified if it to be a viable option for dewatering this type of material. Scholars have investigated various ways of enhancing the mechanical dewatering of micro/nanocellulose, e.g. by modifying the suspension and/or using assisted filtration techniques. This will be explored further in *3.3 DEWATERING MICRO/NANOCELLULOSE*.

One way of modifying the process is by tuning the chemical environment and thereby altering the electrostatic interactions between the particles, which play an important role during filtration. This can be achieved by the addition of ions, for example, resulting in the negative charges of the cellulose particles being shielded. There will be less particle repulsion and, instead, attractive van der Waals interactions, which promotes agglomeration. This reduces the surface area subjected to the liquid flow which, in turn, reduces the drag and filtration resistance.

Another way of modifying filtration is to employ assisted filtration techniques. These promote the dewatering of materials that are notoriously difficult to dewater, e.g. materials that tend to form highly compressible filter cakes. The filtration process could be enhanced by the application of an electric field, known as electro-assisted filtration. In this method, an electric field is applied across part of the filter chamber before various electrokinetic phenomena are introduced that could be beneficial to the dewatering process. Wetterling *et al.* [7, 8] showed this method to be efficient in dewatering MCC. Furthermore, they also studied the electro-osmotic dewatering of CNC, i.e. only applying an electric field [9]. The electro-assisted filtration of MFC is only mentioned in the literature, however, in a patent submitted by Heiskanen *et al.* [10]. The distinct discrepancies between crystalline and fibrillated celluloses in terms of morphology and surface properties make it both important and interesting to further investigate electro-assisted filtration as a means of dewatering MFC.

Dewatering plays an essential part in achieving a sustainable large-scale production of micro/nanocelluloses, making it essential to extend knowledge in this area. The work performed in this thesis aims at achieving precisely this.

1.1 OBJECTIVES

The main objective of the work conducted in this thesis was to extend current knowledge on the filtration of microcrystalline and microfibrillated cellulose, as this constitutes an important part of the challenges related to their large-scale production.

This objective can be subdivided as follows:

- To investigate the **impact of ions** on the dead-end filtration of MCC.

- To investigate **electro-assisted filtration** as a means of improving the dewatering of two types of MFC and in order to:
    - Gain further insights on the dewatering mechanism by combining experimental work and molecular dynamic (MD) simulations.
    - Explore the filter cake structure in terms of the orientation of MFC in the electric field.
    - Study the impact of the mechanical degree of fibrillation of commercially-available MFC.
    - Evaluate how the product properties are affected after dewatering.

Throughout this thesis, *micro/nanocellulose* are used when referring to the types of cellulose materials (MCC and MFC) studied.

1.2 OUTLINE OF THE THESIS

A short theoretical background on filtration and cellulose to set the foundation for the following discussion of the research conducted is provided in Chapters 2 and 3, respectively. This is followed by a description of the materials and methods described in Chapter 4. In Chapter 5, the major findings from research, which involves the influence of ions during the filtration of MCC and the electro-assisted filtration of MFC (Figure 1.1), are presented and discussed. Chapters 6 and 7 summarise the thesis, with concluding remarks and a suggestion for future work.

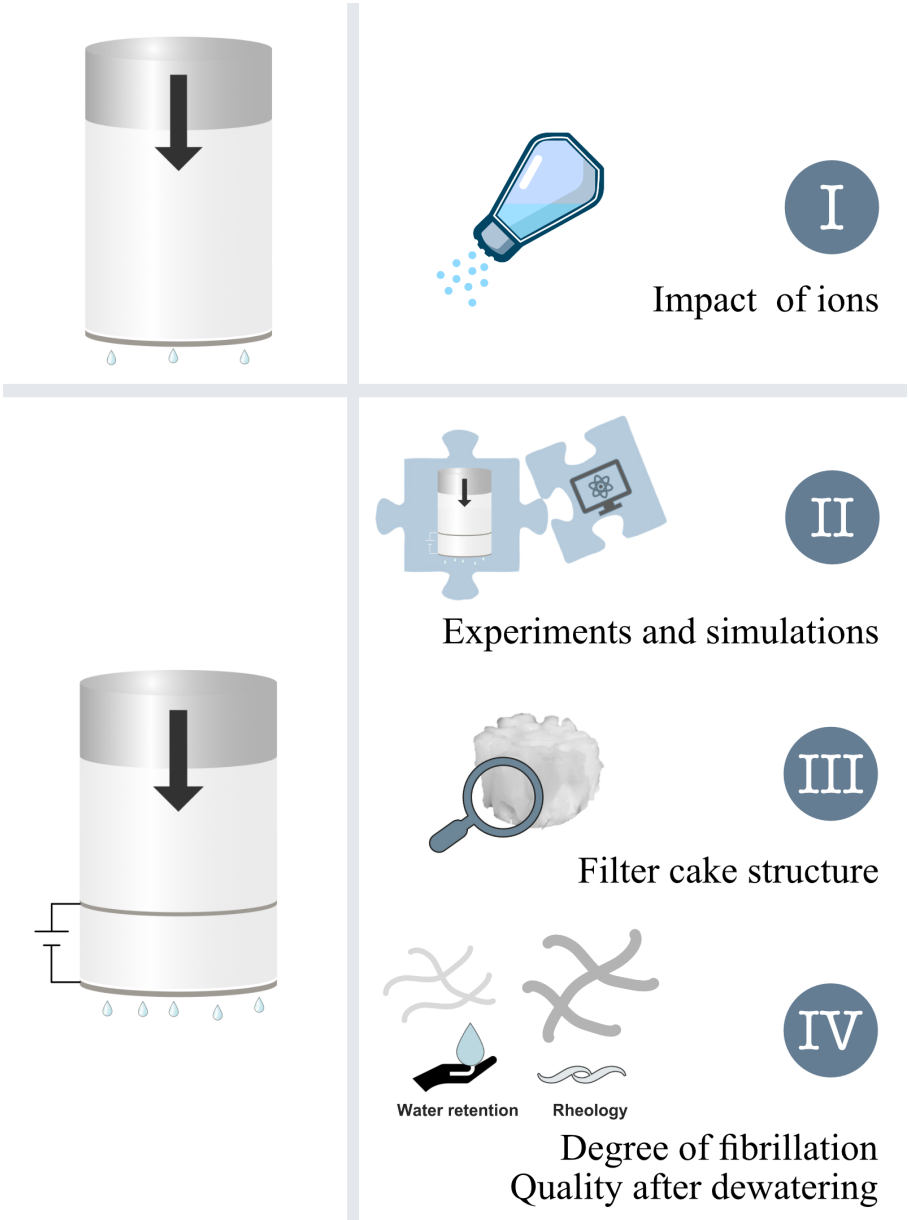

Figure 1.1 Overview of the appended papers (I-IV), which provide the basis of this doctoral thesis.

2

FILTRATION

"Reaction engineering tells whether the process is possible or not, but the separation whether the process is profitable or not"

Prof. Ann-Sofi Jönsson
Avancell Conference, 2019

This chapter presents the fundamentals of dead-end filtration and covers the important equations used in this thesis. Furthermore, the role of electrostatic interactions is highlighted, and the basics of electro-assisted filtration explained.

2.1. DEAD-END FILTRATION

Filtration, such as dead-end filtration, is a key unit operation in many industries, ranging from foodstuffs to refineries, and in the treatment of water and sludge. It is a classical method used in the separation of liquids and solids, for example, and may serve many purposes: separating the reaction medium from the product, purification and water removal. In the perfect scenario, this would be an effortless process and the separation would be complete: the filtrate would be devoid of solids and the filter cake would be free from liquid (if gas blowing is applied as a final step).

This is not, however, an accurate description of reality: the process is actually rather complicated, especially where compressible filter cakes are concerned.

Dead-end filtration involves the suspension being subjected to a pressure difference whereby only the liquid passes through a filter medium: the suspension reaches a dead-end. The pore size of the filter medium only allows particles of a certain size to pass, thereby leading to the consequential build-up of a filter cake as liquid is being removed, so it could also be called cake filtration. Two important events thus transpire during the filtration process: the flow of the liquid through the porous bed, and the build-up of the filter cake.

In order for separation to occur, the driving force, i.e. the pressure difference, must overcome the resistance of both the filter medium and the filter cake. The latter results from the drag forces that arise when the liquid flows through the interstices of the filter cake. When exposed to the liquid flow, the solid particles experience both frictional and form drag. Assuming that the particles are in point contact, these stresses are communicated through the particle bed towards the filter medium. The net solid pressure therefore increases in the direction towards the filter medium.

Constructing a force balance over a thin section of the filter cake yields the following (neglecting gravitational and inertial forces):

$$AP(t) = AP_l(z,t) + F_s(z,t) \qquad (1)$$

where $P(t)$ is the applied pressure, $P_l(z,t)$ is the hydrostatic pressure and $F_s(z,t)$ refers to the compressive force on the solids due to accumulated drag. A fictitious pressure term, $P_s(z,t)$, referred to as solid pressure, is defined as F_s/A. It is important to note that both the hydrostatic and solid pressures are functions of position as well as time, whereas the applied pressure is only a function of time.

It becomes apparent that, when dividing the force balance in (Eq. 1) by the cross-sectional area and taking the differential with respect to distance at constant time[2], the hydrostatic and solid pressures must be in balance if the applied pressure is constant: as the hydrostatic pressure decreases, the solid pressure increases. At the beginning of the filtration, either before a filter cake has been formed or at the surface of a filter cake, the hydrostatic pressure equals the applied pressure; at the bottom of the filter cake, i.e. at the filter medium, the solid pressure equals the pressure drop across the filter cake, see Figure 2.1.

[2] $dP_L + dP_s = 0$

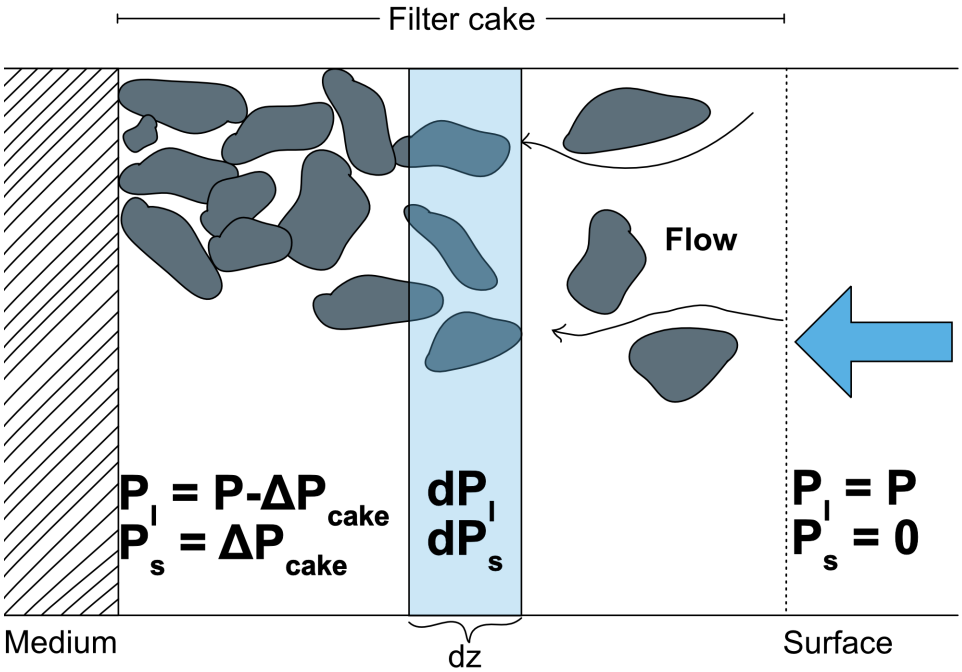

Figure 2.1 Schematic illustration of the filter cake including the hydrostatic pressure (P_l) and solid pressure (P_s). ΔP_{cake} represents the pressure drop across the filter cake.

The liquid flow through the filter cake can be modelled as flow through a porous medium. Many important discoveries on such flows were realised during the 19th century and presented by Darcy in his renowned work on the fountains of Dijon [11]. Although Darcy himself did not include viscosity in the original expression, the equation presented in Eq. 2 is often referred to as Darcy's law. In the differential form, it is expressed as:

$$v = -\frac{K}{\mu}\frac{dP_l}{dz} \qquad (2)$$

where v is the superficial flow velocity (in direction from the filter medium into the cake), K is the permeability of the bed, μ is the dynamic viscosity and dP_l/dz is the hydrostatic pressure gradient.

The relation between the permeability of the bed (filter cake) and the filtration resistance is defined according to Eq. 3 thus:

$$K = \frac{1}{\alpha \rho_s \varphi} \qquad (3)$$

where α is the specific filtration resistance, ρ_s is the solid density and φ is the solidosity, which is the volume of solids and the total volume.

The average filtration resistance, α_{av}, is a parameter of certain importance when assessing the filtration performance, and is defined according to Eq. 4:

$$\frac{1}{\alpha_{av}} \equiv \frac{1}{\Delta P_{cake}} \int_0^{\Delta P_{cake}} \frac{dP_s}{\alpha} \qquad (4)$$

The average filtration resistance is commonly calculated from the general filtration equation[3] (Eq. 5) [12], in which both the resistance of the filter cake (in the first term on right hand side) and the filter medium (in the second term) are included:

$$\frac{dt}{dV} = \frac{\mu c \alpha_{av}}{A^2 \Delta P} V + \frac{\mu R_m}{A \Delta P} \qquad (5)$$

where A is the area of the filter medium, c is the mass of solids to filtrate, V is the volume of filtrate, R_m is the resistance of the filter medium and ΔP is the pressure difference across the filter cake and filter medium. In the case of constant pressure filtration, plotting dt/dV against V yields a linear plot from which the average filtration resistance can be calculated from the slope of the line.

The general filtration equation is derived under the following assumptions:

- The superficial velocity is uniform throughout the filter cake.
- The filter cake structure is uniform and the solid particles are stationary.
- All particles are retained in the filter cake.
- No blinding of the filter medium occurs.

2.1.1. Compressible filter cakes – the importance of local properties

The nature of a filter cake is considered as "incompressible" if its structure, and thus properties, are the same in every position within the filter cake. This is, nevertheless, not true for most filter cakes and they are referred to as being "compressible". The general structure of a compressible filter cake is not constant: it changes with time as the solid compressive pressure increases, which infers an increasingly higher solidosity towards the filter medium. It therefore becomes important to evaluate the local properties, such as local filtration resistance and local solidosity, when dealing with compressible filter cakes.

The effective stress on the solid particles increases in the direction towards the filter medium. The particulate network cannot sustain this, and a structural collapse occurs. This means that it is not possible for the solid particles in the filter cake to be stationary. To account for the liquid velocity relative to that of the solids, Shirato *et al.* [13] modified Darcy's equation (Eq. 6) accordingly:

$$v - \frac{1-\varphi}{\varphi} v_{solid} = -\frac{K}{\mu} \frac{dP_l}{dz} \qquad (6)$$

[3] Sometimes referred to as *Ruth's equation.*

Although it is important to take into consideration the velocity of the solids in highly concentrated suspensions that form highly compressible filter cakes it is regarded, in practice, as being much less than that of the flowing liquid, and v_{solid} is therefore often approximated as zero.

The permeability, and thus the properties, of a compressible filter cake varies in the direction of the flow because of its inability to withstand the increasing compressive pressure: e.g. the solidosity increases as the compressive pressure increases towards the filter medium. The solidosity can be related to the porosity according to Eq. 7.

$$\varphi = 1 - \varepsilon \qquad (7)$$

There are several methods, direct and indirect, that can be used to measure local solidosity, such as cake dissection [14], nuclear magnetic resonance [15], conductivity measurements [16] and γ-ray attenuation [17]. The latter, which has been used in this work, is a non-invasive method that allows it to be calculated using Beer-Lambert's law for two phases, as given in Eq. 8.

$$-ln\frac{\eta_\gamma}{\eta_{\gamma 0}} = \mu_{\gamma,l} d_\gamma + (\mu_{\gamma,s} - \mu_{\gamma,l})\varphi \qquad (8)$$

where η_γ is the number of counts recorded per time, $\eta_{\gamma 0}$ is the number of counts for the empty filter cell, μ_γ is the attenuation factor (l and s denoting liquid and solid, respectively), d_γ is the average path length of the radiation and φ is the solidosity.

Furthermore, the non-uniformity of the filter cake leads to variations in the local filtration resistance. This can be calculated by combining Eqs. 2 and 3, and expressed by Eq. 9 thus:

$$\alpha = -\frac{1}{\mu v \rho_s \varphi}\frac{dP_l}{dz} \qquad (9)$$

Fitting the experimental data to models allows the degree of compressibility of different conditions to be compared. There is, however, a lack of suitable models bearing physical relevance and they are, instead, merely empirical. Tiller and Leu [18] have put forth an important set of semi-empirical relations for compressible filter cakes, Eqs. 10 and 11. In the doctoral thesis of Leu [19], it was suggested that the values of n, β and φ_0 be categorised as reported in Table 2.1.

$$\varphi_i = \varphi_0\left(1 + \frac{P_s}{P_0}\right)^\beta \qquad (10)$$

$$\alpha_i = \alpha_0\left(1 + \frac{P_s}{P_0}\right)^n \qquad (11)$$

Here, φ_0 and α_0 may be interpreted as the solidosity and local filtration resistance at zero compressible pressure, respectively. P_0, β and n are mere empirical parameters, where the two latter are related to the compressibility of the specific material. The five parameters may be determined by simultaneous fitting of local experimental data.

Table 2.1 Categorisation of the model parameters in Eqs. 10 and 11 according to Leu [19].

	Low compressibility	*Medium compressibility*	*High compressibility*
α_0 [m/kg]	10^9	10^{10}	10^{11}
φ_0 [-]	0.30	0.20	0.10
β [-]	0.05	0.15	0.30
n [-]	0.20	0.60	1.20

2.2. ELECTROSTATIC INTERACTIONS AND THE IMPACT OF IONS

The interaction between solid particles plays an important role in the filtration process. Understanding how these interactions can be altered, and the consequences of doing so, is therefore of significant value. Interparticle interactions are mainly comprised of repulsive electrostatic interactions, attractive van der Waals forces, friction and interlocking of the particles. The focus of this thesis is on the former, i.e. the influence of electrostatic interactions.

One way of altering electrostatic interactions is by modifying the ionic environment of the suspensions. In order to explain this effect, the well-known electrolytic double layer (EDL) theory must be clarified first. When a solid particle is submerged in a polar medium, it gains a surface charge due to mechanisms involving ionisation, ion adsorption and ion dissolution [20]. To achieve electroneutrality, the charged particle is surrounded by a double layer of counterions in appropriate concentrations: these two regions are known as the “stern layer” and the “diffusive layer” (Figure 2.2). The stern layer is thin and has a fixed layer of almost immobile counterions, whereas the diffusive layer is comprised of mobile ions with charge densities that vary with distance from the surface of the solid particle.

Upon the addition of ions, the diffusive layer of the EDL will be compressed because of the increasing concentration of counterions. This, in turn, means that the repulsive electrostatic interactions will diminish at a certain distance from the surface of the particle: the surface charges become shielded. If the repulsive electrostatic interactions become sufficiently weaker, the attractive van der Waals forces will be predominant instead and particle agglomeration promoted. Should this occur, the total surface area subjected to the liquid flow will be reduced, as will be the drag forces. Such agglomeration could also affect the structure of the filter cake.

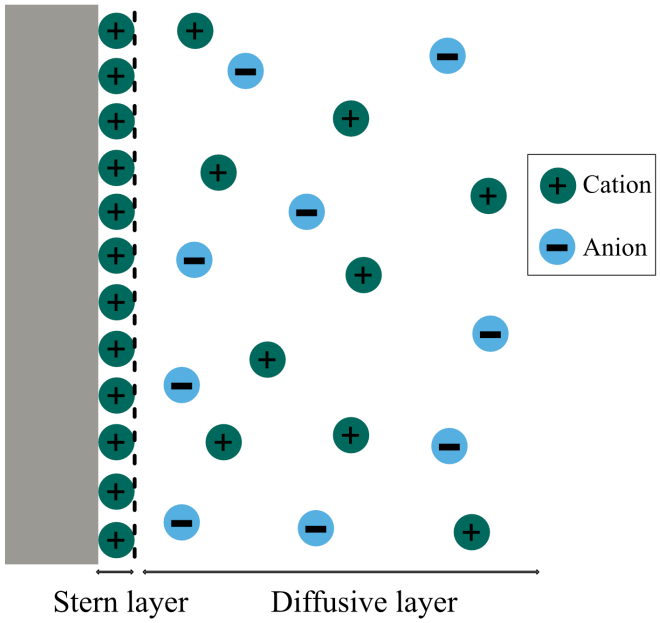

Figure 2.2 The EDL model, illustrating the case of a particle with a negative surface charge (grey).

2.3. ELECTRO-ASSISTED FILTRATION

Conventional filtration (i.e. pressure-driven) is not always the most suitable option. This is true, for instance, when filtering particles with a large specific surface area (e.g. nanomaterials) which results in a filter cake with high filtration resistance. This would be a time-consuming filtration process and/or require excessive filter areas. The filtration of such materials may be enhanced by employing assisted filtration techniques, whereby additional driving forces are introduced via an external field, e.g. magnetic [21], acoustic [22] or electric [23].

If the filtration process is assisted by an external electric field, the method is referred to as electro-assisted filtration[4]. It has been reported as a means of improving the dewatering of materials that are notoriously difficult to dewater, such as sewage sludge [24,25], clays [26,27] and various biopolymers (such as chitosan and xanthan) [28,29]. More recently, the application of an external electric field was discovered as being an efficient method of enhancing the dead-end filtration of MCC [8]. Assistance by an electric field has also been used to mitigate fouling during membrane filtration [30,31].

Although mostly occurring in an academic context, a few industrial applications can nevertheless be found within the field of electro-assisted dewatering, e.g. in companies such as Korea Water Technology (E-LO, the world's first drum-type electro-osmosis dehydrator) and Electrokinetic (several models for electrodewatering).

[4] Sometimes also referred to as *electrofiltration* or *electrodewatering*.

2.3.1. The application of an electric field

Electro-assisted filtration takes advantage of the fact that most particles gain a surface charge upon dispersion in a polar medium. The electrokinetic phenomena introduced by the application of an electric field may serve as an additional driving force in the separation process. The three transport mechanisms related to the electrokinetic phenomena involving the interactions between the charged solid surface, the double layer and the liquid are depicted in A, B, and C in Figure 2.3, together with additional effects caused by the application of an electric field (D and E). The examples given below are for a particle carrying a negative surface charge, the electric field is in the same direction as the flow, the electrodes are placed with the cathode underneath the filter medium and the anode is located higher up in the filter chamber.

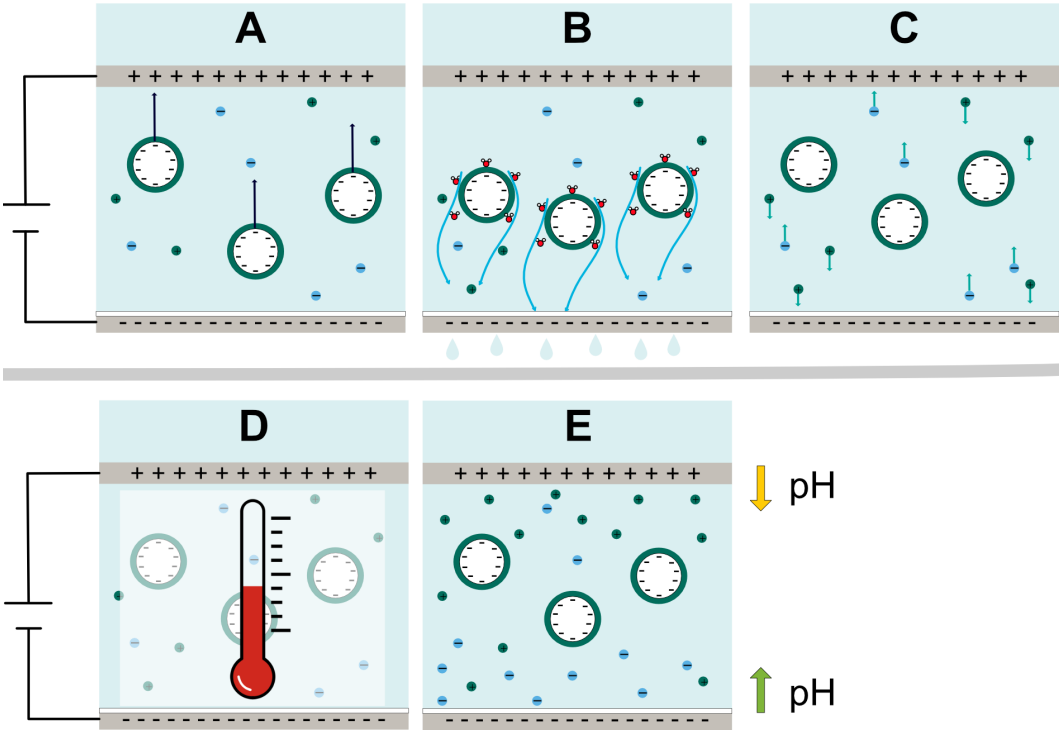

Figure 2.3 Illustration of important electrokinetic phenomena: (A) electrophoresis, (B) electroosmosis, (C) ion migration, (D) ohmic heating and (E) electrolysis reactions.

A. Electrophoresis is the movement of a charged particle relative to that of a liquid. This could certainly be important for dewatering as it may perturb the formation of a "skin" on top of the filter medium or, depending on the placement of the electrodes, have implications for the formation of the filter cake structure and thereby affect the resistance of the filter cake. The actual migration of the solid particles is only possible if the particles are free to move and not locked in a certain position or hindered by, for example, a filter cake or electrode. The particles in the network nevertheless experience an electrophoretic force in the presence of an electric field.

The Helmholtz-Smoluchowski equation (Eq. 12) can be used to express the electrophoretic velocity of the solid particles [20]:

$$\frac{v_{EF}}{E} = \frac{\varepsilon_r \varepsilon_0 \zeta}{\eta} \qquad (12)$$

where v_{EF} is the electrophoretic velocity, E is the strength of the electric field applied, ε_r is the relative dielectric constant of the fluid, ε_0 is the permittivity of vacuum, ζ is the zeta potential and η is the dynamic viscosity of the dispersion medium.

B. Electro-osmosis is the chief mechanism by which water is transported through a porous filter cake whilst under the influence of an electric field. Upon the application of an electric field, the cations in the diffuse layer of the EDL are pulled towards the cathode along with the bulk water, thereby facilitating dewatering. The electroosmotic flow of water is in the direction opposite to the electrophoresis, so the Helmholtz-Smoluchowski equation (but in the opposite direction) could be useful for describing its velocity.

C. Ion migration is the migration of ions towards the respective electrode. The ions may be present in the original suspension or formed in the electrolysis reactions, as described in e) below.

D. Ohmic heating is caused by the passage of a current through a system with electrical resistance, which results in an increase in temperature. The temperature rise is proportional to the current and leads to a reduction in the viscosity, thereby aiding filtration. However, overheating can lead damage of, for example, electrodes and filter medium and consequently have a negative effect on the process [32].

E. Electrolysis reactions occur at the electrodes [23, 26, 27]:

Anode:

$$2H_2O\ (l) \rightarrow 4H^+ + O_2\ (g) + 4e^- \qquad [A1]$$

$$M \rightarrow M^{n+} + ne^- \qquad [A2]$$

Cathode:

$$2H_2O\ (l) + 2e^- \rightarrow 2OH^- + H_2\ (g) \qquad [C1]$$

$$M^{n+} + ne^- \rightarrow M \qquad [C2]$$

where M is the material of the electrode and M^{n+} is its cation. Reaction [A2] dominates in the case of oxidising metals [33].

The electrolysis reactions result in an alkaline environment in the vicinity of the cathode and a higher acidity at the anode but may, however, migrate within the filter cake. It is

important to remember here that the pH may impact the surface charge (and hence the zeta potential) of the solid material being dewatered, depending on the pH sensibility of the solid material. Flushing the anodes has been suggested as a means of minimising problems related to the formation of electrolysis products [34,35].

2.3.2. Important factors affecting electro-assisted filtration

Several factors are known to impact electro-assisted filtration: some are related to process conditions and others to the properties of the suspension. Some important factors are the same as for conventional dead-end filtration since mechanical pressure is also applied during electro-assisted filtration. Naturally, the applied mechanical pressure contributes significantly to pressing the bulk water out of the filter cake and filter medium and accelerates the filtrate flow, but the full extent of its impact depends on the compressibility of the filter cake: a higher applied pressure is not necessarily synonymous with a higher filtrate flux. Moreover, the surface area subjected to the liquid flow will still be of importance to the drag force.

Additional factors are decisive when dewatering is executed using electro-assisted filtration rather than conventional filtration. An example of such a factor is the electric field strength, as Eq. 12 shows. The electric field mode can be either constant voltage or constant current. Furthermore, the design of a filtration set-up affects the dewatering process. This includes, for example, the design and material of the electrodes [33], potential flushing of the anodes [34, 35], the direction of the electric field (parallel or perpendicular to the flow [36]) and the distance between the electrodes.

Factors relevant to the suspension include the zeta potential of the particles (and hence electrophoretic movement), as shown in Eq. 12: a higher zeta potential shows a greater response to the electric field. The zeta potential is impacted by both the pH and ionic concentration, where the latter not only affects the zeta potential but also the conductivity of the suspension. A higher ionic concentration, and thus a higher conductivity, results in an increased electrical current and, consequently, a higher energy demand [7].

3

CELLULOSE

"Cellulose is the most abundant biopolymer on Earth"

...is often the opening phrase in publications involving cellulosic materials, and this chapter is clearly no exception. It describes the cellulose fibre down to its polymeric units, explains the novel cellulosic materials and their potential and, finally, addresses difficulties related to dewatering.

3.1. FROM FIBRE TO POLYMERIC UNITS

Cellulose is presented as being one of the cornerstones in the transition of industry based on finite fossil-based resources to one based on renewable raw materials. It is found in abundance in nature and, thanks to e.g. pulp mills, the infrastructure for its processing is already partly in place. Raw materials rich in cellulose include grass, tunicates and wood; in the latter, cellulose constitutes up to 40-45% of the biomass (depending on the species) [37]. In addition, cellulose can also be produced from bacteria [38]. The focus of this thesis is, however, on cellulose sourced from wood.

The wide range of wood-sourced cellulose is due to the hierarchical structure presented in Figure 3.1A, which spans from the actual tree (m) to fibres (µm) and monomeric units (Å). Structures/building blocks at some of the length scales are already very well established in today's society, e.g. the use of pulp fibres in paper and packaging, regenerated cellulose fibres in viscose

textiles and polymeric units in speciality chemicals such as carboxymethyl cellulose. Nanoscale structures isolated from the cellulose microfibrils found in between the fibre and the monomeric units (Figure 3.1A) are commonly referred to as nanocelluloses; despite having been featured in a multitude of scientific publications to date, they are not yet established as a major commercial product.

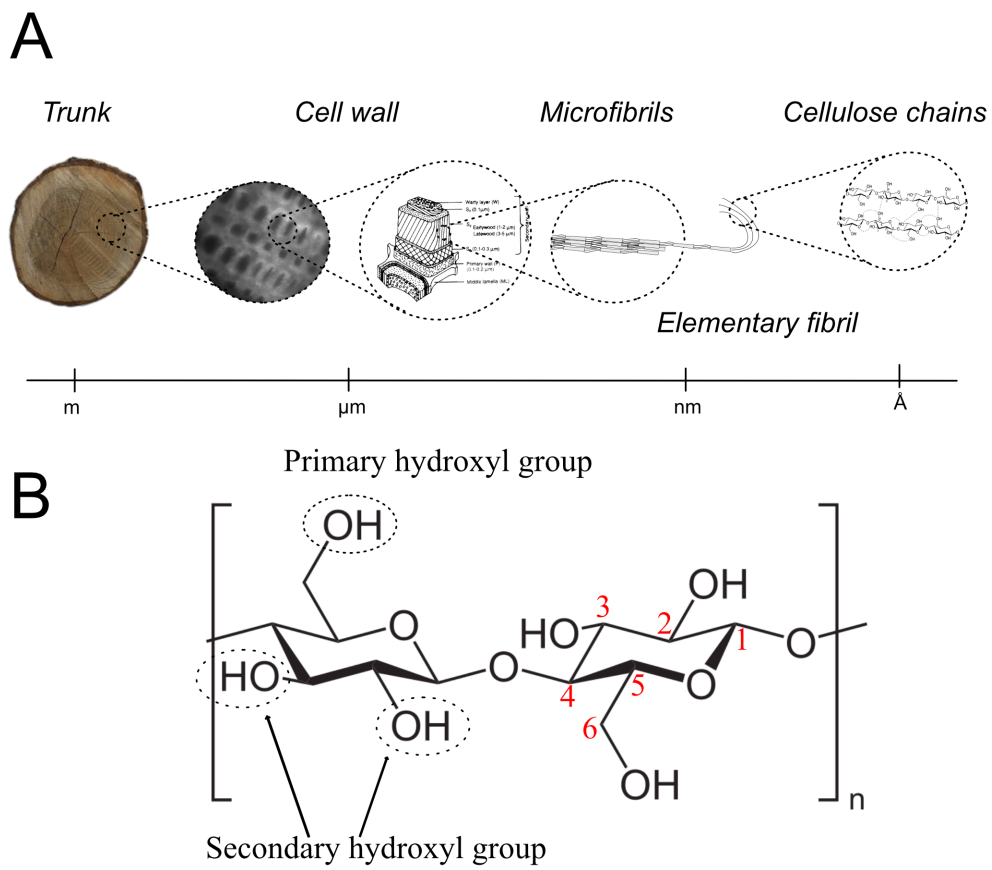

Figure 3.1 Overview of cellulose. (A) Schematic illustration of the hierarchical structure, with an approximate length scale of width given. Cell wall model is adapted from Huang *et al.* [39]. (B) A cellobiose unit, with the hydroxyl groups shown in dashed circles and the carbon number in red.

In a living wood cell, the cellulose chains are extruded from cellulose-synthesizing hexametric complexes in the plasma membrane and are comprised of D-anhydroglucopyranose units linked together by β-(1→4)-glucosidic bonds. Each glucose unit has a primary hydroxyl group (located on C6) and two secondary hydroxyl groups (C2 and C3), Figure 3.1B. Strong intra and inter hydrogen bonding between the hydroxyl groups of the glucose units provide the cellulose chain with its stiff character, which allows for the formation of sheets. Further, the cellulose sheets are stacked up on top of each other and interact through attractive van der Waals forces; they are stabilised further through hydrophobic effects to form elementary fibrils [40] with a diameter of 3-4 nm [41]. Not all details of this process are known, and it continues to be the subject of debate whether, for example, 18, 24 or 36 cellulose chains constitute the elementary fibril [42]. Another

widely debated topic is the development of the "twist" in the elementary fibril [43] that is argued to disturb the ordered regions and thus be the cause of the presence of both ordered and disordered regions, where the latter are more prone to reactions. The elementary fibrils are aggregated further into so-called microfibrils[5] which, in turn, can aggregate to form macrofibrils by interacting via van der Waals forces and hydrogen bonding.

The wood cell wall is multi-layered and comprised of the middle lamella (M), the primary wall (P) and the secondary layer consisting of three layers (S1, S2 and S3). The middle lamella is rich in lignin, whilst the other layers contain varying amounts of cellulose, hemicelluloses, and lignin in a complex matrix. Cellulose microfibrils are found in a random pattern in the primary layer, whereas they are located at alternating angles in relation to the cell axis in the secondary layer: the microfibril angle is important for the flexibility of the cell wall [44].

3.2. MICRO/NANOCELLULOSE

Nanocellulose commonly refers to isolated structures from cellulose microfibrils that have dimensions in the nanoscale: it is an expensive material that is challenging to produce. If complete isolation to nanoscale dimensions is not achieved, the material will be a heterogeneous blend of structures in micro as well as nanoscale: a mixture that does not yet have a proper name in the literature. Therefore, as established in the beginning of this thesis (*1.1 OBJECTIVES*), the term *micro/nanocellulose* will be used throughout when referring to these materials.

Figure 3.2 illustrates the two sub-classes that micro/nanocelluloses are typically divided into, namely *crystalline* and *fibrillated.* The inherent differences between these two sub-classes in terms of e.g. morphology and surface properties result in two very different materials and will be explained in *3.2.1 Crystalline cellulose* and *3.2.2 Fibrillated cellulose*, respectively. In brief, crystalline cellulose has a high crystallinity and is comprised of short and rod-like fractions, whereas fibrillated cellulose has long and flexible fibrils that can entangle and form a network.

[5] Although the terminology is under debate among scholars, some refer to microfibrils as elementary fibrils whilst others claim that microfibrils consist of several elementary fibrils.

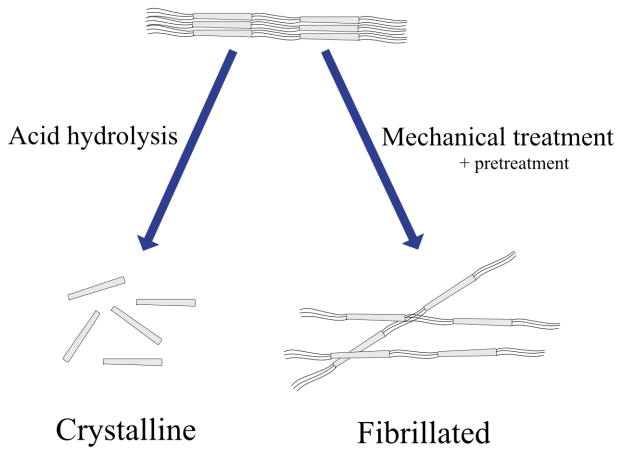

Figure 3.2 Schematic illustration of the two classifications of micro/nanocellulose: crystalline and fibrillated.

In the last decade, micro/nanocellulose has become a progressively popular topic in the research community, with the number of publications increasing annually (Figure 3.3). This is partly due to the inevitable transition towards a bio-based society in which renewable materials, such as cellulosic biomass, will play a vital role. Furthermore, nanocelluloses have additional benefits that stem from their large surface area to volume ratio, an example of which is a significant water holding capacity. However, a high degree of water retention is not only a benefit because it also causes difficulties related to dewatering, as will be described later on. In addition, the classical features of cellulose materials still hold, e.g. the high number of accessible hydroxyl groups makes it possible to tune its functionality.

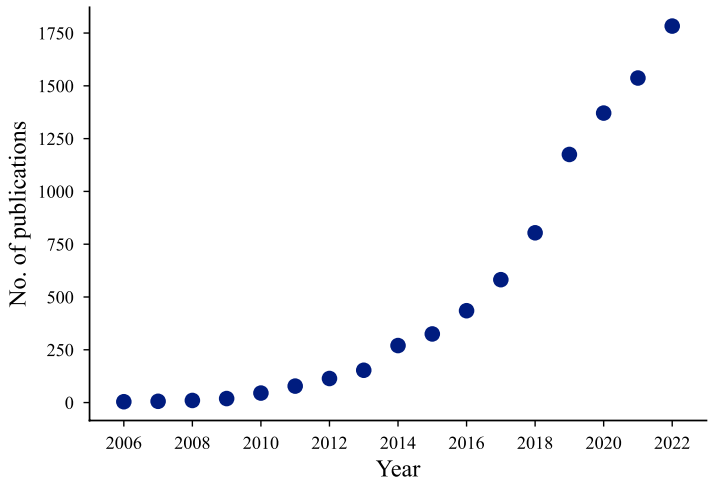

Figure 3.3 Number of publications versus year (2006-2022). Retrieved from Scopus (2023-05-09) [ALL=nanocellulose].

Micro/nanocellulose has partly left the academic sphere, and there are now some companies that produce these materials on an industrial scale, e.g. CelluForce (crystalline) and Fiberlean Technologies (fibrillated). The big breakthrough has nevertheless yet to transpire: this is due, in part, to challenges related to the removal of water in the dilute product streams, and will be discussed further in *3.3 DEWATERING MICRO/NANOCELLULOSE.*

3.2.1. Crystalline cellulose

The first reports on the isolation of crystalline cellulose appeared in the transition between the 1940s and 1950s. Nickerson and Habrle [45], along with Rånby [46], reported that the acidic treatment of cellulosic fibres led to degradation of the disordered part of the cellulose fibre and resulted in fractions of rod-shaped particles of high crystallinity: the discovery of nanocrystalline cellulose had been made.

The isolation of CNC is still commonly achieved by acid hydrolysis of the less ordered parts of the cellulose fibrils, typically using highly concentrated sulphuric or hydrochloric acid, and is followed by sonification and purification. The resulting product is comprised of highly crystalline, stiff fractions with typical dimensions of 50-4000 nm in length and 3-20 nm in width. The dimensions, as well as the shape of the cross-section, depend on the source of the raw material and isolation method [47].

If complete isolation to nanocrystals is not achieved, the resulting material is referred to as microcrystalline cellulose. MCC has a lower crystallinity index than CNC, and the particle/agglomerate size is bigger. Avicel ® is an industrially-available MCC that is used, for example, in toothpaste and cosmetics.

3.2.2. Fibrillated cellulose

The isolation of fibrillated cellulose was realised later than crystalline cellulose, but it is not a new material. In fact, it was first reported approximately 40 years ago by Herrick *et al.* [48] and Turbak *et al.* [49], who used high-pressure homogenisers to isolate the cellulose microfibrils mechanically. Although research continued during the second half of the 1980s [50,51], there was a lack of interest from industry that was due partly to the high energy demand associated with the mechanical treatment needed to separate the cellulose fibrils. It was not until the early 21st century that industrial interest began to appear. This was related to a combination of two factors: the expiration of Turbak's patent [52] in 2004 and efforts that were made to reduce the energy demand by using predominantly enzymatic [53] and chemical pre-treatment [50,54]. The findings of Saito and Isogai [54] were especially successful: they used 2,2,6,6-tetramethylpiperidine-1-oxyl (TEMPO)-mediated oxidation to introduce negative charges on the fibril surface by converting the primary hydroxyls to carboxylate groups (see *3.2.3 TEMPO-mediated oxidation*).

The diversity of the fibrillated material is conveyed from the definition of *cellulose nanofibril* given below [55]; this is not one single material, but rather a family of materials. The source of raw material, the possible pre-treatment and the mechanical isolation process all influence a wide range of the product's characteristics. Furthermore, the nomenclature and variety of abbreviations used is broad: microfibrillated cellulose (MFC) and cellulose nanofibrils (CNF) are two frequently-used terms. In this doctoral thesis, the following distinction between the two is made for the purpose of clarity: CNF refers to material prepared through complete isolation to elementary fibril and MFC refers to materials in which complete isolation has not been achieved but bundles of elementary fibrils (i.e. microfibrils) occur.

ISO/Tappi Standard 20477:2023

"***Cellulose nanofibre*** is composed of at least one elementary fibril that can contain branches of a significant fraction which are in the nanoscale."

The following notes are also added:

- Dimensions are typically 3-100 nm in cross-section and typically up to 100 µm in length.
- Cellulose nanofibrils produced from plant sources by mechanical processes can be accompanied by hemicellulose and, in some cases, lignin.
- Some cellulose nanofibrils might have functional groups on their surface as a result of the manufacturing process.

A flexible nature is characteristic for fibrillated cellulose, but not crystalline cellulose. Also, cellulose fibrils have an even higher aspect ratio which, due to their flexible nature, can cause them to entangle and produce strong networks and form gels, even at low concentrations [56].

Fibrillated cellulose has been suggested as having the potential of being used in a wide span of applications [57], some of which are presented in Figure 3.4. The great ability to hold water and modify rheology makes it suitable for use in areas such as cosmetics and skin care products [58,59], foodstuffs [60,61], paint and coatings [62]. Its use as a mechanical strength agent in, for example, paper products [63–66] is possible due to the ability to interact with the surface of cellulose fibres: strong networks are formed as a result of physical entanglement, hydrogen bonding and hydrophobic interactions between the fibrils. Also, good barrier properties mean that it can be used in various films and barriers [67–69]. According to Li *et al.* [70] the applications mentioned above are considered possible today, or in the near future, whereas it is suggested that future uses will involve use in membranes [71,72], biomedical applications [73] and optoelectronics [74–76].

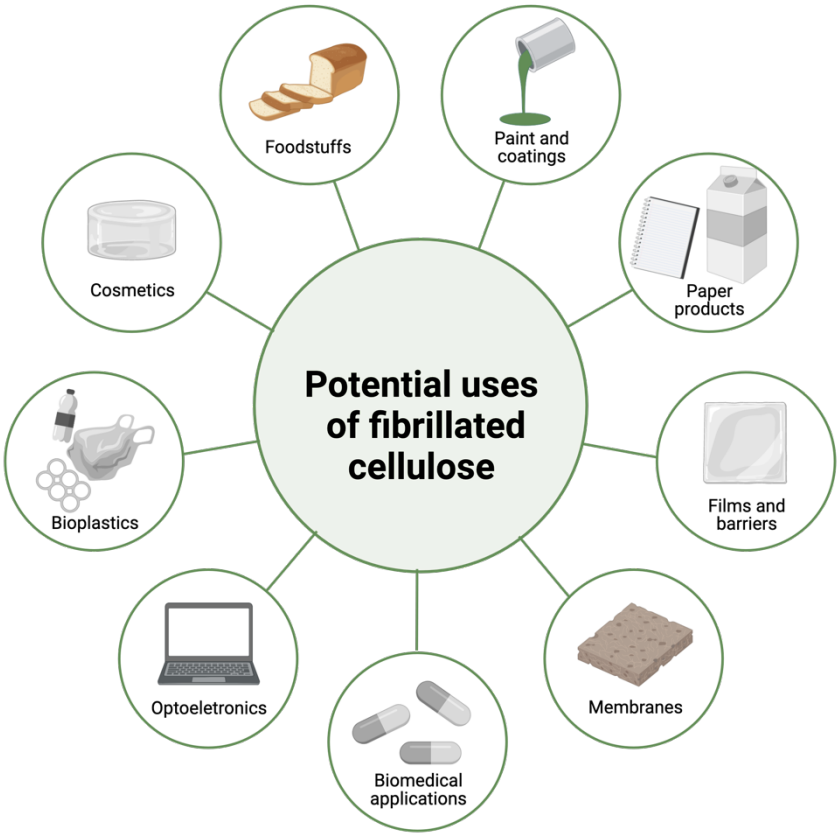

Figure 3.4 Potential uses of fibrillated cellulose. Created with BioRender.com.

There are currently several companies that produce various qualities of fibrillated cellulose exist, e.g. Borregaard AS (Exilva ®), Daicel Industries (CELISH ®), Norske Skog (CEBINA ®), FiberLean Technologies (FiberLean ® MFC), Weidmann Fiber Technology (Celova ®) and Sappi (Valida ®). The University of Maine also produces and sells fibrillated cellulose.

3.2.3. TEMPO-mediated oxidation

TEMPO-mediated oxidation is one method of reducing the energy demand of mechanical fibrillation, which is achieved by the introduction of negative charges onto the fibril surface. This promotes repulsion forces between the fibrils, with the consequence that less energy is then required to separate them.

The reaction scheme shown in Figure 3.5 displays the mechanism of a reaction system with NaBr/NaClO/TEMPO [77]. The primary oxidant, NaClO, first oxidises the TEMPO in its radical form to a nitrosonium cation which, in turn, oxidises the primary hydroxyl group (C6) to an aldehyde and further to a carboxylate group [78]. Studies have also shown that the conversion to C6-carboxylate groups can be achieved using NaBrO and/or NaClO. NaBrO is used as an

additional catalyst and oxidises the N-hydroxy-TEMPO [79]; in the meantime, it is being reduced to NaBr, which is then re-oxidised back to NaBrO with NaClO. This means that only NaClO is consumed during the reaction. The reaction, which is typically performed at pH ~10, requires that small amounts of NaOH be added continuously to the reaction medium to maintain a constant pH throughout.

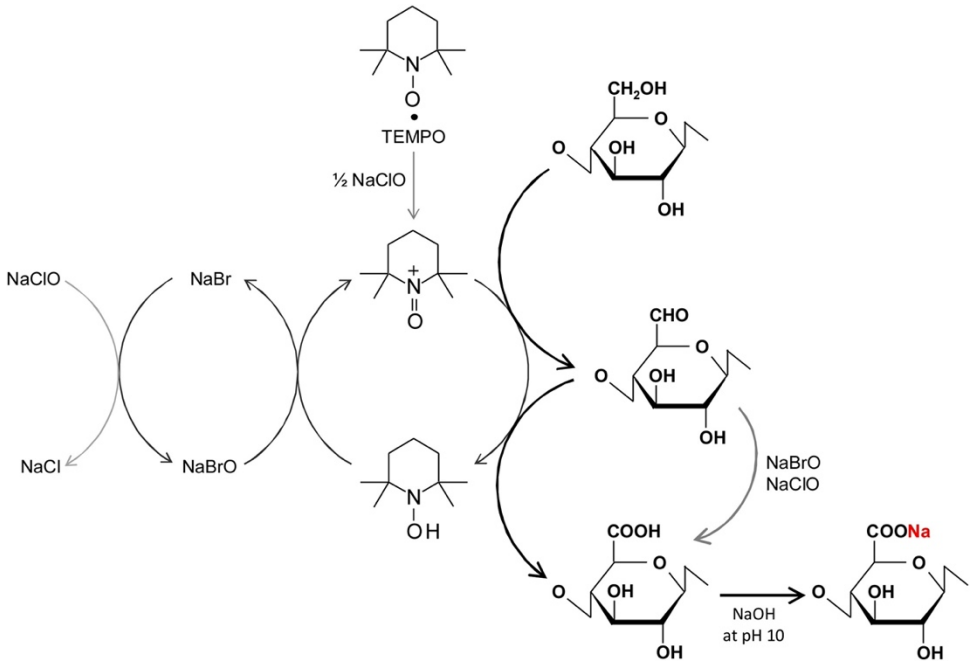

Figure 3.5 Reaction scheme of TEMPO-mediated oxidation. Reprinted courtesy of The Royal Society of Chemistry [77].

3.3. DEWATERING MICRO/NANOCELLULOSE

3.3.1. Why is mechanical dewatering necessary?

Micro/nanocelluloses are produced at dilute conditions (e.g. 1 kg of the final product can have a composition of 0.99 kg water and as little as 0.01 kg MFC) to provide a lower viscosity or to reduce the risk of clogging during mechanical separation. Transportation and storage costs will otherwise be steep if the majority of the water in the product is not removed. Water removal is thus an essential part of improving the overall economic performance: it has been expressed as being one of the greatest challenges that must be overcome in improving the commercial attractiveness of these materials [2,4,70,80–82].

The high moisture content of the final product can also be a cause of concern for product applications in which water is not tolerable. A selection of the aforementioned applications of MFC shown in Figure 3.4 allows MFC to be added in the form of an aqueous solution or a wet

gel, for example, to bulk products such as paper, foodstuffs, paint and coatings, and can also be used in cosmetics and biomedical applications. In other applications, however, incompatibility with water can be an issue and it therefore cannot be present.

Water removal can be achieved through methods based on thermal drying but, given the high heat of evaporation of water and the excessive quantity of water that is to be removed, this is unrealistic from an economical perspective. In addition, drying is associated with severe problems related to redispersion of the dried material: this stems from partial aggregation of the cellulose structures, referred to as *hornification*[6] in the pulp and paper industry, that aggravates the re-dispersibility of the material.

3.3.2. Why is filtration challenging?

Filtration is the mechanical dewatering technique used most often for solid/liquid separation. However, the extensive surface area of crystalline and especially fibrillated micro/nanocellulose means that there is excessive drag and the filtration resistance is therefore high. Compressible materials have also been shown, under certain conditions, to deposit a dense initial layer of particles on the surface of the filter cloth, thereby forming a "skin" with a very high flow resistance [86,87]. Furthermore, in the case of MFC, the flexible fibrils (with a wide distribution in size), may slide over each other to form a compact mat [88].

Further complexity is added to the dewatering process in the case of fibrillated cellulose due to its gel-like nature, which endows it with a high water-trapping capacity. Water retention can be modified by altering the fibril-fibril interactions: lowering the pH, for example, would cause the protonation of charged entities and result in stronger attractive fibril-fibril interactions. This was demonstrated in a patent issued in 2016 to Laukkanen *et al.* [89], as well as in a study by Fall *et al*. [90], to be an efficient way of increasing the dewatering rate during the dead-end filtration of a variety of MFC. Reducing the gel point, which is defined as the lowest fibrous volume fraction at which all the primary flocs are interconnected and form a self-supporting network, is also a way of tackling this issue. This can be achieved by the addition of polyelectrolytes [91,92].

Furthermore, it is also important that valuable characteristics (e.g. available surface area) are not diminished after dewatering. Although the risk of hornification is not as severe as in the case of thermal drying, studies have shown that the available surface area of MFC is reduced already at modest dry contents of 8.2 wt% [93]. Moreover, sufficient re-dispersibility is key if the dewatering is to be regarded as successful, i.e. there is a trade-off between water content (transportation and storage costs) and properties of the material [5,6].

[6] The reversibility and mechanism of hornification remain under debate, despite being discussed for decades [83–85].

3.3.3. What has been done?

The methods presented in Table 3.1 have been used to study the dewatering of micro/nanocellulose. A number of research groups have explored how dewatering is influenced by the chemical environment (e.g. pH and ionic strength) [86,87,90,94] and various types of assisted dewatering techniques, such as the use of an electric field [7–9], shear [95–97] and ultrasound [98]. The objective of the studies summarised in the table was to assess dewatering; two studies focusing on the fabrication of nanopapers ([91,99]) are also included.

All of the studies in Table 3.1 handle dilute suspensions (0.05-4 wt% fibrillated cellulose, 5-10 vol% MCC, 2.3 wt% CNC), but the dewatering equipment and quantities to be dewatered vary; in the case of filtration, different filter media have been used. It is important to bear this in mind when comparing the results. For example, Fall *et al.* [90] reported impressive dry contents (21-33 wt%) when dewatering 1 wt% CNF/MFC using dead-end filtration; it is important to recognize here that the resulting filter cake would be very thin because only 91 g of suspension was dewatered ($Ø_{filter}$=50 mm). In the MFC filtration experiments conducted in this thesis, the same filter area was used but using approx. 500 mL of MFC, which gave a thicker filter cake. Regardless of the discrepancies between the tabulated studies, the researchers all concluded that, without any modification or assistance, dewatering micro/nanocellulose is nevertheless difficult.

The importance of electrostatic interactions during dead-end filtration was described in *2.2 ELECTROSTATIC INTERACTIONS AND THE IMPACT OF IONS.* These can be controlled by the chemical environment, e.g. pH and/or ionic strength of the suspension. The influence of pH during the dead-end filtration of MCC [86,87] and MFC/CNF [90] has been demonstrated, and clearly shows that, as the surface charges are protonated, electrostatic repulson is dampened and dewatering is enhanced. The pKa of the carboxyl groups present on the fibre is around 3-4 [100] so, if the pH is >3-4, the consequence is that carboxyl groups are deprotonated and electrostatic repulsions between the cellulosic particles will predominate. Any modification that is made to the surface of the fibres affects the critical pH value.

The impact ionic strength has on the dead-end filtration of CNF/MFC was studied by Sim *et al.* [94] and Fall *et al.* [90], who demonstrated that the beneficial impact of ionic strength is pronounced as long as the zeta potential of the particle is reduced. In the case of MFC, the ionic environment also affects the osmotic pressure and hence the swelling of the fibril network. An increased concentration of ions reduces the swelling of the fibril network because it reduces the concentration gradient of the charges between within the fibril network (where the concentration is high) and the surrounding solution. Wetterling *et al.* [7] also investigated the impact of ionic strength (NaCl) during the electro-assisted filtration of MCC, and concluded that it affected both filtration (as particles agglomerated in the presence of NaCl) and electrokinetic phenomena (i.e. impact on conductivity). The first paper in this thesis probes further into the impact ions have on the dead-end filtration of MCC.

It is not only the particle surface charge that plays an important role in the dewatering of micro/nanocellulose: other surface modifications have also been demonstrated to influence it. Chemical surface modification was studied by Sethi *et al.* [99], who hypothesized that the reason for the slow rate of dewatering was due to the high hydrophilicity of the MFC. The hydrophilicity was reduced by subjecting the cellulose surface to sonication-assisted modification with lactic acid, which subsequently improved dewatering.

However, the surface modifications introduced do not typically aid dewatering. An example of such an alteration is the increased ruggedness of MCC particles, which was studied by Wetterling *et al.* [101]. Increasing the surface ruggedness increased the total surface area of the particles, which gave a higher filtration resistance. In the case of MFC, the degree of mechanical fibrillation is an important parameter that not only affects the properties of the end-product but also dewatering. The way in which the degree of mechanical fibrillation influences the dewatering of MFC requires further evaluation, and is explored in Paper IV.

Rather than modifying the suspension to improve dewatering, another method that can be employed involves the use of assisted dewatering techniques. The dewatering of furnishes containing MFC/CNF under the assistance of shear has been investigated extensively by Dimic-Misic *et al.* [95–97], who also studied its influence on rheology. Among other things, they demonstrated the relationship between dewatering and rheology: dewatering was enhanced by the assistance of shear due to the shear-thinning behaviour of the furnish that resulted from the breakage of the suspension's microstructure.

Dewatering MFC with the assistance of ultrasound waves was explored recently by Ringania *et al.* [98]. Using this method, they succeeded in removing a maximum of 72% of the water from a 1 wt% MFC suspension.

Electro-assisted filtration, in which an electric field is applied across a part of the filter chamber, was proven by Wetterling *et al.* [7,8] to be a successful way of enhancing the dewatering of MCC; the use of an electric field alone was sufficient to achieve dewatering of CNC [9]. MFC has a completely different morphology than MCC and CNC, as previously highlighted in this chapter, making it both important and interesting to study the electro-assisted filtration of this material; more is uncovered in Papers II-IV.

Table 3.1 Overview of the literature pertaining to the dewatering of micro/nanocellulose.

Dewatering technique	Micro/nanocellulose	Conditions	Cited in
Dead-end Filtration (overpressure)	1 wt% MFC/CNF (91 g) Enzymatically pretreated Carboxymethylated Industrially produced	Piston-press (Ø=50 mm), Stepwise increase of pressure from 0.5 to 6 bar Munktell 00H filter paper (particle retention: 1-2 µm) Studied effect of pH and ionic strength	Fall *et al.* [90]
	1.5 wt% MFC (60 g) produced from bleached eucalyptus kraft pulp	Pressure dewatering equipment, 7 bar Filter medium: n.d. Studied effect of ionic strength (NaCl, $CaCl_2$)	Sim *et al.* [94]
	5–10 vol% MCC	Filter press (Ø=60 mm, volume approx. 500 mL) A variety of filter media with a nominal pore size of 0.45 µm were used: polyethersulphone (PES), regenerated cellulose & cellulose nitrate Studied effect of filter medium, pH and mechanical ruggedness of MCC	Mattsson *et al.* [86,87] Wetterling *et al.* [101]

Vacuum filtration to form nanopapers	0.35 wt% MFC produced by grinding of bleached softwood sulphite pulp	Buchner funnel, 70 kPa (vacuum) Filter medium: polyvinylidene difluoride (PVDF) membrane Nominal pore size: 0.65 µm Studied effect of sonication-assisted surface modification (lactic acid)	Sethi *et al.* [99]
	0.05-0.6 wt% MFC from Daicel Chemical Industries Ltd.	British hand sheet maker (5 MPa) Studied the addition of polyelectrolyte (cationic polyacrylamide, CPAM, polyamide–amine–epichlorohydrin and PAE)	Varanasi and Batchelor [91]
Compression	0.15 wt% MFC (200 mL) from Daicel Chemical Industries Ltd.	Compression load cell Studied the addition of polyelectrolyte (CPAM)	Li *et al.* [92]
Assisted dewatering techniques			
Shear-assisted vacuum dewatering	1-4 wt% CNF/MFC suspensions and 5-15% furnishes	Vacuum dewatering (50 kPa, vacuum) Filter medium: Whatman nucleopore membrane Nominal pore size: 0.2 µm	Dimic-Misic *et al.* [95–97]
Ultrasound-assisted dewatering	3 wt% MFC (5 g) from The University of Maine	Ultrasound equipment	Ringania *et al.* [98]

Electro-assisted filtration	5 vol% MCC	Filter press described in Wetterling *et al.* [8] with a modified filter cell (Ø=50 mm) Filter medium: PES Nominal pore size: 0.45 µm Applied pressure: 3 bar Applied electric field: 10, 30 and 60 V/cm Also studied the effects of ionic concentration during electro-assisted filtration (NaCl)	Wetterling *et al.* [7,8]
Electro-osmotic dewatering	2.3 wt% CNC	Filter press described in Wetterling *et al.* [8] with a modified filter cell (Ø=50 mm) Applied electric field: 5-30 V/cm Filter medium: PES Nominal pore size: 0.1 µm	Wetterling *et al.* [9]

4

MATERIALS AND METHODS

This chapter describes the materials and methods used in Papers I-IV. Further details and experimental protocols can be found in the respective papers.

4.1. MATERIALS

Microcrystalline cellulose (Avicel ® PH-105) supplied by DuPont Nutrition was the model material used in Paper I. According to the manufacturer, it had an average nominal particle size of 19 µm, which was determined by a method based on laser diffraction. 2 M NaCl (VWR GPR Rectapur) was used to adjust the concentration of NaCl in the suspension.

Two types of MFC were used in Papers II-IV:

- TEMPO-MFC, produced from dissolving pulp (see *4.3.2 TEMPO-MFC*)
- Commercially-available MFC, sourced from Borregaard AS. It had a dry content of approx. 2 wt% and was supplied in two different degrees of mechanical fibrillation.

4.2. FILTRATION EQUIPMENT

4.2.1. Dead-end filtration

A pneumatically-driven piston press (Figure 4.1), capable of handling pressures up to 60 bar, was used for all filtration experiments. The inner diameter of the filter cell is 60 mm and it has a total height of 175 mm. The lower part, which has a height of 115 mm and is constructed of Plexiglas, is placed upon a perforated bottom plate. Eight pressure capillaries are mounted through the bottom plate; they have circular holes 0.6 mm in diameter that are located perpendicular to the flow at distances from the bottom plate of 0.5, 1, 2, 3, 5, 7, 9 and 12 mm, respectively. The top of each pressure capillary is conical in shape to minimise disturbance to the flow.

Prior to the filtration experiments, the capillaries are flushed thoroughly with degassed water to remove air that would otherwise cause entrapment of the suspension and thereby provide inaccurate measurements. The pressure capillaries are connected to pressure transducers (Kristal Instrument AG, accuracy of 10 kPa) and the absolute hydrostatic pressure is recorded in LabVIEW™ (software version 15.0, National Instruments) every other second. LabVIEW is also used to record the mass of the filtrate using a balance (Mettler Toledo SB 32000) with an accuracy of 0.5 g.

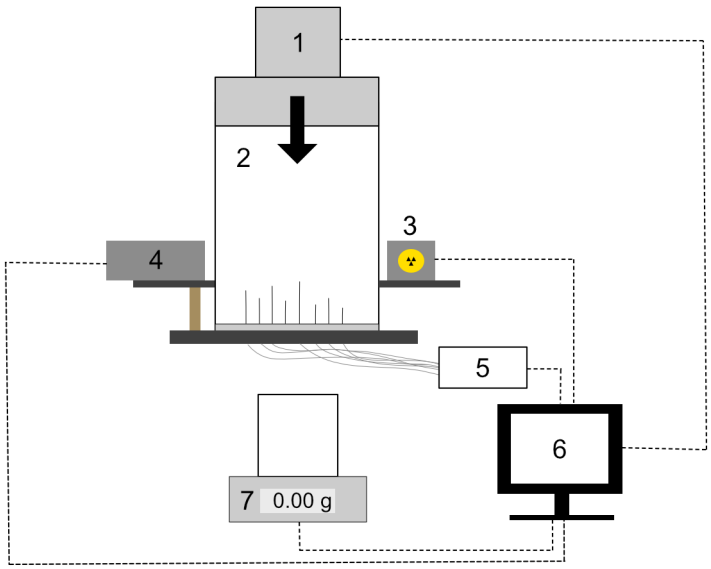

Figure 4.1 Schematic diagram of the filtration unit. 1: Piston press with its position recorded. 2: Plexiglas filter cell, with 8 pressure capillaries located at different heights. 3: ^{241}Am source of 10^9 Bq. 4: NaI (Tl) scintillator. 5: Pressure transducers. 6: Data acquisition unit. 7: Balance.

Solidosity measurements were conducted using a γ-emitting ^{241}Am source of 10^9 Bq as the source of radiation. The attenuation of the γ-radiation in a 1 mm thick slice of the cake was measured using a NaI(Tl) scintillator (Crismatec™ , ORTEC DigiBASE) and recorded in MAESTRO ®-32

(software version 6.0, ORTEC). A moveable rack was used for mounting the radiation source and the scintillator. The number of counts for the empty filter cell was measured for 10 minutes. A recording time of 30 s was used for the filtration of suspensions with additions of NaCl due to the short filtration time needed; the time was changed to 3 minutes for the suspension without an addition of ions. The absolute deviation of the solidosity was estimated as being ±0.02- 0.05, and the error between individual measurements lower than 0.03.

4.2.2. Electro-assisted filtration

To allow for electro-assisted filtration, the filtration set-up was adjusted [8], see Figure 4.2; the metallic bottom plate and piston head were exchanged for plastic alternatives. Also, the lower part of the filter cell was adapted: the inner diameter was reduced to 50 mm to accommodate a supporting rack that carries the upper electrode that is a mesh (10x10 mm (Papers II-IV) or 5x5 cm (Paper III)) of platinum wire with a diameter of 0.25 mm. The bottom electrode is a platinum mesh (Unimesh 300) and is placed on the bottom plate, beneath the filter medium and support filter. The two electrodes are separated at a constant distance of 25 mm and connected to a DC power supply (EA-PSI 5299-02 A, Elektro-Automatik). The two K-type thermocouples coated in PFA that are used for measuring the temperature are placed at distance of 5 and 20 mm from the filter medium, respectively.

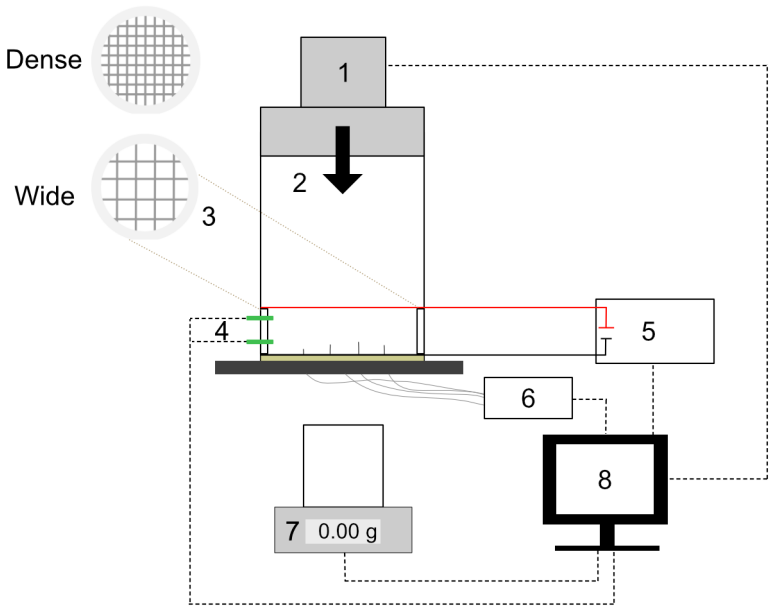

Figure 4.2 Schematic diagram of the electro-assisted filtration unit. 1: Piston press with its position recorded. 2: Plexiglas filter cell, with 4 pressure capillaries located at different heights. 3: Close-up of two anode meshes of different calibres. 4: Thermocouples. 5: Power supply (current, voltage and power recorded). 6: Pressure transducers. 7: Balance. 8: Data acquisition unit.

4.3. PREPARATION OF THE SUSPENSIONS

The preparation of all suspensions included homogenisation or dispersion using IKA Ultra-Turrax ® T50 with a dispersing element S50 N-G45F (Figure 4.3A). Figure 4.3B illustrates the operational principle: the rotor moves at a high speed, causing the medium to be sucked into the dispersion head and then forced radially through the rotor and stator teeth. The high shearing forces between the rotor and stator cause particle/particle cluster disintegration and, owing to turbulence, efficient mixing occurs.

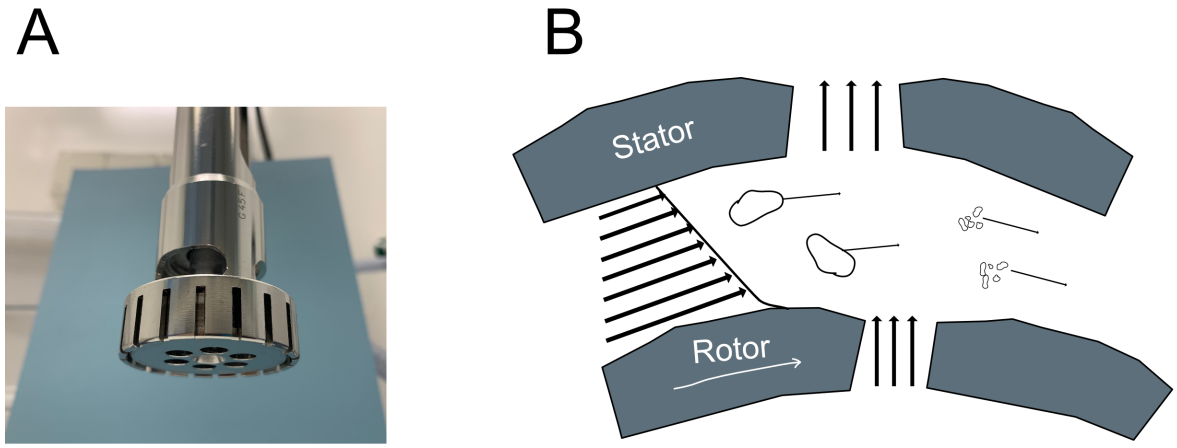

Figure 4.3 (A) Image of the dispersion head used. (B) Schematic illustration of the rotor-stator principle adapted from the IKA website.

4.3.1. MCC

A 10 vol% suspension was prepared by suspending MCC in 2 L of deionized water, whereafter the suspension was dispersed using IKA Ultra-Turrax ® T50 with a dispersing element (S50 N-G45F). From this suspension, a 5 vol% suspension was prepared and stirred continuously overnight. The ionic concentration of the suspension was adjusted by adding a calculated amount of 2 M NaCl to 1 L of MCC suspension under simultaneous stirring 1 h prior to the filtration experiment. Six conditions were investigated: 0.0, 0.10, 0.15, 0.20, 0.50 and 1.0 g/L NaCl.

4.3.2. TEMPO-MFC

The procedure used for the TEMPO-mediated oxidation of the dissolving pulp was based on the work by Brodin and Theliander [102]. The reaction was initialised by the dropwise addition of NaClO (5 mmol/g pulp) to an aqueous suspension containing 40 g (dry basis) of dissolving pulp, NaBr (1 mmol/g pulp) and catalytic amounts of TEMPO (0.1 mmol/g pulp). The reaction was carried out at 1% pulp consistency and at room temperature in a baffled vessel (⌀ = 190 mm) under constant stirring with a four-pitch blade impeller (⌀ = 90 mm). Throughout the reaction, the pH was kept at 10.1 ± 0.1 (pH meter SevenCompact™ S210, Mettler Toledo) by the addition of 0.5 M NaOH. After 70 minutes, the reaction was quenched using 200 mL 99% EtOH.

The oxidised fibres were then separated by vacuum filtration, and smaller fibre fragments were retained by recirculating the first volume of filtrate. The oxidised pulp was washed thoroughly with deionized water until the conductivity of the filtrate was stabilized (>23 µS/cm). Further, the pulp was stored in plastic bags at 4 ºC until required for treatment and analysis.

A 1 wt% TEMPO-MFC was prepared by mechanical disintegration of the oxidised pulp, using an IKA Ultra-Turrax ® T50 with a dispersing element (S50 N-G45F) operating at 10 000 rpm for 4 min/g TEMPO-oxidised pulp. The dry content of the oxidised pulp was determined by a Sartorius moisture analyser and performed in a minimum of duplicates. The suspension was kept in an ice bath in order to limit the increase in temperature that occurs during mechanical treatment.

4.3.3. MFC

1.0 wt% suspensions were prepared in 300 g portions from the approx. 2 wt% batches by diluting a known amount with deionised water, followed by mechanical dispersion using IKA Ultra-Turrax ® T50 with a dispersing element (S50 N-G45F) operating at 10 000 rpm for 4 min.

4.4. EXPERIMENTAL CONDITIONS

All experiments were performed at room temperature (~22 ˚C). A hydrophilic polyethersulphone (PES) filter (Supor ®, PALL Corporations) was used as the filter medium, with a grade 5 Munktell filter (Ahlström-Munksjö) that served as an underlying support. Table 4.1 reports the experimental conditions employed, along with the pore size of the filter medium used in the different studies.

Table 4.1 Summary of the experimental conditions used in Papers I-IV. P=applied pressure; E=electric field strength used in the electro-assisted filtration experiments conducted at the applied pressure given in P; EOD=electric field strength used in the electro-osmotic dewatering experiments. * = omitted in the electro-assisted filtration experiments.

Paper	Suspension	Nominal pore size of filter medium [µm]	Experimental conditions (P, E, EOD)
I	5 vol% MCC NaCl: 0-1.0 g/L	0.45	P: 3 bar
II	1 wt% TEMPO-MFC	0.1	P: 3 bar E: 6, 12, 24 V/cm EOD: 24 V/cm
III	1 wt% TEMPO-MFC	0.1	P: 3 bar E: 6, 24 V/cm EOD: 24 V/cm
IV	1 wt% MFC Two degrees of mechanical fibrillation	0.45	P: 0.3, 1.7*, 3.0 bar E: 16, 32 V/cm EOD: 32 V/cm

4.4.1. Dead-end filtration of MCC

Dead-end filtration experiments were performed using varying ionic concentrations at a constant applied filtration pressure of 3 bar.

4.4.2. Filtration of MFC

All dead-end filtration experiments were run at constant applied pressure whereas the electro-assisted filtration experiments were at both constant applied pressure and constant voltage. In addition, experiments involving only an applied electric field, i.e. electro-osmotic dewatering, were also included.

4.4.2.1. Papers II & III: TEMPO-MFC

The dead-end filtration experiments were performed using only an applied pressure of 3 bar. In the electro-osmotic dewatering experiments, only an applied electric field of 24 V/cm was used. In Paper II, three levels of applied electric field strength were examined during electro-assisted filtration at 3 bar: 6, 12 and 24 V/cm. The middle level was omitted in Paper III, with only 6 and 24 V/cm being evaluated.

4.4.2.2. Paper IV: MFC

Dead-end filtration experiments were carried out at applied pressures of 0.3, 1.7 and 3 bar respectively; electro-osmotic dewatering used only an applied electric field of 32 V/cm. Electro-assisted filtration was performed at two different applied pressures of 0.3 and 3 bar, and two levels of applied electric field, namely 16 and 32 V/cm.

The same filter medium and underlying support filter paper used in Paper I were employed since the 0.1 µm used in Papers II and III was deemed unnecessarily dense.

4.5. ANALYSIS OF FILTER CAKE STRUCTURE

In Paper III, the filter cake structures obtained after electro-assisted filtration and electro-osmotic dewatering were studied both qualitatively (scanning electron microscopy, SEM) and quantitatively (small and wide-angle X-ray scattering).

4.5.1. Qualitative analysis

Sections of freeze-dried filter cake were prepared with a sharp razor blade and mounted onto a SEM stub using carbon tape, whereafter they were sputter-coated with gold (4 nm). A low accelerating voltage was used (3 kV) in all SEM analysis in order prevent the samples from burning.

4.5.2. Quantitative analysis

WAXS explores features smaller than 1 nm, and thus can be used for studying the crystal structures of cellulose. Furthermore, as the cellulose crystals are assumed to be aligned in the direction of the cellulose fibril [103], this technique can be used to assess the degree of cellulose fibril orientation in the filter cake. Although either of the cellulose crystal reflections can be used, see Figure 4.4, a q-region of 1.1 ± 0.05Å $^{-1}$, corresponding to the (1−10/110) plane of cellulose I, was chosen in Paper III. Further details pertaining to the WAXS measurements can be found in the paper, which is appended.

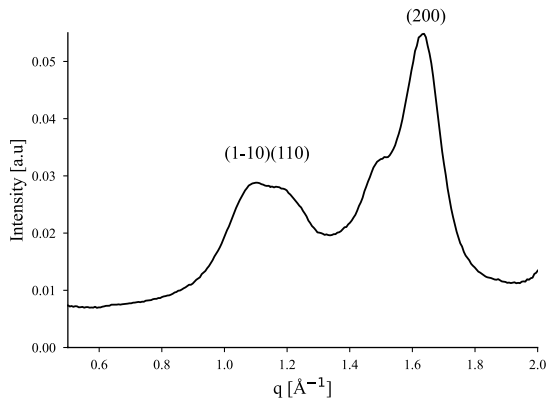

Figure 4.4 Radially-integrated intensity profile obtained from WAXS measurements of TEMPO-MFC. The crystal planes are indicated in the figure.

The degree of orientation, f_c, (Eq. 13) was estimated by employing the full width at half maximum (fwhm) of the azimuthal profile and Gaussian fitting of the WAXS data. The data was treated using DataAnalysis WorkbeNch (DAWN)[104].

$$f_c = \frac{180 - fwhm}{180} \qquad (13)$$

A perfectly aligned sampled would have an f_c approaching one, whereas that of a completely anisotropic sample would be approaching zero.

4.6. QUALITY ANALYSIS AFTER DEWATERING

It is important to know how, and if, the quality of the MFC is altered after dewatering because this could have implications on the final usage of the material. Thus, in Paper IV, the impacts made on two important material properties, namely water retention value (WRV) and rheology, were evaluated after dewatering.

Prior to quality analysis, the dry content of the filter cakes was determined gravimetrically after drying at 105 °C overnight, whereafter 2.0 wt% suspensions were prepared. pH and conductivity were adjusted using 0.05-0.5M NaOH and 0.05-0.2M NaCl to correspond to that of the original 2.0 wt% suspensions of 5.1 ± 0.1 and 92 ± 9 µS/cm, respectively. The samples were left to stabilise overnight.

4.6.1. Water retention value (WRV)

WRV is used to estimate the amount of water that can be retained per gram of MFC. A method based on centrifugation was employed to determine the WRV before and after dewatering. In brief, a 0.3 wt% suspension of MFC was prepared by dilution with milliQ water. The sample was centrifuged (5810 R, Eppendorf) in 50 mL falcon tubes for a set time at 1000g, whereafter the supernatant was discarded. Knowing the amount of MFC in the tube and the mass of the bottom phase after centrifugation, the WRV could be calculated (g water/g MFC).

4.6.2. Rheology

The rheology of the original and dewatered suspensions was investigated using a cylindrical rheometer (Physica MCR-301, Anton Paar GmbH) with a sandblasted bob and cup. All tests were performed at room temperature with a concentration of 0.4 wt% being used, which corresponds to a semi-dilute regime where the MFC still behaves as a gel [105].

MFC is a so-called viscoelastic material, i.e. it exhibits both elastic and viscous properties. These properties were studied using oscillatory tests at a frequency of 1 Hz. An amplitude sweep, with an oscillation strain ranging from 0.01 to 100%, was used first to determine the linear viscoelastic regime (LVE) and the yield stress, determined from a 10% reduction in the storage modulus (G') [106] (Figure 4.5).

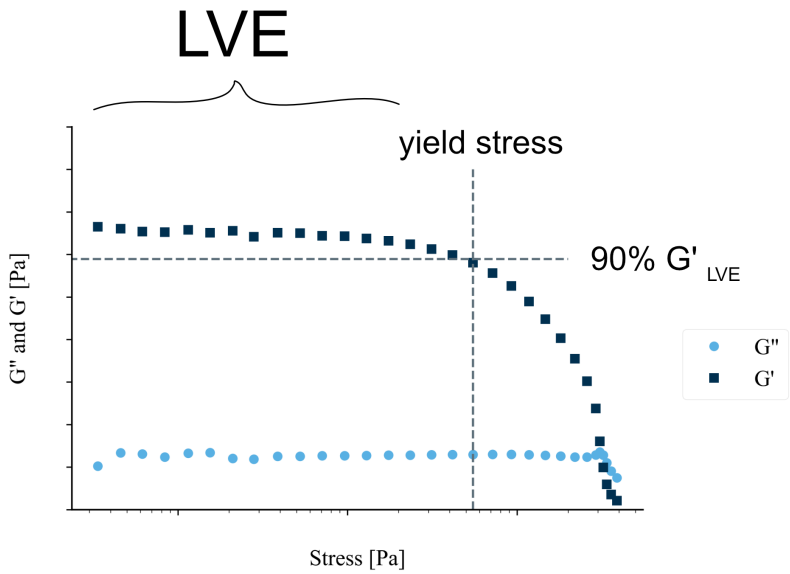

Figure 4.5 Graph used to determine yield stress from amplitude sweep. The horizontal grey dashed line represents a 10% reduction of the plateau value of G' and the yield stress is taken as its intersection with G' (vertical grey dashed line).

Time sweep measurements were made thereafter, at an oscillation strain in the LVE region, to determine the equilibrium storage and loss moduli. The storage modulus (G') corresponds to the elastic response of the material, whereas the loss modulus (G'') corresponds to the viscous response [106]. Flow sweep measurements were performed from 0.001 to 1000 s^{-1} in order to study flow behaviour and the shear thinning effect.

4.7. MATERIAL CHARACTERISATION

All the material characterisation techniques employed in Papers I-IV are summarised below, in Table 4.2.

Table 4.2 Summary of the characterisation techniques used in Papers I-IV.

	Pulp		**MFC**		**MCC**
	Dissolving	TEMPO-oxidised	TEMPO-MFC	Commercial	
Compositional analysis	✓			✓	✓
Density					✓
Carboxylate groups *ATR-IR*	✓				
Conductometric titration	✓	✓	✓	✓	
Surface charge *Zeta potential*			✓		✓
Polyelectrolyte titration				✓	
Size *Focused Beam Reflectance Measurement (FBRM ®)*					✓
Laser diffraction				✓	✓
Fibre analyser (kajaani)				✓	
Surface area *B.E.T.*			✓		✓
Morphology *SEM*			✓	✓	✓

4.7.1. Compositional analysis

The composition of the raw materials, in terms of monosugars and lignin, was determined according to a method based on the work by Theander and Westerlund [107]: the raw material was disintegrated into a solution of monosugars and acid soluble lignin (ASL) through acid hydrolysis with sulphuric acid. The major part of the lignin does, however, remain as a precipitate, referred to as Klason lignin (KL).

The monosugars were quantified using high performance anion exchange chromatography with a pulsed amperometry detection (HPAEC) system (Dionex ICS-5000 equipped with CarboPac PA1 columns), using fucose as an internal standard. NaOH/NaAc (aq.) and NaOH (aq.) were the eluents used. The ASL was quantified by measuring the absorbance with UV at 205 nm (Specord 205, AnalytikJena) utilising an absorptivity constant of 110 $dm^3g^{-1}cm^{-1}$, whereas the amount of KL was determined gravimetrically.

4.7.2. Density

The solid density of MCC was determined using a pycnometer (AccupPyc II 1340, Micromeritics), with helium as the displacement gas.

4.7.3. Carboxylate groups

Pulp was analysed before and after the TEMPO-mediated oxidation using Fourier Transform Infrared (FT-IR) spectroscopy (PerkinElmer Frontier) with Attenuated Total Reflectance (ATR) sampling accessory: the sample was placed on top of an ATR crystal and secured with a clamp. The infrared spectrum was recorded in transmittance mode with a resolution of 4 cm^{-1} recording from a wavenumber of 400 to 5000 cm^{-1}.

Conductometric titration was used to calculate the carboxylate content (mmol/g TEMPO-MFC) according to a method by Mautner *et al.* [108]: a sample of 0.15 g (dry weight) TEMPO-MFC was diluted to 60 mL with deionised water and 5 mL of 10 mM NaCl solution. The resulting solution was then left to stabilise before the pH was adjusted to 2.5-3. The conductivity was logged using a digital conductivity meter (model CO 301, VWR) during titration with 40 mM NaOH at a dosing rate of 0.1 mL/min (TitroLine 7000, SI analytics). Throughout the titration process, nitrogen was bubbled through the system to limit the influence of carbon dioxide. The carboxylate content was calculated according to Eq. 14 thus:

$$n = \frac{(v_1 - v_0)c_{NaOH}}{m} \qquad (14)$$

where n is the carboxylate content (mmol/g TEMPO-MFC), v_1 and v_0 are the volumes of NaOH (mL) at the intersection points between the plateau and the linear regions, respectively, and is determined graphically, c_{NaOH} is the concentration of NaOH (mmol/L) and m is the mass of TEMPO-MFC (g).

The carboxylate content of the unoxidized pulp was determined by the SCAN-CM 65:02 protocol. In this case, *m* equals the mass of pulp in Eq. 14 and therefore *n* equals mmol/g pulp.

The protocol employed in Paper IV can be found in Larsson *et al.* [109], and the same set-up was used.

4.7.4. Surface charge

The surface charge was measured using zeta potential and polyelectrolyte titration.

4.7.4.1. Zeta potential

In Paper 1, the zeta potential of 5 vol% MCC suspensions with a concentration of 0-1 g/L NaCl was measured using DelsaMax PRO (Beckman Coulter). Furthermore, the zeta potential of the PES membrane in an ionic environment (0.06-1 g/L NaCl) was measured using Anton Paar SurPASS streaming potential analyser for planar geometry.

The zeta potential of the TEMPO-MFC was measured in a 0.05 wt% solution, and with a background concentration of NaCl, to ensure a finite double layer thickness around the fibrils, as suggested by Foster *et al.* [110].

4.7.4.2. Polyelectrolyte titration

Polyelectrolyte titration assesses only the surface charges; it is important that the molecular weight of the polyelectrolyte is sufficiently high to avoid penetration through the cell wall. The polyelectrolyte used was poly(diallyldimethylammonium chloride) (pDADMAC) with a known surface charge; the titrations were performed using Stabino Polyelectrolyte titrator (Particle Metrix Gmbh, Meerbusch).

4.7.5. Size determination

Particle/agglomerate size was analysed using focused beam reflectance measurement (FBRM), laser diffraction and fibre analyser (kajaani).

4.7.5.1. FBRM ®

FBRM ® (G400, Mettler Toledo) was used to study variations in the sizes of the MCC agglomerates/particles when being subjected to increasing concentrations of NaCl (Paper I). The principle of this technique can be summarised thus: a focused beam of laser light is passed through a sapphire window located at the end of the FBRM probe. This laser light scans in a circular path and, when it encounters a particle, the back-scattered light is directed back to the probe. Using the time required for the laser beam to cross through the particle and the scanning rate of the laser beam allows the chord length (reported as #/s in the iC FBRM software) of the particle/agglomerate to be calculated which, in turn, can be related to the particle size. The minimum detectable chord length is 1 μm.

4.7.5.2. Laser diffraction

The particle size distribution of MCC was determined by laser diffraction (Malvern Mastersizer 2000). It should be noted that the particles are assumed to have a spherical geometry, and it is therefore not as representative if the particles have a high aspect ratio.

In Paper IV, a Microtrac S3500 laser diffraction analyser was used to study the smaller fractions that could not be captured by the fibre analyser.

4.7.5.3. Fibre analyser

KajaaniFS300 Fibre Analyzer (Metso) was used in Paper IV to analyse the length and width of the larger fibril fragments. It should, however, be emphasized that the equipment has a detection limit of 0.02 mm for length.

4.7.6. Specific surface area

Nitrogen physisorption (Tristar 3000, Micromeritics) at 77 K using the Brunauer–Emmett–Teller (B.E.T.) method was employed to evaluate the specific surface area. All samples were subjected to a solvent exchange procedure in order to preserve the water-swollen state and prevent irreversible collapse of the pores upon drying. In the method used, adapted from Wang *et al.* [111], water is first replaced by acetone and then followed by displacement washing. This is repeated 5 times, whereafter the same procedure is repeated with cyclohexane. The material is then dried overnight in a nitrogen atmosphere.

4.7.7. Morphology

Morphology was investigated by SEM using FEI Quanta200 ESEM (Papers I and II) and LEO Ultra 55 SEM (Papers III and IV). MCC was studied in its water-swollen state and had thus been undergoing the aforementioned solvent exchange (*4.7.6 Specific surface area*) prior to analysis.

In the case of the TEMPO-MFC, a droplet of 0.005 wt% TEMPO-MFC was allowed to air-dry overnight on top of a polished SEM stub. In Paper IV, a 0.01 wt% MFC suspension was filtered through a nanoporous aluminium oxide membrane (FlexiPor 20 nm, SmartMembranes GmbH) before carbon tape was used to attach it to a SEM stub.

5

RESULTS AND DISCUSSION

This chapter presents the main findings of the four papers on which this thesis is based. It starts by demonstrating the impact of ions during the dead-end filtration of MCC, followed by the electro-assisted filtration of MFC and the discovery of a peculiar filter cake structure. Finally, the impact ions have on the material properties after dewatering is examined.

5.1. THE IMPACT OF IONS DURING DEAD-END FILTRATION

Electrostatic interactions play an important role during dead-end filtration and may affect the structure of the filter cake being formed and the filtration resistance. The electrostatic interactions are controlled by the chemical environment and can be altered by, for example, adjusting the ionic strength. Cellulose and ions in an aqueous solution interact in various ways whilst cellulosic materials are being processed, for instance during the washing of pulp or the rinsing of regenerated cellulose. Paper I therefore investigated the impact of ions (Na^+, Cl^-) during the dead-end filtration of MCC (as a model material).

Microcrystalline cellulose

The MCC used in this work had a solid density of 1560 kg/m^3; its composition was 97% glucose and 3% mannose and xylose. The particle/agglomerate shape was cylindrical, as illustrated in the SEM micrograph in Figure 5.1. Laser diffraction revealed that 50 vol% of the particles had a particle size < 20.5 ± 0.9 µm (Table 5.1), and the B.E.T. surface area was 39 ± 2 m^2/g.

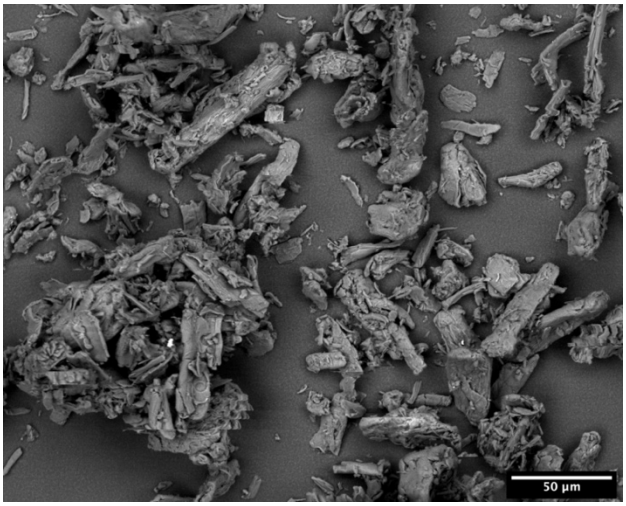

Figure 5.1 SEM micrograph of MCC after undergoing a solvent-exchange procedure.

Table 5.1 Summary of the particle size distribution in the mechanically-treated plain suspension determined by laser diffraction and specific surface area measured by the B.E.T. method. The subscripts 10, 50 and 90 indicate that x vol% of the particles are smaller than the value stated.

D_{10} [µm]	D_{50} [µm]	D_{90} [µm]	$A_{B.E.T}$ [m^2/g]
8 ± 0.4	20.5 ± 0.9	45.7 ± 3	39 ± 2

5.1.1. Addition of ions

Upon the addition of NaCl, the zeta potential of the MCC particles decreases, see Figure 5.2A. A modest amount of 0.2 g/L was sufficient to screen the surface charges efficiently, and reduced the absolute value of the zeta potential from 34.6 to 2.9 mV. A further addition of ions does not cause a significant reduction of the zeta potential.

The effect of increasing ionic concentration can also be observed using FBRM (Figure 5.2B), where this resulted in a shift of the chord length to the right, thereby indicating particle agglomeration. This aligns well with zeta potential measurements, as a reduction in the surface charge would result in weaker electrostatic repulsion between the particles, and attractive forces become dominant instead. No clear difference is visible between 0.5-1.0 g/L NaCl.

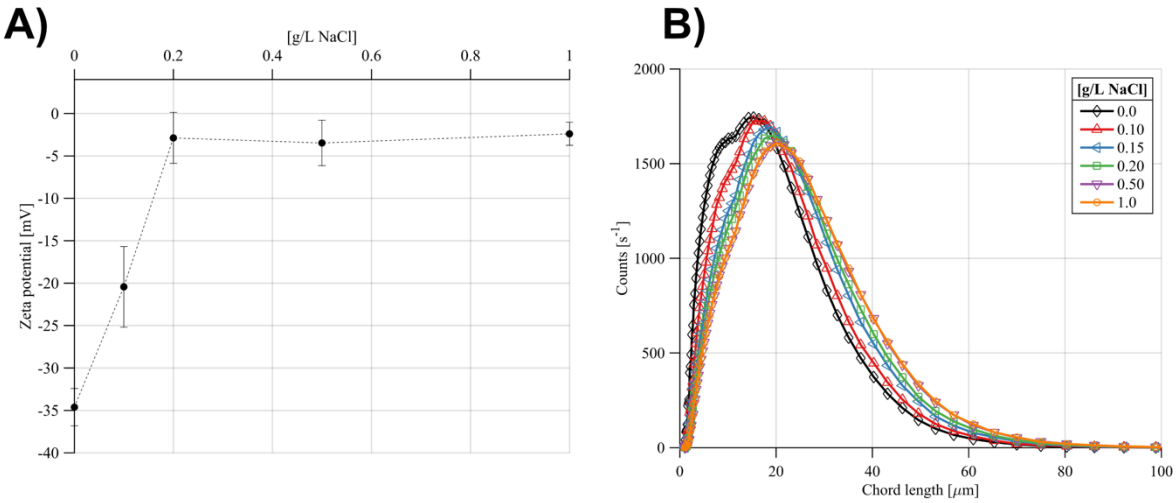

Figure 5.2 (A) Zeta potential of MCC versus g/L NaCl, with dashed lines for reader guidance. (B) Chord length distribution.

5.1.2. Filtration behaviour

The pronounced impact of ions during dead-end filtration is apparent in Figure 5.3, where the filtrate volume is plotted against time. The addition of ions improved dewatering significantly; the trend followed the one observed in the FBRM measurements, where no clear difference between the two highest concentrations could be noted. The impact on the average filtration resistance is displayed in Table 5.2 which, once again, illustrates the clear influence of the addition of ions: the average filtration resistance decreased as the concentration of ions increased.

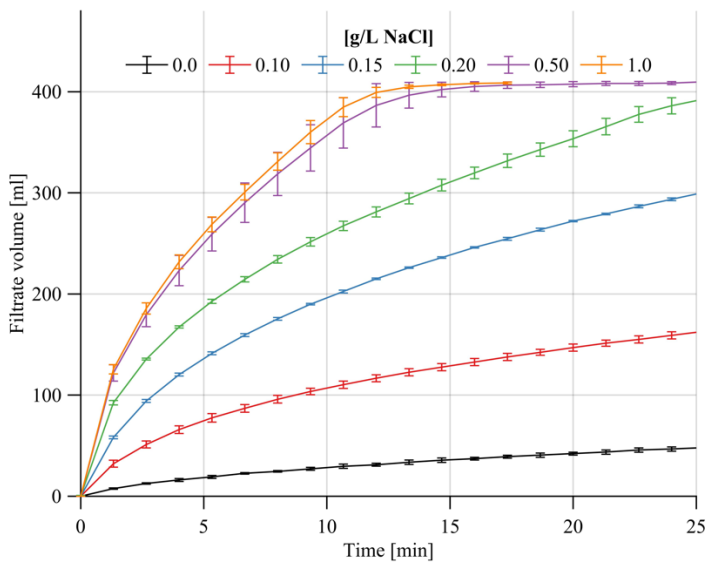

Figure 5.3 Filtrate volume vs. time at varying ionic concentrations.

Table 5.2 Average filtration resistance, including standard deviation.

[g/L NaCl]	*0.0*	*0.10*	*0.15*	*0.20*	*0.50*	*1.0*
α_{av}*10^{-11} [m/kg]	143 ± 10	42 ± 6.5	11 ± 0.1	5.2 ± 0.3	2.0 ± 0.3	1.8 ± 0.2

The beneficial effect on the dewatering is probably related to the agglomeration of the MCC particles in the presence of ions (Figure 5.2). Agglomeration leads to a reduction of the total surface area subjected to the liquid flow, which reduces the drag and, consequently, lowers the filtration resistance. The agglomeration did not, however, appear to have any significant impact on the solidosity of the filter cake formed (Figure 5.4).

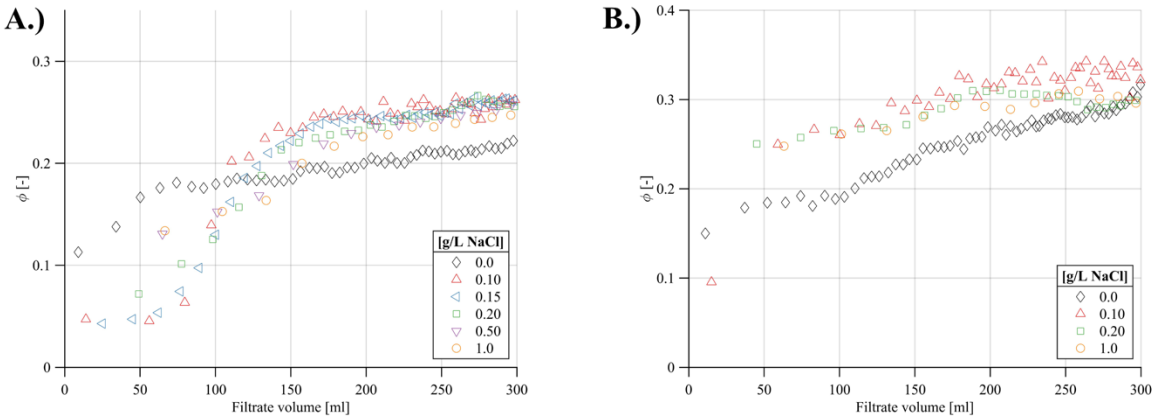

Figure 5.4 Solidosity profiles measured at 13 mm (A) and 7 mm (B). The legend states the concentration of NaCl added to the suspension.

The filtration resistance was extensive if no ions were added (Table 5.2). One possible reason for the very high filtration resistance could be related to partial/complete blocking of the internal pores of the filter medium, although this is deemed rather unlikely given that the nominal pore size (0.45 µm) is much smaller than that of the MCC particles. A more plausible reason is the formation of a dense initial layer of particles deposited on top of the filter medium, a "skin", which has been observed in studies on MCC [86,87]. Its origin is likely related to particle-particle and/or particle-membrane interactions. However, the zeta potential of the PES membrane was, just as in the case of MCC, negative for all ionic concentrations (Table 5.3). Neither the formation of a "skin" nor its absence in the presence of ions could be explained by electrostatic interactions between the solid particles and membrane.

Table 5.3 Zeta potential of the PES membrane at different ionic concentrations.

[g/L NaCl]	*0 (0.06)*	*0.1*	*0.2*	*0.5*	*1.0*
ζ potential [mV]	−93.7 ± 0.9	−89.2 ± 0.4	−68.3 ± 0.4	−43.1 ± 0.1	−28.9 ± 0.3

Arandia *et al.* [112] also encountered resilient cake layers when studying the crossflow filtration of MCC: to understand their formation, MD simulations were employed, and the cellulose-cellulose and cellulose-PES membrane interactions studied. The free energy profiles of the cellulose-cellulose interactions revealed the presence of a primary minima (i.e. a region dominated by attractive forces) at low centre-of-mass (COM) distances, into which region it was suggested

that the cellulose particles migrate when the solid pressure is sufficiently high. This could explain, in part, the strength of the cake layer formed.

5.1.3. Evaluation of compressibility

The local filtration data (local filtration resistance and local solidosity versus solid pressure) was fitted to the semi-empirical models given in Eqs. 10 and 11 in *2.1.1 Compressible filter cakes – the importance of local properties* and classified according to the categorisation presented in Table 2.1. The plain suspension was not included in this analysis because the hydrostatic pressure profile did not display any difference between the different pressure probes, which was a consequence of the formation of a "skin".

Table 5.4 reports the fitted model parameters; it is suggested that the values of β and *n* correspond to moderate to high compressibility. The values of α_0 and *n* decrease slightly with increasing ionic concentration, which could indicate a reduced compressibility. In the case of β, it is not possible to observe any clear trends with respect to ionic concentration as the difference was minor.

Table 5.4 Model parameters obtained by fitting local filtration data to Eqs. 10 and 11.

[g/L NaCl]	φ_0 [-]	P_0 [kPa]	β [-]	$\alpha_0 * 10^{-11}$ [m/kg]	n [-]
0.10	0.21	31.6	0.13	14	0.87
0.15	0.22	31.6	0.15	2.5	0.89
0.20	0.23	31.6	0.15	1.9	0.79
0.50	0.23	31.6	0.15	1.3	0.69
1.0	0.23	31.6	0.14	1.3	0.71

It should nevertheless be emphasized that the data obtained for 0.1 g/L NaCl was more difficult to fit and should therefore be interpreted with caution. At this ionic concentration, the local filtration resistance did not exhibit the same pressure dependency as the other ionic concentrations, which display similar trends (see Figure 5.5). A possible reason for this could be related to the stability of the agglomerates formed and/or particle/agglomerate size distribution. The electrostatic repulsion between the particles could still be rather high at this low ionic concentration (Figure 5.2A), which could lead to slightly different compaction mechanisms.

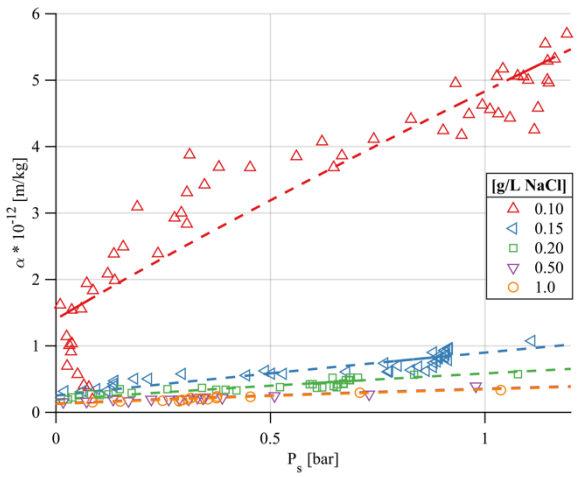

Figure 5.5 Local filtration resistance vs. solid pressure. The markers correspond to the local filtration data and the dashed lines to the data fitted from Eqs. 10 and 11.

5.2. IMPACT OF ELECTRIC FIELD

Rather than modifying the suspension to improve its dewatering, assisted filtration techniques can be used instead. Electro-assisted filtration, in which an electric field is applied across part of the filter chamber, was proven by Wetterling *et al.* [7,8] to be a successful way of enhancing the dewatering of MCC; the use of an electric field alone was sufficient to achieve dewatering of CNC [9]. Electro-assisted filtration was therefore investigated in Papers II-IV as a means of improving the dewatering of MFC. MFC has a completely different morphology to MCC: the microfibrils are long and flexible and may entangle to form networks with water-trapping properties.

Micro/nanofibrillated cellulose is not considered as being one homogenous material since the production method results in a material with a wide spread of characteristics, such as surface area, surface charge and functionalities. In order to interpret the following results, the properties of the MFC to be dewatered must thus be considered first, e.g. surface charge and fibril dimensions, because these may cause the pressure and/or electric field to influence the electro-assisted filtration process in different ways.

TEMPO-MFC (Papers II and III)

The morphology of the TEMPO-MFC displays a polydisperse fibril network, with a large variety of fibril dimensions ranging from bundles of fibrils to more isolated fibrils (Figure 5.6). This material has a very large surface area, determined by nitrogen physisorption to be 218 ± 12 m^2/g (solvent-exchanged state). The introduction of carboxylate groups (1.07-1.08 mmol/g TEMPO-MFC) resulted in a net repulsion between the fibrils and a negative zeta potential, as shown in Table 5.5.

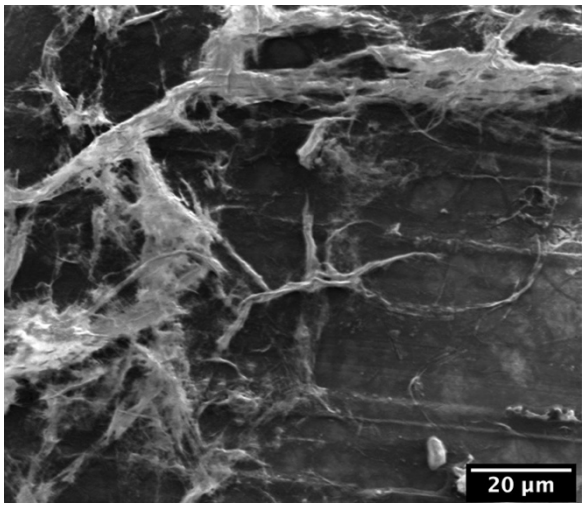

Figure 5.6 SEM micrograph of TEMPO-MFC.

Table 5.5 Summary of the zeta potential, carboxylate content (determined by conductometric titration) and B.E.T. surface area (determined by the nitrogen physisorption of the TEMPO-MFC used in Papers II).

ζ potential [mV]	Carboxylate content [mmol/g TEMPO-MFC]	B.E.T. surface area [m^2/g TEMPO-MFC]
−42.3 ± 1.5 (Paper II)	1.08 ± 0.02 (Paper II)	218 ± 12

Commercially-available MFC

MFC available commercially was used in this study. It was produced mechanically, was not modified chemically, and was supplied in two different degrees of mechanical fibrillation, referred to as *low* and *high*.

The more fibrillated material resulted in fibrils with smaller dimensions, but a higher surface charge (Table 5.6). Determined by polyelectrolyte titration, the surface charge for the low and high degrees of fibrillation at unadjusted pH (5.7) was 10.9 ± 1.2 and 13.9 ± 2.2 μeq/g, respectively. Measured at unadjusted ionic strength, the zeta potential was −28.8 ± 7.0 and −34.5 ± 4.2 mV, respectively.

Table 5.6 Summary of the particle size distribution of the two degrees of fibrillated MFC used in Paper IV, determined by microtrac (see *4.7.5.2 Laser diffraction*). The subscripts 10, 50 and 90 indicate that x vol% of the particles are smaller than the value stated.

Degree of fibrillation	D_{10} [μm]	D_{50} [μm]	D_{90} [μm]
Low	6.58	34.30	137.7
High	6.26	20.37	64.08

Their respective morphologies, seen in Figure 5.7, show similarities with TEMPO-MFC, i.e. a wide size distribution of fibrils and fibril bundles.

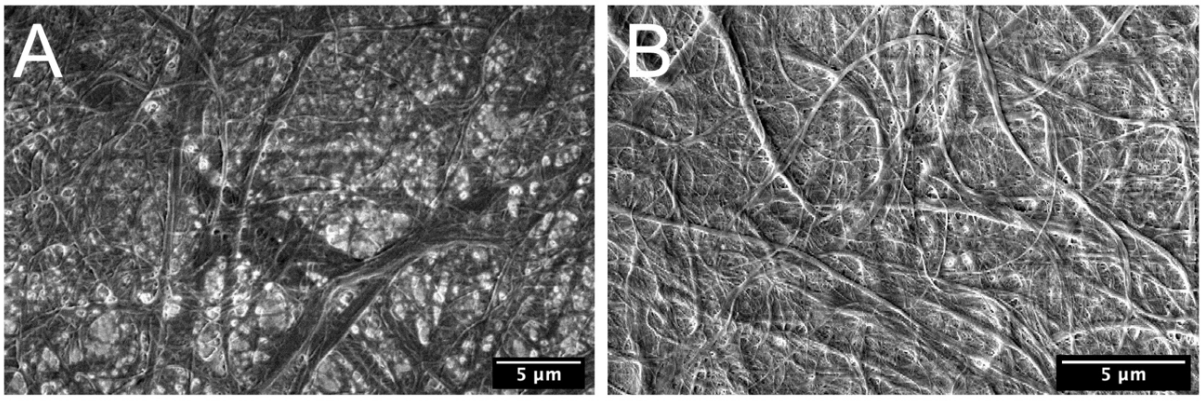

Figure 5.7 SEM micrographs of MFC with a low (A) and high (B) degree of fibrillation.

5.2.1. Electro-assisted filtration of microfibrillated cellulose

Figure 5.8 compares the dewatering of TEMPO-MFC and commercially-available MFC carried out with an applied pressure of 3 bar and varying levels of electric field (0-32 V/cm). Even though no direct comparison can be made between the two, as the experiments were performed at varying electric field strengths and filter media with different pore size (0.1 vs. 0.45 µm), it is evident that the use of electro-assisted filtration greatly improves dewatering compared to conventional filtration (black lines). It can also be observed that the dewatering rate is proportional to the electric field strength, as predicted by the Helmholtz-Smoluchowski equation and reported in a multitude of studies, e.g. [7, 8]. Furthermore, the two types of MFC present different dewatering profiles: that of commercially-available MFC resembles a classical filtration process, with a declining filtrate flux over time, whilst TEMPO-MFC reaches a plateau and remains rather constant. This is discussed further in *5.2.1.1 A comparison of the two types of microfibrillated cellulose used.*

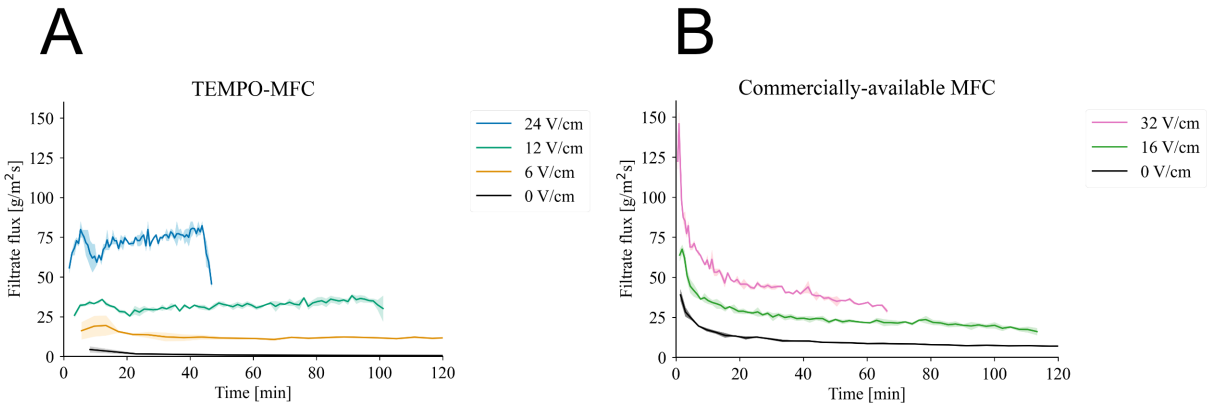

Figure 5.8 Filtrate flux during the electro-assisted filtration of (A) TEMPO-MFC and (B) commercially-available MFC (low degree of fibrillation) at 3.0 bar and applying electric fields of varying strength. Shaded areas show the standard deviation.

The average dry content of the filter cakes after dewatering reaches its highest when pressure and electric field are combined. The highest average dry content between the electrodes that could be achieved was approx. 8.5% (TEMPO-MFC 3 bar and 24 V/cm), i.e. >85% of the water could be removed whilst requiring much less energy than for thermal drying (Figure 5.9). It should be emphasised that, locally, the dry content is higher. In the case of TEMPO-MFC, the material aggregated onto the anode, thereby achieving the highest dry contents in this region, whereas in the case of commercial MFC, the greatest dry contents were achieved closest to the cathode (i.e. at the bottom of the filter cell). As the electrophoretic movement of the MFC is dependent on the zeta potential, it is not surprising that the TEMPO-MFC has the higher dry content at the anode.

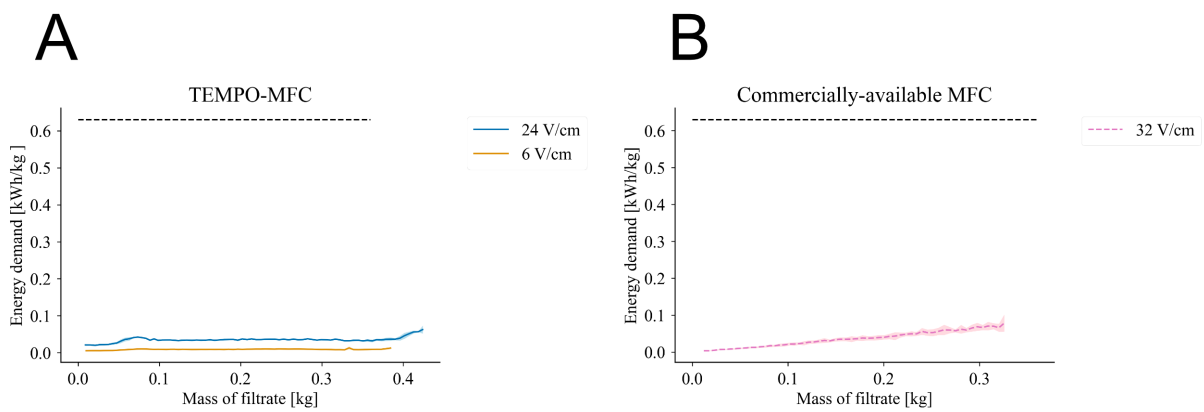

Figure 5.9 Energy demand required [kWh/kg water] for electro-assisted filtration at 3 bar for (A) TEMPO-MFC, using 6 and 24 V/cm, and (B) MFC (high degree of fibrillation), using 32 V/cm. The dashed black lines show the energy needed to evaporate water at atmospheric pressure.

When conventional filtration is employed, the filtration resistance is excessive, partly due to the probable formation of a skin that is highly resistant to flow. This effect was especially pronounced for the TEMPO-MFC: after 24 hours of conventional filtration, the filter cake formed was only millimetre-thick. However, when electro-assisted filtration was used, it appeared to perturb the formation of the thin particulate layer. This is deemed as being one factor of particular importance to the improved dewatering, and is likely due to electrophoresis, which not only prevents the formation of the skin but also influences the resulting structure of the filter cake. This may have influenced dewatering, as this structure has a high over-all permeability; it is discussed further in *5.2.3 On the structure of filter cakes*

In addition, ohmic heating causes an increase in the temperature between the electrodes. The temperature rise was rather minor, especially at the lower electric field strengths (< 3°C), and did not result in any formation of char, even at the higher electric field strengths evaluated. Even though the temperature was rather low, it still affected the liquid viscosity, which can be calculated using Eq. 15 [113]. If the temperature rises from 20 to 35 °C, it results in an almost 30% reduction in the viscosity of the liquid, and hence a corresponding increase in the filtrate flux, if all other conditions are constant.

$$\mu = 2.414 * 10^{-5} * 10^{247.8/(T-140)} \qquad (15)$$

Electrolysis reactions occurred at the respective electrodes, thereby causing the filtrate to be alkaline, whilst the average pH of the filter cake was acidic. The pH of the filtrate rose rapidly, indicating that the electrolysis reactions are swift. The impact of pH on the surface charge of the commercially-available MFC is shown in Figure 5.10, where a decrease in pH is seen to cause a reduction in the surface charge due to protonation of the carboxyl groups: similar trends are

expected for TEMPO-MFC. It should be noted here that, below a pH of 3, the surface charge was too low for measurements to be made using polyelectrolyte titration.

A reduction in the surface charge would mean that the electrostatic repulsion between the particles is reduced, and attractive forces may instead lead to the formation of particle agglomerates that could, in turn, benefit dewatering, as demonstrated by e.g. Fall *et al.* [90]. Moreover, a reduction in the surface charge also means that the electric field has less impact.

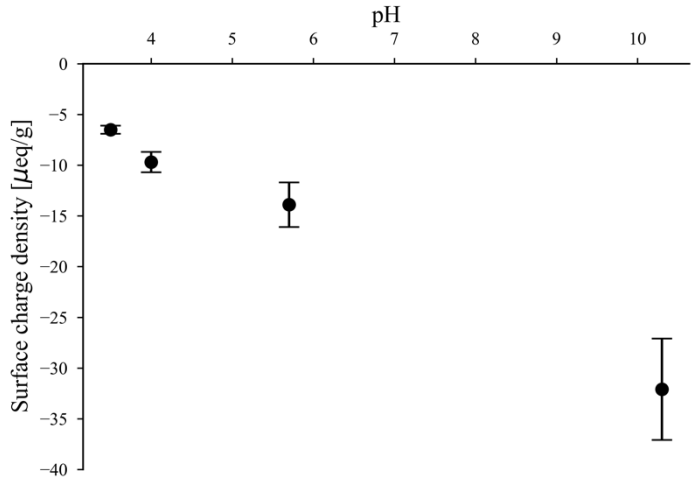

Figure 5.10 Surface charge density of MFC with a low degree of fibrillation, measured by polyelectrolyte titration and as a function of pH.

5.2.1.1. A comparison of the two types of microfibrillated cellulose used

A couple of noteworthy observations can be made from Figure 5.8, namely:

I. The influence of the electric field differs

TEMPO-MFC has a stronger response to the electric field and results in a higher filtrate flux, despite a tighter filter medium (0.1 vs. 0.45 µm) and a lower electric field strength being used than for commercial MFC (24 V/cm vs. 32 V/cm). This illustrates the great importance of surface charge (effect of chemical pre-treatment) on the electro-assisted filtration.

II. The dewatering profiles display different trends

The dewatering rate of TEMPO-MFC reaches a plateau and remains approximately constant, whereas the dewatering profile of commercial MFC is similar to that of conventional filtration, where the filtrate flux declines with time, and is associated with the build-up of a filter cake.

A possible explanation for the different dewatering profiles is probably related to the formation of two different filter cake structures (Figure 5.11). In the case of TEMPO-

MFC, the filter cake has a clearly pronounced channelled structure, with pillars of TEMPO-MFC in the direction of the electric field. Its more or less constant dewatering rate favours the hypothesis that it is the pillars of TEMPO-MFC that grow as dewatering proceeds rather than forming a traditional filter cake, i.e. the membrane area available is basically constant throughout the filtration process.

In the case of the commercially-available MFC, the filter cake has some indications of a channelled structure, but not as pronounced as for TEMPO-MFC. Furthermore, as the dewatering rate does not remain constant throughout dewatering, it is likelier that a more traditional filter cake build-up occurs. Although it is plausible that the discrepancy between the two filter cake structures and their respective formation is related to the lower surface charge (no introduction of carboxylate groups) of the commercial MFC, other explanations should not be excluded at this point.

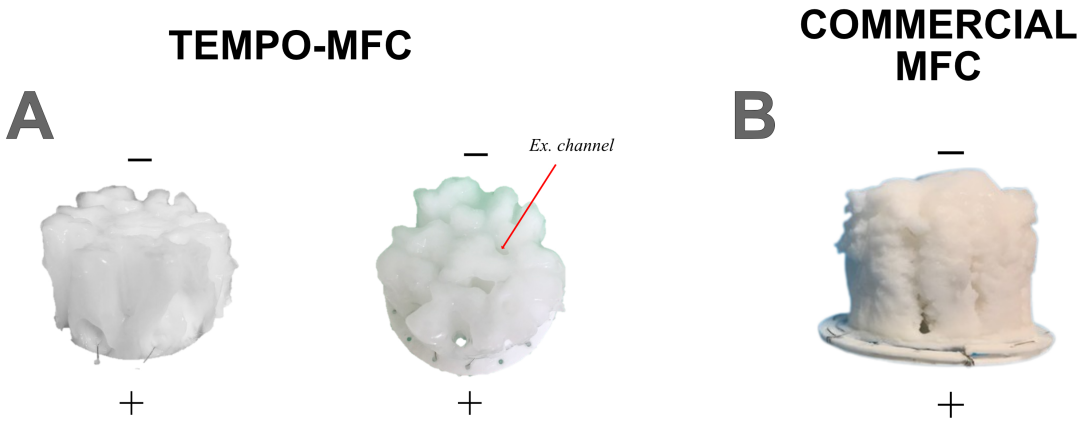

Figure 5.11 Images of filter cake structures resulting from electro-assisted filtration at 3 bar and 12 V/cm for TEMPO-MFC (A) and 16 V/cm for MFC (B). Anode (+) and cathode (−) are labelled. The red arrow in (A) shows a typical flow channel.

5.2.2. Dewatering mechanism

MD simulations were used to study the dewatering mechanism on the molecular level in order to gain deeper knowledge of the dewatering mechanism involved in the electro-assisted dewatering of TEMPO-MFC. TEMPO-oxidised cellulose microfibrils were modelled as oligomers according to Figure 5.12 and are hereafter referred to as TOC. These were comprised of 11 glucose units with each alternate hydroxymethyl group being replaced by a carboxylate group. The simulations were performed in cooperation with Dr Nabin Karna; a comprehensive description of the simulations can be found in Paper II.

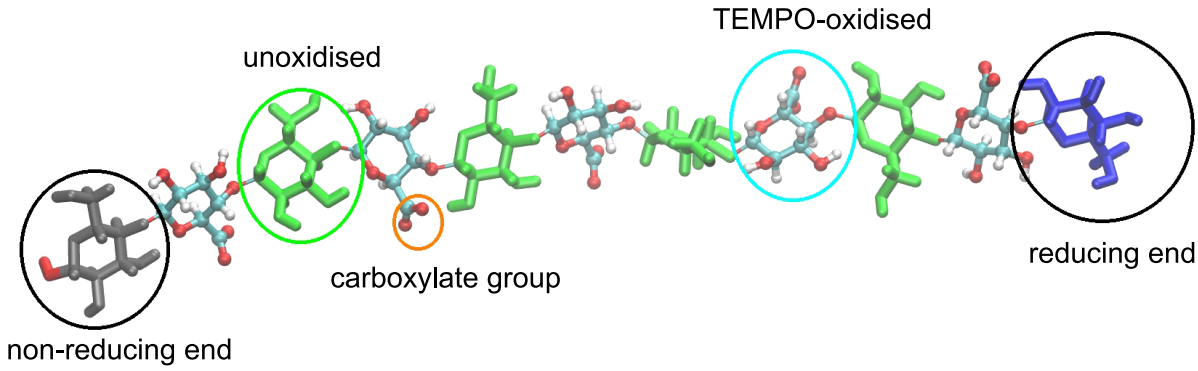

Figure 5.12 Model of TOC, where each alternate hydroxymethyl group is replaced by a carboxylate group.

The pressure and/or electric field were studied in terms of:

- Effect on the movement of TOC
- Effect on the interfibrillar water
- Simultaneous effect of both the TOC movement and flow of water molecules

The focus of this thesis is on the two latter.

5.2.2.1. Effect on interfibrillar water

An electric field affects the solid particles in the system as well as the water molecules. Water is not only present as a bulk of free water molecules but also trapped between cellulose microfibrils and adsorbed or chemically-bound water. The latter is not of interest here since this water cannot be removed through filtration techniques. The effect of pressure and/or electric field on the interfibrillar water was, however, studied using the simulation set-up depicted in Figure 5.13A.

The resulting velocity profiles between two TOC slabs are seen in Figure 5.13B. They display a plug-flow profile when the effect of electric field alone is studied (unfilled circles), which is characteristic of electro-osmotic flow [114], and a traditional parabolic shape when the effect of pressure is included (red and blue circles), as described by the Hagen-Poiseuille equation[7]. The maximum velocity is achieved when a pressure effect of 20 bar and electric field of 0.5 V/nm is investigated: this velocity is 360% higher than that observed for a pressure effect of 20 bar alone, but only 14% greater than that of 0.5 V/nm alone. It illustrates that, under the conditions examined, the electric field plays the most important role in releasing the water from the space between the TOC.

[7] $-\frac{dP}{dx} = \frac{32\mu v}{D^2}$

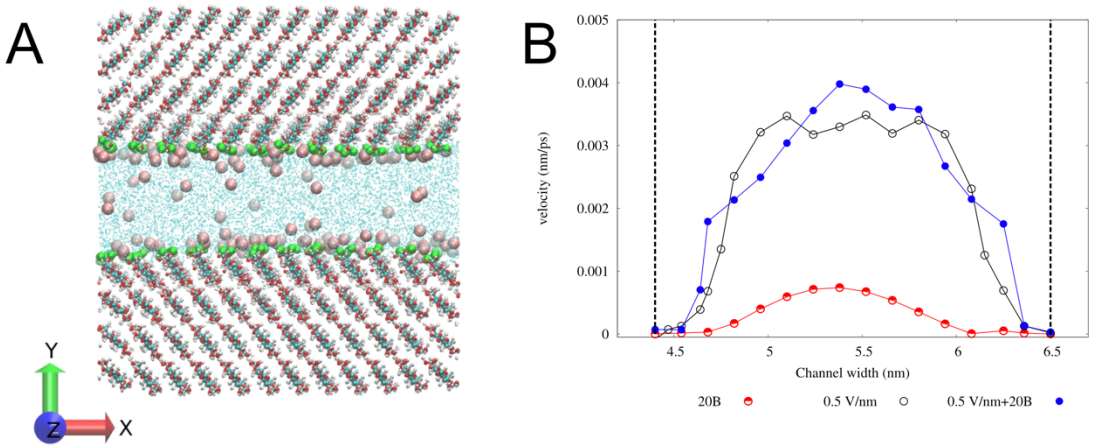

Figure 5.13 (A) Set-up used to study the flow of water trapped between the fibrils; simulated pressure effect and/or electric field are applied in the positive x-direction. (B) Velocity profiles of the water molecules trapped between the TOC fibrils. 20B corresponds to a simulated pressure effect of 20 bar.

5.2.2.2. Simultaneous effect on the movement of TOC and flow of water molecules

The simulation set-up described in Figure 5.14 was used to study the simultaneous effect on the flow of water molecules and TOC movement. For the convenience of computational cost, the simulation set-up replicates a microscopic part of the electro-assisted filter cell and is uses a time span of mere nanoseconds. In addition, the effect of the electrolysis reactions was not included: neither interlockings nor friction between the TOC fibrils.

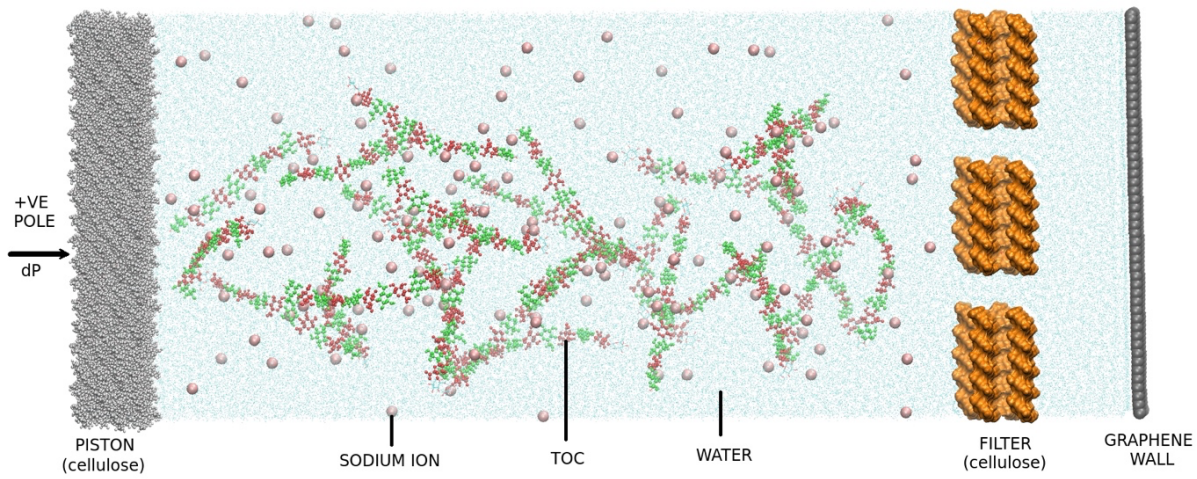

Figure 5.14 Schematic diagram of the set up considered for studying the electro-assisted dead-end filtration. Pink spheres: sodium ions. Blue spheres: water molecules. Uncharged cellulose walls represent the piston and filter medium. A graphene wall, imposed on the filter end to prevent water molecules from escaping, applies a negative pressure to the system.

Figure 5.15A illustrates the flow of water molecules/ns for two levels investigated of the pressure effect of 10 and 20 bar (10B, 20B) and/or electric field strengths of 0.5 and 1 V/nm. The results

presented concur with the insights gained from the experimental work as they illustrate that pressure alone is not sufficient to achieve efficient dewatering, although it is the combination of pressure and electric field that yields the highest rate of dewatering. Increasing the electric field strength increases the dewatering rate.

These simulations also show how the COM distance changes with time (Figure 5.15B): as the strength of the electric field increases, the velocity of the TOC oligomers towards the anode increases. As well as preventing a skin from forming on the filter membrane, this movement also leads to the release of water molecules that were previously trapped between the TOC oligomers; this bulk of free water can then be expelled by the additional pressure exerted.

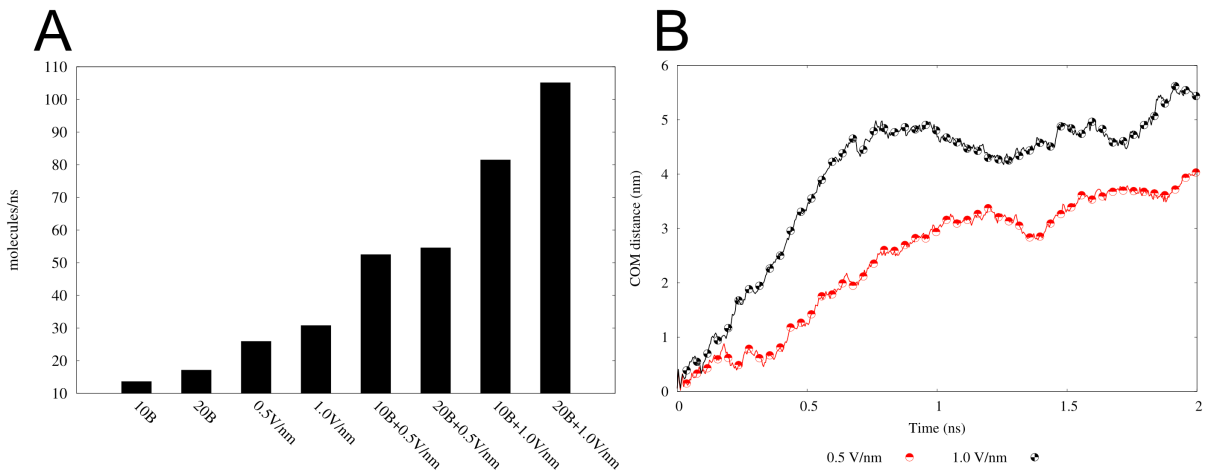

Figure 5.15 (A) Dewatering rate after 0.5 ns of simulation. (B) COM distance vs. time for electro-assisted filtration simulation with an applied pressure effect of 20 bar and an electric field of 0.5 V/nm (red) and 1 V/nm (black).

5.2.3. On the structure of filter cakes

Electro-assisted filtration of the TEMPO-MFC resulted in a filter cake with an interesting structure (Figure 5.11A) that has not previously been reported for either MCC [8] or CNC [9]. The hypothesis suggested in Paper II (illustrated in Figure 5.16) was that the TEMPO-MFC assembled in the direction of the electric field, which was uneven owing to the design of the anode mesh (see insert Figure 5.16), and resulted in the formation of pillars. Furthermore, as the liquid flows through the square openings of the anode mesh, it combines with the opposing electrophoretic force and thereby stabilises the channelled structure. There was, however, uncertainty as to whether or not the TEMPO-MFC was aligned in the direction of the electric field, so this was investigated in Paper III.

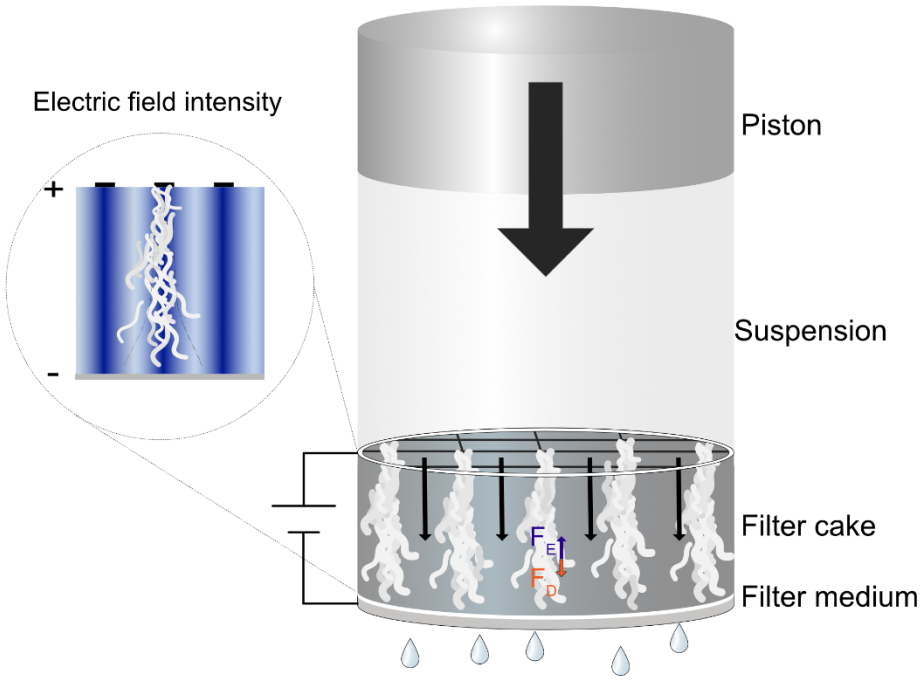

Figure 5.16 The mechanism suggested for the formation of the channelled filter cake structure. The thin black arrows represent liquid flow through some of the square openings of the anode mesh. Blue arrow (F_E): electrophoretic force. Orange arrow (F_D): force due to applied pressure. Insert: close-up of the part of the filter cell between the electrode, seen from the front. The gradient shows the intensity of the electric field, where a darker colour represents a higher intensity.

The alignment of fibrillated cellulose in the presence of an external electric field has been proven in several experimental [115–119] and simulation [120] studies already, mostly using alternating current (AC). It was therefore deemed plausible that the cellulose microfibrils have also aligned in the direction of the electric field during electro-assisted filtration (DC). It should, however, be emphasised that the mechanism responsible for the alignment of the cellulose fibrils in an AC electric field may differ to that in a DC field, but this was not explored.

Visual observations of the structures obtained with an electric field alone (Figure 5.17A) and using a combination of electric field and pressure (Figure 5.18A) show clear signs of the cellulose microfibrils aligning in the direction of the electric field. The micrographs display the preferred orientation in the electric field alone (Figure 5.17B), but this is not as clear in the case of electro-assisted filtration (Figure 5.18B). The overall impression nevertheless is that the microfibrils have a preferred orientation in the filter cake.

Interestingly enough, the structure obtained when electro-osmotic dewatering is applied to MFC is completely different from that displayed when dewatering CNC [9], where the resulting structure lacked channels. It should, however, be noted that the morphology and surface charge differ significantly between CNC and MFC, which give rise to different packing. Where the discrepancies found between the experimental conditions of these studies are concerned, the

suspension used when studying CNC had a higher solids content and a higher dry content was achieved. Moreover, the residence time between the two studies also differed, which could also have been significant.

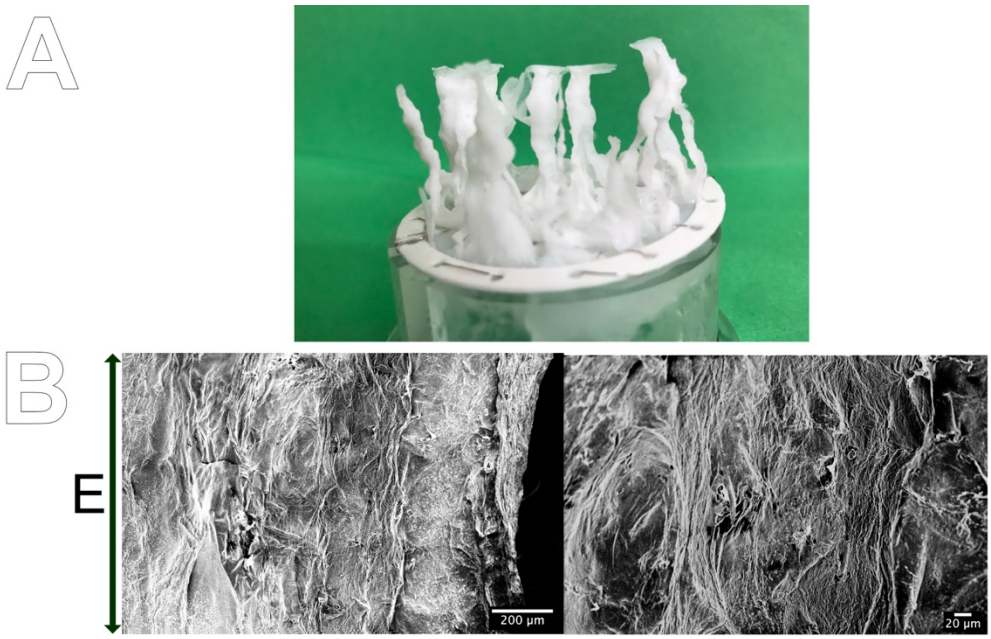

Figure 5.17 (A) Structures obtained from the electro-osmotic dewatering of TEMPO-MFC at 24 V/cm; SEM micrographs at different magnifications. (B) Scale bars, from left to right: 200 and 20 µm.

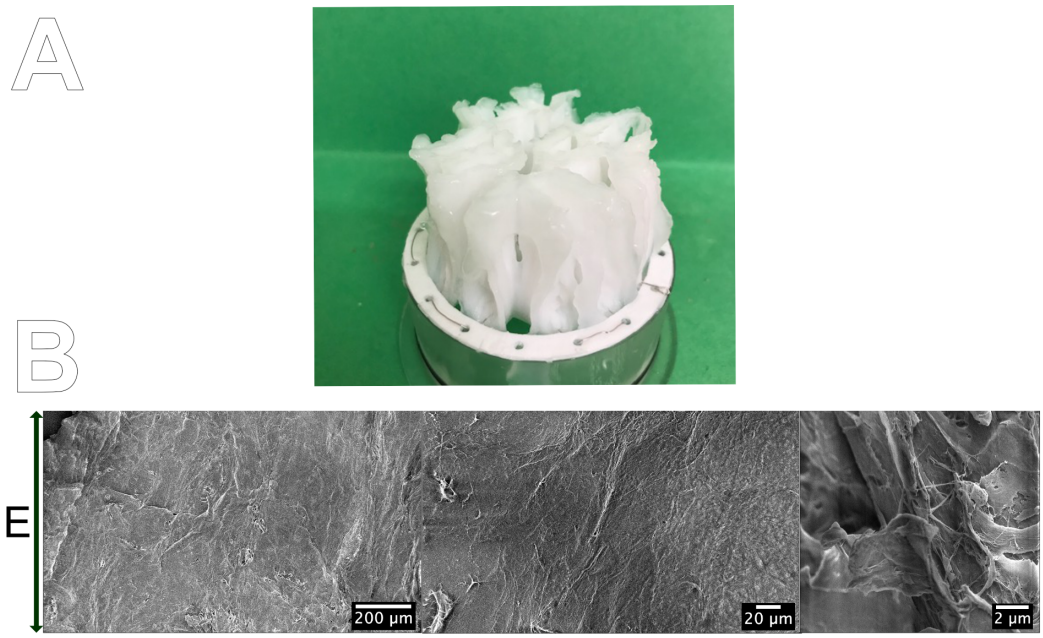

Figure 5.18 (A) Filter cake structures obtained after the electro-assisted filtration of TEMPO-MFC at 3 bar and 24 V/cm; SEM micrographs at different magnifications. (B) Scale bars, from left to right: 200, 20 and 2 µm.

The orientation index, f_c, shown in Table 5.7 was calculated from the azimuthally integrated WAXS data using Eq. 13 and ranged between 0.49-0.57, indicating only a partially preferred orientation. Compared to values reported previously in the literature, these might appear low: Mittal *et al.* [121], for example, studied the flow-alignment of TEMPO-oxidised CNF (3 g/L) into filaments and reported orientation indexes between 0.83 and 0.92. It is, nevertheless, important to recognise the difference in terms of experimental set-up and sample preparation: in the present study, the cellulose concentration is much higher and the flow rate much lower. This, in turn, means that the TEMPO-MFC is unable to orientate fully because it is hindered by entanglements, interlockings and the suchlike. It is therefore not surprising that the resulting f_c is lower.

Table 5.7 Orientation index, f_c, calculated from azimuthal integrated WAXS data using Eq. 13.

	24 V/cm	3 bar 6 V/cm	3 bar 24 V/cm
f_c	0.51 ± 0.05	0.49 ± 0.03	0.57 ± 0.04

The cellulose microfibrils in filter cakes thus appear to have a preferred orientation on the microscopic scale (SEM), but only a partially preferred orientation on the molecular scale (WAXS). This is plausibly related to the high particle concentration that prevails, which makes it impossible for the fibrils to align perfectly since bent fibrils and entanglements may be present.

5.2.4. Impact of the degree of fibrillation

The degree of mechanical fibrillation is one important factor pertaining to the quality of MFC. It affects the production process not only by increasing the energy demand needed for the mechanical separation of fibrils but also in terms of dewatering. A more fibrillated material will have a larger surface area and thus be subjected to more drag, and a higher filtration resistance is therefore anticipated. The impact of an electric field is, however, expected to increase with increasing degree of fibrillation, since it will result in a higher number of surface charges being exposed. It would thus be of certain importance to investigate the combined effect of pressure and electric field.

5.2.4.1. The effect of pressure alone

Conventional filtration resulted in rather low initial filtrate fluxes (Figure 5.19), which indicate the formation of a thin filter cake with a high filtration resistance. The difference between the two degrees of fibrillation is clear: a more fibrillated MFC is more challenging to dewater (Table 5.8), which concurs with the prediction based on the surface properties.

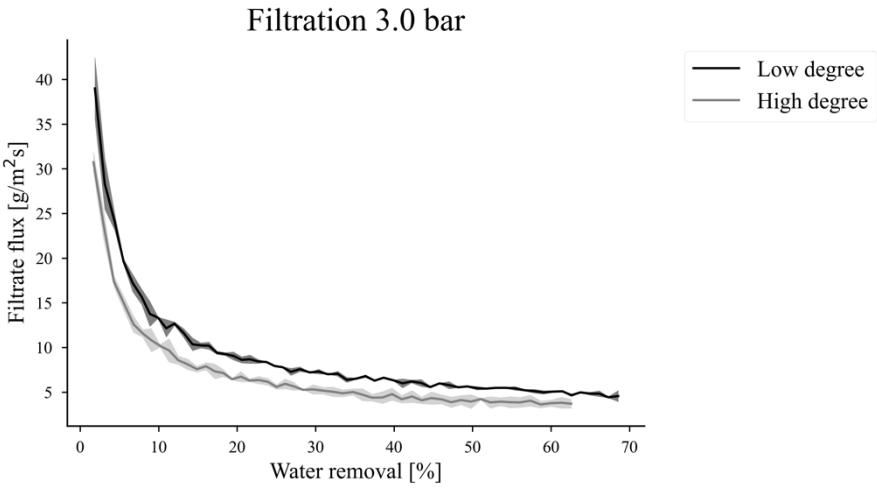

Figure 5.19 Filtrate flux vs. water removal. Shaded areas: standard deviations from duplicate measurements.

The impact of applied pressure was also evaluated, and the average filtration resistance calculated (Eq. 5). From Table 5.8, it can be noted that an increasing applied pressure results in a higher average filtration resistance, which is a typical behaviour of compressible materials [122]. It is therefore uncertain that, despite the higher driving force (ΔP), an increased applied pressure results in an improved dewatering rate, which is evidenced in Figure 5.20 (1.7 and 3 bar).

Table 5.8 Average filtration resistance (determined from Eq. 5) including standard deviations from duplicate measurements. No standard deviation is given for single measurements.

	α_{av} *10^{-13} [m/kg]	
ΔP [bar]	*High degree of fibrillation*	*Low degree of fibrillation*
0.3	0.37 ± 0.12	0.27 ± 0.01
1.7	1.96	1.12
3.0	2.95 ± 0.83	2.05 ± 0.06

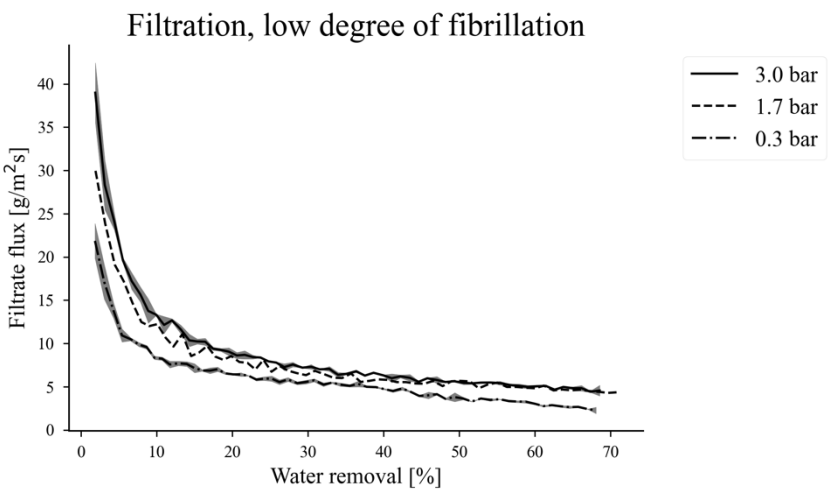

Figure 5.20 Filtrate flux vs. water removal of MFC with a low degree of fibrillation, at applied pressures of 0.3, 1.7 and 3.0 bar.

5.2.4.2. The effect of electric field alone

Figure 5.21 presents the filtrate flux for electro-osmotic dewatering, i.e. an applied electric field alone. There is a slight difference between the two degrees of fibrillation, where the higher degree of fibrillation, with the highest surface charge, displays a somewhat higher filtrate flux; this, too, is in line with what would be expected. It is, nevertheless, clear that an electric field alone was not enough to provide sufficient dewatering.

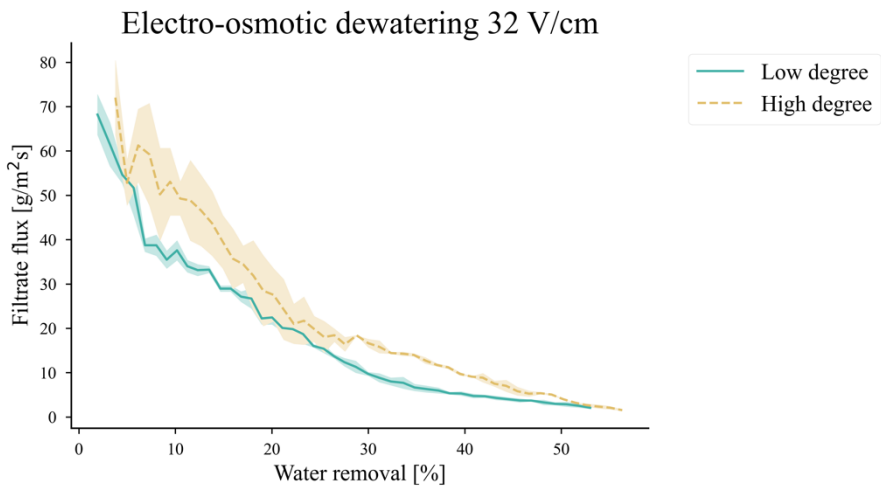

Figure 5.21 Filtrate flux vs. water removal. Shaded areas: standard deviations from duplicate measurements. The legend gives the degree of mechanical fibrillation.

5.2.4.3. The effect of pressure and electric field

The resulting filtrate flux was improved significantly when pressure and electric field were combined, Figure 5.22. In contrast to the observations made when either pressure (Figure 5.19) or electric field (Figure 5.21) were applied alone, no difference could now be noted between the two degrees of fibrillation. It is evident that, when an electric field and pressure are combined, they balance each other out.

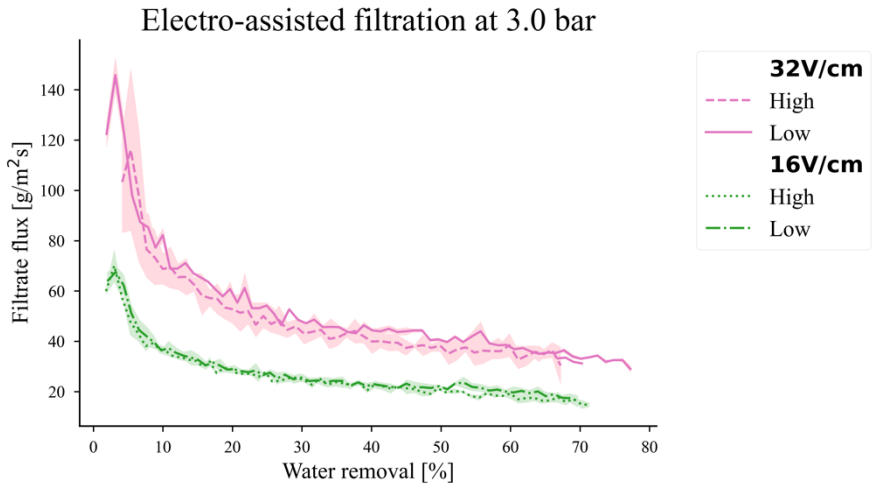

Figure 5.22 Filtrate flux vs. water removal. Shaded areas: standard deviations from duplicate measurements. The legend shows the degree of mechanical fibrillation.

5.2.5. Quality after dewatering

The results presented in Section *5.2 IMPACT OF ELECTRIC FIELD* have proven electro-assisted filtration to be an efficient method for improving the dewatering of microfibrillated cellulose, but the results do not identify the impact it makes on the quality of the product. Dewatering fibrillated cellulose is accompanied by a possible risk of partial "irreversible" aggregation occurring: this would cause a reduction in the surface area available and thereby a loss of valuable properties. The impact of the WRV and rheology of the MFC after dewatering were therefore assessed, since these properties are important for future applications of MFC (e.g. as a rheology modifier).

WRV before and after dewatering is displayed in Figure 5.23 along with the average dry content of the filter cake (height: 25 mm). The decrease in WRV seen after dewatering appeared to be slightly related to an increased dry content of the filter cake (NB: all WRV measurements were conducted at a dry content of 0.3 wt%). A reduction of the WRV indicates that the properties of MFC were affected by dewatering, even though rather modest dry contents were achieved. It is, however, important to remember that the dry content is not uniform and that, locally, it can be higher than those reported in Figure 5.23.

The reduction observed in WRV can be related to a lower accessible surface area as well as a lesser number of accessible hydroxyl groups. These results are in line with the findings reported by Ding *et al.* [93]: they studied the effect of nanocellulose fibre hornification and hydroxyl accessibility during dehydration, and found that a reduction in accessible hydroxyl groups can be observed already at a dry content of 8.2%, and was severely reduced at dry contents >20%.

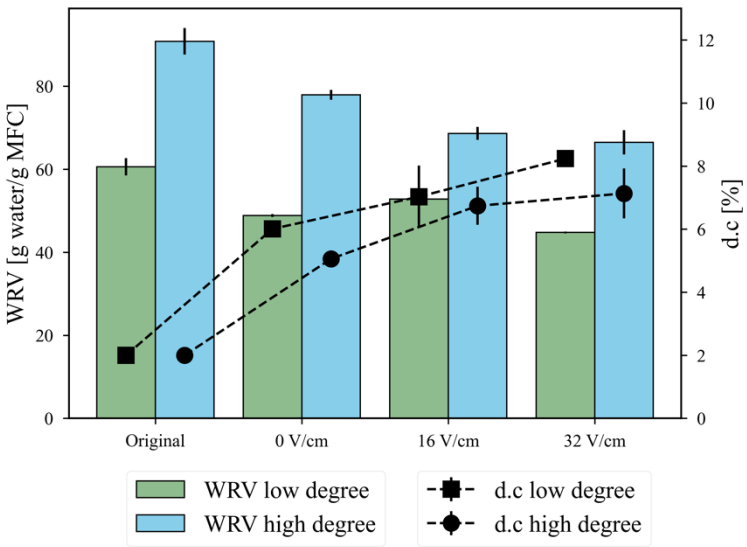

Figure 5.23 WRV (bars) and average dry content (squares and circles) of both degrees of fibrillation. WRV was measured for the original suspension as well as after dewatering at 3 bar and different strengths of electric field.

The MFC still exhibits shear-thinning behaviour after dewatering (Figure 5.24A). This is typical of MFC and is related to the structuring and alignment of the fibrils in the shear direction [123], which causes a reduction in viscosity as the shear rate increases. At the concentration investigated, 0.4 wt%, all MFC samples behave as a gel (G'>G") in the LVE-region, see Figure 5.24B, albeit the reduction in G' and G" observed after dewatering indicates a weaker gel. Also, the yield stress, determined from a 10% reduction in the storage modulus (G') in the amplitude sweep measurements [106] tabulated in Table 5.9, suggests a weaker network after conventional filtration, and especially so after electro-assisted filtration. This means that less stress is necessary to deform the network structure.

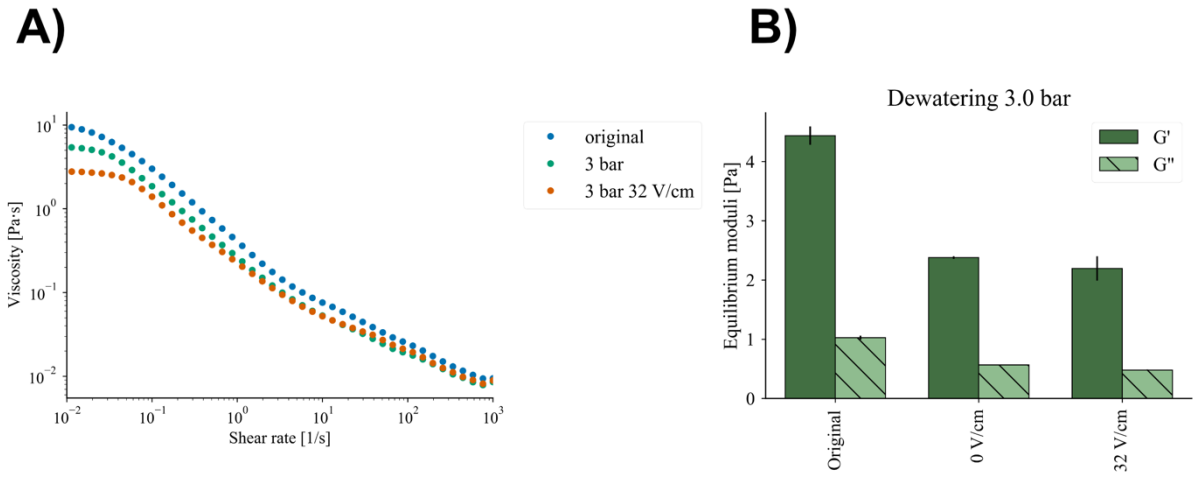

Figure 5.24 Rheology measurements of MFC with a lower degree of fibrillation, before and after dewatering: (A) flow-sweep profile and (B) equilibrium storage and loss moduli. Dark green bars: storage modulus (G'), hatched green bars: loss modulus (G").

Table 5.9 Yield stress of the original suspension and after dewatering, using either 3.0 bar or 3.0 bar and 32 V/cm. The MFC had a lower degree of fibrillation.

	Original	3.0 bar	3.0 bar 32 V/cm
Yield stress [Pa]	0.079 ± 0.005	0.054 ± 0.001	0.046 ± 0.002

The general conclusions drawn from the quality analysis after dewatering pertain to the slight reduction in WRV and network strength, the full reason for which remains to be uncovered. One hypothesis is related to the partial aggregation and/or reshaping/collapse of the MFC bundles after dewatering and the consequential reduction in available surface area. It therefore becomes important to explore the re-dispersion of the dewatered material to assess the recovery of available surface area. In the present study, re-dispersion was achieved using an IKA Ultra-Turrax ® T50 operating at 10 000 rpm, but alternative methods may have the potential for rendering a more efficient recovery of the available surface area. Nevertheless, it is important to bear in mind that there will always be a trade-off between the costs of transportation and re-dispersion.

The extent to which the properties of a material impact on the future performance of products is not obvious, as it is highly dependent on their final function. Potential applications include, for example, the use of MFC in a composite, in which case the final properties of the product are not necessarily only dependent on the properties of the MFC but also on those of the additional ingredient(s). This combined effect remains to be evaluated. Furthermore, the rheological features of MFC can be tailored by size fractionation [105] or tuning the chemical environment [124], which has the potential of being used to re-gain important features.

6

CONCLUDING REMARKS

The aim of the work compiled in this thesis is to extend current knowledge of the filtration of micro/nanocelluloses, since this is an essential component in reducing the total cost of producing these materials and thus in increasing their commercial attractiveness. Although the three micro/nanocelluloses used had inherently different characteristics (e.g. morphology and surface charge), it can be concluded that there are similarities in terms of excessive filtration resistance that can, in part, be attributed to the formation of a dense initial layer of particles, a "skin", closest to the filter medium if no modifications are made. The filter cakes formed are compressible in nature, i.e. the solidosity, and thus the filtration resistance, is not constant throughout.

The importance of electrostatic interactions between MCC particles during dead-end filtration was illustrated in Paper I by altering the ionic concentration by between 0.1 and 1 g/L NaCl. Without the addition of ions, a "skin" with a high flow resistance was formed, but this was perturbed by the addition of ions. The sodium ions shielded the negative surface charges of the MCC particles and promoted agglomeration, as evidenced by measuring the size of the agglomerates/particles using an FBRM. This, in turn, lead to a reduction of the total filtration resistance: this was most likely due to a combination of the absence of a "skin" and the smaller total surface area of the agglomerates that were formed, compared to the single particles. Increasing the ionic concentration reduced the average as well as the local filtration resistance.

The filtration of TEMPO-MFC (Papers II and III) and commercially-available MFC (Paper IV) was improved significantly when electro-assisted filtration was employed: the dewatering rate increased and up to 85% of the water could be removed, whilst requiring considerably less energy than for thermal drying. Electro-assisted filtration of TEMPO-MFC was studied through experiments in combination with MD simulations to reveal further details of the dewatering mechanism. The MD simulations suggested that, apart from the electroosmotic flow of water, the improved dewatering could be attributed to electrophoresis of the negatively charged MFC towards the anode leaving behind water that had previously been trapped; this water could now be pressed out by the pressure applied.

In addition, instead of a conventional filter cake, a channelled structure with high overall permeability was discovered in the experimental work. Such a structure provided high overall permeability and could therefore also have been part of the reason behind the higher dewatering rate. The cellulose microfibrils appeared to assemble in pillars in the direction of the electric field to form the channelled structure of the filter cake. This was evaluated further and the preferred orientation of the cellulose microfibrils in the filter cake on the microscale was observed using SEM. Only partial preferred orientation could be seen on a molecular scale using WAXS, plausibly due to the presence of bent fibrils and/or entanglements, which resulted in deviation from perfect alignment.

The impact of the degree of mechanical fibrillation is an important process parameter when producing MFC. It affects the characteristics of the product (e.g. surface area and surface charge density) and thereby dewatering; this was studied using a commercially-available MFC in Paper IV. When pressure alone was applied, a more fibrillated material showed greater filtration resistance because a higher surface area was subjected to the liquid flow and, hence, there was more drag. The application of an electric field alone showed the opposite: a more fibrillated MFC has a higher surface charge density and therefore the electric field has a greater effect. However, when a combination of pressure and electric field was used, no significant difference could be noticed between the two degrees of fibrillation. In contrast to TEMPO-MFC, the filter cakes did not have a pronounced channelled character.

It is important to know how dewatering affects valuable product characteristics, which is the reason for analysing water retention and rheology: a moderate reduction in the water retention value and rheological features (yield stress, storage and loss moduli) after electro-assisted filtration indicated a weakened network strength. This may be attributed to a reduction of the total surface area that is probably due to the aggregation of the microfibrils and/or the reshaping of the microfibrils/fibril bundles.

7

FUTURE WORK

"All research falls into one of the three following: difficult, boring or already done"

Xiaohui Song

Dewatering micro/nanocelluloses is difficult, yet it is crucial that this unit operation functions efficiently for large-scale production to be successful. This thesis has explored the dewatering of micro/nanocelluloses via modification of the suspension's ionic concentration as well as using electro-assisted filtration. It is not the first thesis on the dewatering of micro/nanocellulose and it will most likely not be the last: several possible routes remain to be explored further, especially with respect to electro-assisted filtration.

Electro-assisted filtration has been demonstrated to improve the dewatering of MFC, both TEMPO-MFC and commercially-available MFC. Although the dewatering of both was enhanced through the assistance of an electric field, their respective dewatering profiles differed owing to the diverse characteristics of the MFC in question. This implies the need for further studies of other qualities of MFC or even CNF, e.g. degree of oxidation, another chemical pre-treatment (such as carboxymethylation) and the presence of hemicellulose as well as lignin.

The formation of the channelled filter cake structures would also be of interest to study further, for example using *in-situ* monitoring techniques employing tomography and/or SAXS/WAXS. From a material perspective, it would also be interesting to discover whether these channelled structures could serve a wider purpose in material applications, because aligned material infers superior strength and stiffness [125].

It is also vital to investigate just how dewatering affects MFC, and the effects on both the water retention value and rheology were therefore assessed after dewatering. Further evaluation is nevertheless required in order to reveal the full reason as to why these properties were affected and whether or not they could be restored after dewatering by other suitable methods of dispersion. The extent to which this change in properties could affect potential future applications should also be assessed. In addition, it would be of interest to study if there is a way of mitigating the hypothesised reduction of available surface area of the microfibrils whilst promoting dewatering and still maintaining the low energy demand (i.e. limiting the ionic strength [7]).

Finally, all experiments in this work have been performed on a lab scale, which means that one inevitable question remains: the matter of scale-up. Prior to scaling up, several concerns raised in this thesis should be addressed:

- *Aggregation of material onto the anode*
  After electro-assisted filtration, it proved challenging to remove TEMPO-MFC from the anode, as it aggregated strongly to it. It is therefore important that the design and material of the anode are such that the filter cake can be removed easily after dewatering: vibration-assisted removal may be a viable option here.

- *Impact of electrolysis products*
  If no or minor alternation of the pH and ionic concentration of the material is allowed, the design of the filter chamber must be such that the products of the electrolysis reactions can easily be removed, e.g. via continuous flushing of the electrodes [35]. For this purpose, a design whereby the electric field is applied perpendicular, rather than parallel, to the flow may be suitable.

- *Techno-economic analysis*
  It is common praxis to make a techno-economic analysis to assess the economic performance of the process. There will for example always be a trade-off between the cost of transportation and that of water removal and potential subsequent re-dispersion.

8

ACKNOWLEDGEMENTS

This Ph.D. project has been funded by a grant from the Swedish Research Council (Vetenskapsrådet), which is gratefully acknowledged. Attendance to several conferences would not have been possible without the stipends from the following: Nils Philblad foundation, Bo Rydin foundation and Gunnar Sundblads forskningsfond.

Furthermore, support and guidance from the following people should be recognised:

- **Prof. Hans Theliander**, my main supervisor, for the immense belief in me. This time has prepared me for life as an independent researcher. As a bonus, you also seem to have liked the silly Ph.D. comics I show.

- **Assoc. Prof. Merima Hasani**, my present co-supervisor, for always having my best at interest. Your help, especially during these last months, has been invaluable!

- **Docent Tuve Mattsson**, my former co-supervisor, for the guidance and support from the sideline in the execution of the first paper.

- **Dr Nabin Karna**, for interesting talks about MD simulations, the purchase of diamonds, Harry Potter and literally everything in between.

- **Dr Polina Naidjonoka**, for guiding me through the jungle that is X-ray scattering.

- Borregaard AS, for the collaboration in Paper IV. A special thanks to **Dr Hans Henrik Øvrebø**, **Anna Vøllo Kristiansen**, **Anne Opstad** and **Anne Marie Falkenberg Olsen**.

- **Chalmers Material Laboratory (CMAL),** for the possibility of running SEM, WAXS and SAXS. In particular, the SEM assistance of **Dr Stefan Gustavsson** and **Ph.D. candidate Aina Edgren** should be recognised.

- **Ms. Maureen Sondell**, for the skilful language review of manuscripts and theses.

- **Isa Bengzon**, my amazing friend and artist, for creating the cover art of my theses.

- All colleagues from **SIKT** and **KART**, past and present, for fun conversations during coffee breaks, noon-meetings and for creating an enjoyable working environment. During the challenging spring, the exceptional help and encouragement from Dr Anders Ahlbom, as well as Ph.D. candidates Amanda Sörensen Ristinmaa, Emma Olsson Månsson and Shirin Naserifar was highly appreciated.

- Administers **Malin Larsson**, **Anna Oskarsson** and **Johanna Spång**, for making everything run smoothly.

- Research Engineer **Michael Andersson-Sarning**, as well as **Torbjörn** and **Esa** from the workshop, for all the practical help with the filtration set-up.

- All teachers, TAs (Anders Ahlbom, You Wayne Cheah and Linus Kron) and students involved in the transport phenomena course, a.k.a. **KAA060**, **KAA061**, or **KBT340**, it was truly a pleasure (OK, maybe not correction of the hundreds of exams…).

- My fellow colleagues in **the local Ph.D. council at K and Life**, for all the hours put into ensuring a high quality of time spent as a Ph.D. student at these departments.

I would also like to highlight the support from my family. A special thanks to my parents for showing by example the importance of a positive attitude – not only in academia – but more importantly, in life. My siblings Maria and Joel, for cheering me when needed (even though neither of you managed to complete the proofreading of this thesis…).

Finally, I would like to thank the person I met the very first day at Chalmers nine years ago, my husband Oscar. You have been so patient: read manuscripts, listened to me explaining problems in transport phenomena, double-checked my dilution calculations and unconditionally supported me throughout this rollercoaster of a journey.

3rd of September, Mölndal

9

REFERENCES

[1] F. Zhang, R. Shen, N. Li, X. Yang, D. Lin, Nanocellulose: An amazing nanomaterial with diverse applications in food science, Carbohydrate Polymers. 304 (2023) 120497. https://doi.org/10.1016/j.carbpol.2022.120497.

[2] A. Barhoum, V.K. Rastogi, B.K. Mahur, A. Rastogi, F.M. Abdel-Haleem, P. Samyn, Nanocelluloses as new generation materials: natural resources, structure-related properties, engineering nanostructures, and technical challenges, Materials Today Chemistry. 26 (2022) 101247. https://doi.org/10.1016/j.mtchem.2022.101247.

[3] D. Klemm, F. Kramer, S. Moritz, T. Lindström, M. Ankerfors, D. Gray, A. Dorris, Nanocelluloses: A New Family of Nature-Based Materials, Angewandte Chemie International Edition. 50 (2011) 5438–5466. https://doi.org/10.1002/anie.201001273.

[4] S. Sinquefield, P.N. Ciesielski, K. Li, D.J. Gardner, S. Ozcan, Nanocellulose Dewatering and Drying: Current State and Future Perspectives, ACS Sustainable Chem. Eng. 8 (2020) 9601–9615. https://doi.org/10.1021/acssuschemeng.0c01797.

[5] Y. Peng, D.J. Gardner, Y. Han, Drying cellulose nanofibrils: in search of a suitable method, Cellulose. 19 (2012) 91–102. https://doi.org/10.1007/s10570-011-9630-z.

[6] P. Posada, J. Velásquez-Cock, C. Gómez-Hoyos, A.M. Serpa Guerra, S.V. Lyulin, J.M. Kenny, P. Gañán, C. Castro, R. Zuluaga, Drying and redispersion of plant cellulose nanofibers for industrial applications: a review, Cellulose. 27 (2020) 10649–10670. https://doi.org/10.1007/s10570-020-03348-7.

[7] J. Wetterling, S. Jonsson, T. Mattsson, H. Theliander, The influence of ionic strength on the electroassisted filtration of microcrystalline cellulose, Industrial & Engineering Chemistry Research. 56 (2017) 12789–12798.

[8] J. Wetterling, T. Mattsson, H. Theliander, Local filtration properties of microcrystalline cellulose : Influence of an electric field, Chemical Engineering Science. 171 (2017) 368–378. https://doi.org/10.1016/j.ces.2017.05.054.
[9] J. Wetterling, K. Sahlin, T. Mattsson, G. Westman, H. Theliander, Electroosmotic dewatering of cellulose nanocrystals, Cellulose. 25 (2018) 2321–2329. https://doi.org/10.1007/s10570-018-1733-3.
[10] I. Heiskanen, K. Backfolk, A. Kotilainen, V. Gaidelis, J. Sidaravicius, Process for treating microfibrillated cellulose and microfibrillated cellulose treated according to the process, US20140088301A1, 2014. https://patents.google.com/patent/US20140088301A1/en (accessed June 3, 2021).
[11] H. Darcy, Les fontaines publiques de la ville de Dijon: Exposition et application des principes à suivre et des formules à employer dans les questions de distribution d'eau : Ouvrage terminé par un appendice relatif aux fournitures d'eau de plusieurs villes, au filtrage des eaux et à la fabrication des tuyaux de fonte, de plomb, de tôle et de bitume, Victor Dalmont, éditeur, 1856.
[12] B.F. Ruth, Studies in Filtration III. Derivation of General Filtration Equations, Ind. Eng. Chem. 27 (1935) 708–723. https://doi.org/10.1021/ie50306a024.
[13] M. Shirato, M. Sambuichi, H. Kato, T. Aragaki, Internal flow mechanism in filter cakes, AIChE Journal. 15 (1969) 405–409. https://doi.org/10.1002/aic.690150320.
[14] G.H. Meeten, A dissection method for analysing filter cakes, Chemical Engineering Science. 48 (1993) 2391–2398. https://doi.org/10.1016/0009-2509(93)81060-9.
[15] H. Saveyn, D. Curvers, L. Pel, P. De Bondt, P. Van der Meeren, In situ determination of solidosity profiles during activated sludge electrodewatering, Water Research. 40 (2006) 2135–2142. https://doi.org/10.1016/j.watres.2006.04.003.
[16] M. Shirato, T. Aragaki, K. Ichimura, N. Ootsuji, Porosity Variation in Filter Cake Under Constant-Pressure Filtration, Journal of Chemical Engineering of Japan. 4 (1971) 172–177. https://doi.org/10.1252/jcej.4.172.
[17] C. Johansson, H. Theliander, Measuring concentration and pressure profiles in deadend filtration, Filtration. 3 (2003) 114–120.
[18] F.M. Tiller, W.F. Leu, Basic data fitting in filtration, J. Chinese Institute Chemical Engineers,. 11 (1980) 61–70.
[19] W.F. Leu, Cake filtration, University of Houston, 1981.
[20] D.J. Shaw, Introduction to colloid and surface chemistry, 3. ed., Butterworth & Co Ltd, 1980.
[21] M. Stolarski, B. Fuchs, S. Bogale Kassa, C. Eichholz, H. Nirschl, Magnetic field enhanced press-filtration, Chemical Engineering Science. 61 (2006) 6395–6403. https://doi.org/10.1016/j.ces.2006.06.009.
[22] M.C. Smythe, R.J. Wakeman, The use of acoustic fields as a filtration and dewatering aid, Ultrasonics. 38 (2000) 657–661. https://doi.org/10.1016/S0041-624X(99)00147-X.
[23] A. Mahmoud, J. Olivier, J. Vaxelaire, A.F.A. Hoadley, Electrical field: A historical review of its application and contributions in wastewater sludge dewatering, Water Research. 44 (2010) 2381–2407. https://doi.org/10.1016/j.watres.2010.01.033.
[24] C. Yuan, C. Weng, Sludge dewatering by electrokinetic technique: effect of processing time and potential gradient, Advances in Environmental Research. 7 (2003) 727–732. https://doi.org/10.1016/S1093-0191(02)00030-8.

[25] M. Citeau, O. Larue, E. Vorobiev, Influence of salt, pH and polyelectrolyte on the pressure electro-dewatering of sewage sludge, Water Research. 45 (2011) 2167–2180. https://doi.org/10.1016/j.watres.2011.01.001.
[26] N.C. Lockhart, Electroosmotic dewatering of clays. I. Influence of voltage, Colloids and Surfaces. 6 (1983) 229–238. https://doi.org/10.1016/0166-6622(83)80015-8.
[27] N.C. Lockhart, Electroosmotic dewatering of clays. II. Influence of salt, acid and flocculants, Colloids and Surfaces. 6 (1983) 239–251. https://doi.org/10.1016/0166-6622(83)80016-X.
[28] G. Gözke, C. Posten, Electrofiltration of Biopolymers, Food Eng. Rev. 2 (2010) 131–146. https://doi.org/10.1007/s12393-010-9016-2.
[29] R. Hofmann, C. Posten, Improvement of dead-end filtration of biopolymers with pressure electrofiltration, Chemical Engineering Science. 58 (2003) 3847–3858. https://doi.org/10.1016/S0009-2509(03)00271-9.
[30] Y. Shen, A.R. Badireddy, A Critical Review on Electric Field-Assisted Membrane Processes: Implications for Fouling Control, Water Recovery, and Future Prospects, Membranes. 11 (2021) 820. https://doi.org/10.3390/membranes11110820.
[31] P. Geng, G. Chen, Electrically and Electrochemically Assisted Nanofiltration: A Promising Approach for Fouling Mitigation, Nanofiltration. (2018). https://doi.org/10.5772/intechopen.75819.
[32] J. Olivier, J.-B. Conrardy, A. Mahmoud, J. Vaxelaire, Electro-dewatering of wastewater sludge: An investigation of the relationship between filtrate flow rate and electric current, Water Research. 82 (2015) 66–77. https://doi.org/10.1016/j.watres.2015.04.006.
[33] M. Citeau, O. Larue, E. Vorobiev, Influence of Filter Cell Configuration and Process Parameters on the Electro-Osmotic Dewatering of Sewage Sludge, Separation Science and Technology. 47 (2012) 11–21. https://doi.org/10.1080/01496395.2011.616567.
[34] J. Desabres, M. Loginov, E. Vorobiev, Model of electrofiltration in a filter press with anode flushing, Drying Technology. 35 (2017) 1182–1194. https://doi.org/10.1080/07373937.2016.1233885.
[35] M. Citeau, M. Loginov, E. Vorobiev, Improvement of sludge electrodewatering by anode flushing, Drying Technology. 34 (2016) 307–317. https://doi.org/10.1080/07373937.2015.1052083.
[36] P. Wu, F. Zhan, Z. Wang, Q. Li, J. Li, Z. Xiong, Y. Shi, K. Pi, D. Liu, A.R. Gerson, Comparison of horizontal and vertical electric field in the treatment of river sediment by electro-dewatering, Drying Technology. 37 (2019) 770–780. https://doi.org/10.1080/07373937.2018.1460850.
[37] M. Ek, G. Gellerstedt, G. Henriksson, 2. The Trees, in: Wood Chemistry and Wood Biotechnology, De Gruyter, Inc., Berlin/Boston, Germany, 2009.
[38] S. Hestrin, M. Aschner, J. Mager, Synthesis of Cellulose by Resting Cells of Acetobacter xylinum, Nature. 159 (1947) 64–65. https://doi.org/10.1038/159064a0.
[39] C.-L. Huang, H. Lindström, R. Nakada, J. Ralston, Cell wall structure and wood properties determined by acoustics—a selective review, Holz Roh Werkst. 61 (2003) 321–335. https://doi.org/10.1007/s00107-003-0398-1.
[40] H. Meier, Chemical and morphological aspects of the fine structure of wood, Pure and Applied Chemistry. 5 (1962) 37–52. https://doi.org/10.1351/pac196205010037.

[41] T. Saito, S. Kimura, Y. Nishiyama, A. Isogai, Cellulose Nanofibers Prepared by TEMPO-Mediated Oxidation of Native Cellulose, Biomacromolecules. 8 (2007) 2485–2491. https://doi.org/10.1021/bm0703970.
[42] A.N. Fernandes, L.H. Thomas, C.M. Altaner, P. Callow, V.T. Forsyth, D.C. Apperley, C.J. Kennedy, M.C. Jarvis, Nanostructure of cellulose microfibrils in spruce wood, PNAS. 108 (2011) E1195–E1203. https://doi.org/10.1073/pnas.1108942108.
[43] T. Dumitrică, Intrinsic twist in Iβ cellulose microfibrils by tight-binding objective boundary calculations, Carbohydrate Polymers. 230 (2020) 115624. https://doi.org/10.1016/j.carbpol.2019.115624.
[44] E. Sjöström, Chapter 1 - THE STRUCTURE OF WOOD, in: E. Sjöström (Ed.), Wood Chemistry (Second Edition), Academic Press, San Diego, 1993: pp. 1–20. https://doi.org/10.1016/B978-0-08-092589-9.50005-X.
[45] R.F. Nickerson, J.A. Habrle, Cellulose Intercrystalline Structure, Ind. Eng. Chem. 39 (1947) 1507–1512. https://doi.org/10.1021/ie50455a024.
[46] B.G. Rånby, A. Banderet, L.G. Sillén, Aqueous Colloidal Solutions of Cellulose Micelles., Acta Chem. Scand. 3 (1949) 649–650. https://doi.org/10.3891/acta.chem.scand.03-0649.
[47] R.J. Moon, A. Martini, J. Nairn, J. Simonsen, J. Youngblood, Cellulose nanomaterials review: structure, properties and nanocomposites, Chemical Society Reviews. Vol. 40, No. 7 (2011): P. 3941-3994. 40 (2011) 3941–3994. https://doi.org/10.1039/c0cs00108b.
[48] F.W. Herrick, R.L. Casebier, J.K. Hamilton, K.R. Sandberg, Microfibrillated cellulose: morphology and accessibility, J. Appl. Polym. Sci.: Appl. Polym. Symp.; (United States). 37 (1983). https://www.osti.gov/biblio/5039044.
[49] A.F. Turbak, F.W. Snyder, K.R. Sandberg, Microfibrillated cellulose, a new cellulose product: properties, uses, and commercial potential, J. Appl. Polym. Sci.: Appl. Polym. Symp.; (United States). 37 (1983). https://www.osti.gov/biblio/5062478.
[50] L. Wågberg, L. Winter, L. Ödberg, T. Lindström, On the charge stoichiometry upon adsorption of a cationic polyelectrolyte on cellulosic materials, Colloids and Surfaces. 27 (1987) 163–173. https://doi.org/10.1016/0166-6622(87)80335-9.
[51] T. Lindström, L. Winter, Mikrofibrillär cellulosa som komponent vid papperstillverkning, STFI-meddelande C159, 1988.
[52] A.F. Turbak, F.W. Snyder, K.R. Sandberg, Suspensions containing microfibrillated cellulose, US4378381A, 1983. https://patents.google.com/patent/US4378381A/en (accessed March 21, 2022).
[53] M. Pääkkö, M. Ankerfors, H. Kosonen, A. Nykänen, S. Ahola, M. Österberg, J. Ruokolainen, J. Laine, P.T. Larsson, O. Ikkala, T. Lindström, Enzymatic Hydrolysis Combined with Mechanical Shearing and High-Pressure Homogenization for Nanoscale Cellulose Fibrils and Strong Gels, Biomacromolecules. 8 (2007) 1934–1941. https://doi.org/10.1021/bm061215p.
[54] T. Saito, A. Isogai, TEMPO-Mediated Oxidation of Native Cellulose. The Effect of Oxidation Conditions on Chemical and Crystal Structures of the Water-Insoluble Fractions, Biomacromolecules. 5 (2004) 1983–1989. https://doi.org/10.1021/bm0497769.
[55] ISO/TS 20477:2023 Nanotechnologies — Vocabulary for cellulose nanomaterial, (2023). https://www.iso.org/obp/ui/en/#iso:std:iso:ts:20477:ed-2:v1:en (accessed August 29, 2023).

[56] O. Nechyporchuk, M.N. Belgacem, F. Pignon, Current Progress in Rheology of Cellulose Nanofibril Suspensions, Biomacromolecules. 17 (2016) 2311–2320. https://doi.org/10.1021/acs.biomac.6b00668.
[57] J.A. Shatkin, T.H. Wegner, E.M. (Ted) Bilek, J. Cowie, Market projections of cellulose nanomaterial-enabled products- Part 1: Applications, TAPPI JOURNAL, Volume 13, Number 5, 2014; Pp. 9-16. 13 (2014) 9–16.
[58] R. Blell, I.M.N. Vold, H.H. Øvrebrø, A. Gonera, Skin care spray compositions comprising microfibrillated cellulose, EP3081208B1, 2019. https://patents.google.com/patent/EP3081208B1/en (accessed March 30, 2022).
[59] R. Blell, I.M.N. Vold, H.H. Øvrebø, A. Gonera, Skin care compositions comprising microfibrillated cellulose, US20180078484A1, 2018. https://patents.google.com/patent/US20180078484A1/en (accessed March 30, 2022).
[60] E.B. Heggset, R. Aaen, T. Veslum, M. Henriksson, S. Simon, K. Syverud, Cellulose nanofibrils as rheology modifier in mayonnaise – A pilot scale demonstration, Food Hydrocolloids. 108 (2020) 106084. https://doi.org/10.1016/j.foodhyd.2020.106084.
[61] R. Aaen, S. Simon, F. Wernersson Brodin, K. Syverud, The potential of TEMPO-oxidized cellulose nanofibrils as rheology modifiers in food systems, Cellulose. 26 (2019) 5483–5496. https://doi.org/10.1007/s10570-019-02448-3.
[62] T. Salo, K. Dimic-Misic, P. Gane, J. Paltakari, Application of pigmented coating colours containing MFC/NFC: Coating properties and link to rheology, Nordic Pulp & Paper Research Journal. 30 (2015) 165–178. https://doi.org/10.3183/npprj-2015-30-01-p165-178.
[63] A. Balea, E. Fuente, M.C. Monte, N. Merayo, C. Campano, C. Negro, A. Blanco, Industrial Application of Nanocelluloses in Papermaking: A Review of Challenges, Technical Solutions, and Market Perspectives, Molecules. 25 (2020) 526. https://doi.org/10.3390/molecules25030526.
[64] Ø. Eriksen, K. Syverud, Ø. Gregersen, The use of microfibrillated cellulose produced from kraft pulp as strength enhancer in TMP paper, Nordic Pulp & Paper Research Journal. 23 (2008) 299–304. https://doi.org/10.3183/npprj-2008-23-03-p299-304.
[65] R. Hollertz, V.L. Durán, P.A. Larsson, L. Wågberg, Chemically modified cellulose micro- and nanofibrils as paper-strength additives, Cellulose. 24 (2017) 3883–3899. https://doi.org/10.1007/s10570-017-1387-6.
[66] A. Winter, W. Gindl-Altmutter, D. Mandlez, W. Bauer, R. Eckhart, J. Leitner, S. Veigel, Reinforcement effect of pulp fines and microfibrillated cellulose in highly densified binderless paperboards, Journal of Cleaner Production. 281 (2021) 125258. https://doi.org/10.1016/j.jclepro.2020.125258.
[67] N. Lavoine, I. Desloges, A. Dufresne, J. Bras, Microfibrillated cellulose – Its barrier properties and applications in cellulosic materials: A review, Carbohydrate Polymers. 90 (2012) 735–764. https://doi.org/10.1016/j.carbpol.2012.05.026.
[68] S. Belbekhouche, J. Bras, G. Siqueira, C. Chappey, L. Lebrun, B. Khelifi, S. Marais, A. Dufresne, Water sorption behavior and gas barrier properties of cellulose whiskers and microfibrils films, Carbohydrate Polymers. 83 (2011) 1740–1748. https://doi.org/10.1016/j.carbpol.2010.10.036.
[69] I. Siró, D. Plackett, M. Hedenqvist, M. Ankerfors, T. Lindström, Highly transparent films from carboxymethylated microfibrillated cellulose: The effect of multiple homogenization steps on key properties, Journal of Applied Polymer Science. 119 (2011) 2652–2660. https://doi.org/10.1002/app.32831.

[70] T. Li, C. Chen, A.H. Brozena, J.Y. Zhu, L. Xu, C. Driemeier, J. Dai, O.J. Rojas, A. Isogai, L. Wågberg, L. Hu, Developing fibrillated cellulose as a sustainable technological material, Nature. 590 (2021) 47–56. https://doi.org/10.1038/s41586-020-03167-7.
[71] Y.C. Gorur, M.S. Reid, C. Montanari, P.T. Larsson, P.A. Larsson, L. Wågberg, Advanced Characterization of Self-Fibrillating Cellulose Fibers and Their Use in Tunable Filters, ACS Appl. Mater. Interfaces. 13 (2021) 32467–32478. https://doi.org/10.1021/acsami.1c06452.
[72] A.W. Carpenter, C.-F. de Lannoy, M.R. Wiesner, Cellulose Nanomaterials in Water Treatment Technologies, Environ. Sci. Technol. 49 (2015) 5277–5287. https://doi.org/10.1021/es506351r.
[73] H. Seddiqi, E. Oliaei, H. Honarkar, J. Jin, L.C. Geonzon, R.G. Bacabac, J. Klein-Nulend, Cellulose and its derivatives: towards biomedical applications, Cellulose. 28 (2021) 1893–1931. https://doi.org/10.1007/s10570-020-03674-w.
[74] A. Hajian, S.B. Lindström, T. Pettersson, M.M. Hamedi, L. Wågberg, Understanding the Dispersive Action of Nanocellulose for Carbon Nanomaterials, Nano Lett. 17 (2017) 1439–1447. https://doi.org/10.1021/acs.nanolett.6b04405.
[75] M.M. Hamedi, A. Hajian, A.B. Fall, K. Håkansson, M. Salajkova, F. Lundell, L. Wågberg, L.A. Berglund, Highly Conducting, Strong Nanocomposites Based on Nanocellulose-Assisted Aqueous Dispersions of Single-Wall Carbon Nanotubes, ACS Nano. 8 (2014) 2467–2476. https://doi.org/10.1021/nn4060368.
[76] W. Tian, M.A. Vahid, M.S. Reid, Z. Wang, L. Ouyang, J. Erlandsson, T. Pettersson, L. Wågberg, M. Beidaghi, M.M. Hamedi, Multifunctional Nanocomposites with High Strength and Capacitance Using 2D MXene and 1D Nanocellulose, Advanced Materials. 31 (2019) 1902977. https://doi.org/10.1002/adma.201902977.
[77] A. Isogai, T. Saito, H. Fukuzumi, TEMPO-oxidized cellulose nanofibers, Nanoscale. 3 (2011) 71–85. https://doi.org/10.1039/C0NR00583E.
[78] A.E.J. de Nooy, A.C. Besemer, H. van Bekkum, Highly selective nitroxyl radical-mediated oxidation of primary alcohol groups in water-soluble glucans, Carbohydrate Research. 269 (1995) 89–98. https://doi.org/10.1016/0008-6215(94)00343-E.
[79] A. Isogai, T. Hänninen, S. Fujisawa, T. Saito, Review: Catalytic oxidation of cellulose with nitroxyl radicals under aqueous conditions, Progress in Polymer Science. 86 (2018) 122–148. https://doi.org/10.1016/j.progpolymsci.2018.07.007.
[80] T. Benselfelt, N. Kummer, M. Nordenström, A.B. Fall, G. Nyström, L. Wågberg, The Colloidal Properties of Nanocellulose, ChemSusChem. n/a (n.d.) e202201955. https://doi.org/10.1002/cssc.202201955.
[81] J.Y. Zhu, U.P. Agarwal, P.N. Ciesielski, M.E. Himmel, R. Gao, Y. Deng, M. Morits, M. Österberg, Towards sustainable production and utilization of plant-biomass-based nanomaterials: a review and analysis of recent developments, Biotechnology for Biofuels. 14 (2021) 114. https://doi.org/10.1186/s13068-021-01963-5.
[82] N. Barrios, R. Marquez, J.D. McDonald, M.A. Hubbe, R.A. Venditti, L. Pal, Innovation in lignocellulosics dewatering and drying for energy sustainability and enhanced utilization of forestry, agriculture, and marine resources - A review, Advances in Colloid and Interface Science. (2023) 102936. https://doi.org/10.1016/j.cis.2023.102936.
[83] R. Pönni, T. Vuorinen, E. Kontturi, PROPOSED NANO-SCALE COALESCENCE OF CELLULOSE IN CHEMICAL PULP FIBERS DURING TECHNICAL TREATMENTS, BioResources. 7 (2012) 6077–6108. https://doi.org/10.15376/biores.7.4.6077-6108.

[84] J.M.B.F. Diniz, M.H. Gil, J. a. a. M. Castro, Hornification—its origin and interpretation in wood pulps, Wood Sci Technol. 37 (2004) 489–494. https://doi.org/10.1007/s00226-003-0216-2.
[85] F.A. Sellman, T. Benselfelt, P.T. Larsson, L. Wågberg, Hornification of cellulose-rich materials – A kinetically trapped state, Carbohydrate Polymers. 318 (2023) 121132. https://doi.org/10.1016/j.carbpol.2023.121132.
[86] T. Mattsson, M. Sedin, H. Theliander, Filtration properties and skin formation of micro-crystalline cellulose, Separation and Purification Technology. 96 (2012) 139–146. https://doi.org/10.1016/j.seppur.2012.05.029.
[87] T. Mattsson, M. Sedin, H. Theliander, On the local filtration properties of microcrystalline cellulose during dead-end filtration, Chemical Engineering Science. 72 (2012) 51–60. https://doi.org/10.1016/j.ces.2012.01.022.
[88] M.A. Hubbe, J.A. Heitmann, REVIEW OF FACTORS AFFECTING THE RELEASE OF WATER FROM CELLULOSIC FIBERS DURING PAPER MANUFACTURE, BioResources. 2 (2007) 500–533.
[89] A. Laukkanen, M. Nuopponen, Method and apparatus for processing fibril cellulose and fibril cellulose product, US9409998B2, 2016. https://patents.google.com/patent/US9409998B2/fr (accessed April 5, 2023).
[90] A. Fall, M. Henriksson, A. Karppinen, A. Opstad, E.B. Heggset, K. Syverud, The effect of ionic strength and pH on the dewatering rate of cellulose nanofibril dispersions, Cellulose. 29 (2022) 7649–7662. https://doi.org/10.1007/s10570-022-04719-y.
[91] S. Varanasi, W. Batchelor, Superior non-woven sheet forming characteristics of low-density cationic polymer-cellulose nanofibre colloids, Cellulose. 21 (2014) 3541–3550. https://doi.org/10.1007/s10570-014-0370-8.
[92] Q. Li, P. Raj, F.A. Husain, S. Varanasi, T. Rainey, G. Garnier, W. Batchelor, Engineering cellulose nanofibre suspensions to control filtration resistance and sheet permeability, Cellulose. 23 (2016) 391–402. https://doi.org/10.1007/s10570-015-0790-0.
[93] Q. Ding, J. Zeng, B. Wang, D. Tang, K. Chen, W. Gao, Effect of nanocellulose fiber hornification on water fraction characteristics and hydroxyl accessibility during dehydration, Carbohydrate Polymers. 207 (2019) 44–51. https://doi.org/10.1016/j.carbpol.2018.11.075.
[94] K. Sim, J. Lee, H. Lee, H.J. Youn, Flocculation behavior of cellulose nanofibrils under different salt conditions and its impact on network strength and dewatering ability, Cellulose. 22 (2015) 3689–3700. https://doi.org/10.1007/s10570-015-0784-y.
[95] K. Dimic-Misic, A. Puisto, J. Paltakari, M. Alava, T. Maloney, The influence of shear on the dewatering of high consistency nanofibrillated cellulose furnishes, Cellulose. 20 (2013) 1853–1864. https://doi.org/10.1007/s10570-013-9964-9.
[96] K. Dimic-Misic, A. Puisto, P. Gane, K. Nieminen, M. Alava, J. Paltakari, T. Maloney, The role of MFC/NFC swelling in the rheological behavior and dewatering of high consistency furnishes, Cellulose. 20 (2013) 2847–2861. https://doi.org/10.1007/s10570-013-0076-3.
[97] K. Dimic-Misic, J. Rantanen, T.C. Maloney, P.A.C. Gane, Gel structure phase behavior in micro nanofibrillated cellulose containing in situ precipitated calcium carbonate, Journal of Applied Polymer Science. 133 (2016). https://doi.org/10.1002/app.43486.
[98] U. Ringania, J. Harrison, R.J. Moon, M.S. Bhamla, Dewatering of cellulose nanofibrils using ultrasound, Cellulose. 29 (2022) 5575–5591. https://doi.org/10.1007/s10570-022-04626-2.

[99] J. Sethi, K. Oksman, M. Illikainen, J.A. Sirviö, Sonication-assisted surface modification method to expedite the water removal from cellulose nanofibers for use in nanopapers and paper making, Carbohydrate Polymers. 197 (2018) 92–99. https://doi.org/10.1016/j.carbpol.2018.05.072.
[100] E. Sjöström, The origin of charge on cellulosic fibers, Nordic Pulp & Paper Research Journal. 4 (1989) 90–93. https://doi.org/10.3183/npprj-1989-04-02-p090-093.
[101] J. Wetterling, T. Mattsson, H. Theliander, Effects of surface structure on the filtration properties of microcrystalline cellulose, Separation and Purification Technology. 136 (2014) 1–9. https://doi.org/10.1016/j.seppur.2014.08.031.
[102] F.W. Brodin, H. Theliander, ABSORBENT MATERIALS BASED ON KRAFT PULP: PREPARATION AND MATERIAL CHARACTERIZATION, BioResources. 7 (2012) 1666–1683. https://doi.org/10.15376/biores.7.2.1666-1683.
[103] T. Nissilä, J. Wei, S. Geng, A. Teleman, K. Oksman, Ice-Templated Cellulose Nanofiber Filaments as a Reinforcement Material in Epoxy Composites, Nanomaterials. 11 (2021) 490. https://doi.org/10.3390/nano11020490.
[104] M. Basham, J. Filik, M.T. Wharmby, P.C.Y. Chang, B. El Kassaby, M. Gerring, J. Aishima, K. Levik, B.C.A. Pulford, I. Sikharulidze, D. Sneddon, M. Webber, S.S. Dhesi, F. Maccherozzi, O. Svensson, S. Brockhauser, G. Náray, A.W. Ashton, Data Analysis WorkbeNch (DAWN), J Synchrotron Radiat. 22 (2015) 853–858. https://doi.org/10.1107/S1600577515002283.
[105] G. Cinar Ciftci, P.A. Larsson, A.V. Riazanova, H.H. Øvrebø, L. Wågberg, L.A. Berglund, Tailoring of rheological properties and structural polydispersity effects in microfibrillated cellulose suspensions, Cellulose. 27 (2020) 9227–9241. https://doi.org/10.1007/s10570-020-03438-6.
[106] T. Mezger, 8. Oscillatory tests, in: The Rheology Handbook: For Users of Rotational and Oscillatory Rheometers, Vincentz Network, 2020: pp. 153–247. https://doi.org/10.1515/9783748603702-009.
[107] O. Theander, E.A. Westerlund, Studies on dietary fiber. 3. Improved procedures for analysis of dietary fiber, J. Agric. Food Chem. 34 (1986) 330–336. https://doi.org/10.1021/jf00068a045.
[108] A. Mautner, F. Mayer, M. Hervy, K.-Y. Lee, A. Bismarck, Better together: synergy in nanocellulose blends, Phil. Trans. R. Soc. A. 376 (2018) 20170043. https://doi.org/10.1098/rsta.2017.0043.
[109] P.A. Larsson, A.V. Riazanova, G. Cinar Ciftci, R. Rojas, H.H. Øvrebø, L. Wågberg, L.A. Berglund, Towards optimised size distribution in commercial microfibrillated cellulose: a fractionation approach, Cellulose. 26 (2019) 1565–1575. https://doi.org/10.1007/s10570-018-2214-4.
[110] E.J. Foster, R.J. Moon, U.P. Agarwal, M.J. Bortner, J. Bras, S. Camarero-Espinosa, K.J. Chan, M.J.D. Clift, E.D. Cranston, S.J. Eichhorn, D.M. Fox, W.Y. Hamad, L. Heux, B. Jean, M. Korey, W. Nieh, K.J. Ong, M.S. Reid, S. Renneckar, R. Roberts, J.A. Shatkin, J. Simonsen, K. Stinson-Bagby, N. Wanasekara, J. Youngblood, Current characterization methods for cellulose nanomaterials, Chem. Soc. Rev. 47 (2018) 2609–2679. https://doi.org/10.1039/C6CS00895J.
[111] X. Wang, T. Maloney, H. Paulapuro, Internal Fibrillation in Never-dried and Once-dried Chemical Pulps, Appita Journal. 56 (2003) 455–459.

[112] K. Arandia, N.K. Karna, T. Mattsson, A. Larsson, H. Theliander, Fouling characteristics of microcrystalline cellulose during cross-flow microfiltration: Insights from fluid dynamic gauging and molecular dynamics simulations, Journal of Membrane Science. 669 (2023) 121272. https://doi.org/10.1016/j.memsci.2022.121272.
[113] R.W. Fox, A.T. McDonald, P.J. Pritchard, Introduction to fluid mechanics, 6th ed, Wiley, New York, 2004.
[114] D. Erickson, Electroosmotic Flow (DC), in: D. Li (Ed.), Encyclopedia of Microfluidics and Nanofluidics, Springer US, Boston, MA, 2008: pp. 560–567. https://doi.org/10.1007/978-0-387-48998-8_446.
[115] A. Kadimi, K. Benhamou, Z. Ounaies, A. Magnin, A. Dufresne, H. Kaddami, M. Raihane, Electric Field Alignment of Nanofibrillated Cellulose (NFC) in Silicone Oil: Impact on Electrical Properties, ACS Appl. Mater. Interfaces. 6 (2014) 9418–9425. https://doi.org/10.1021/am501808h.
[116] S. Kalidindi, Z. Ounaies, H. Kaddami, Toward the preparation of nanocomposites with oriented fillers: electric field-manipulation of cellulose whiskers in silicone oil, Smart Mater. Struct. 19 (2010) 094002. https://doi.org/10.1088/0964-1726/19/9/094002.
[117] H.G. Wise, H. Takana, F. Ohuchi, A.B. Dichiara, Field-Assisted Alignment of Cellulose Nanofibrils in a Continuous Flow-Focusing System, ACS Appl. Mater. Interfaces. 12 (2020) 28568–28575. https://doi.org/10.1021/acsami.0c07272.
[118] D. Bordel, J.-L. Putaux, L. Heux, Orientation of Native Cellulose in an Electric Field, Langmuir. 22 (2006) 4899–4901. https://doi.org/10.1021/la0600402.
[119] H.C. Kim, J.W. Kim, L. Zhai, J. Kim, Strong and tough long cellulose fibers made by aligning cellulose nanofibers under magnetic and electric fields, Cellulose. 26 (2019) 5821–5829. https://doi.org/10.1007/s10570-019-02496-9.
[120] R.M. Muthoka, P.S. Panicker, J. Kim, Molecular Dynamics Study of Cellulose Nanofiber Alignment under an Electric Field, Polymers (Basel). 14 (2022) 1925. https://doi.org/10.3390/polym14091925.
[121] N. Mittal, F. Ansari, K. Gowda.V, C. Brouzet, P. Chen, P.T. Larsson, S.V. Roth, F. Lundell, L. Wågberg, N.A. Kotov, L.D. Söderberg, Multiscale Control of Nanocellulose Assembly: Transferring Remarkable Nanoscale Fibril Mechanics to Macroscale Fibers, ACS Nano. 12 (2018) 6378–6388. https://doi.org/10.1021/acsnano.8b01084.
[122] F.M. Tiller, C.S. Yeh, W.F. Leu, Compressibility of Paniculate Structures in Relation to Thickening, Filtration, and Expression—A Review, Separation Science and Technology. 22 (1987) 1037–1063. https://doi.org/10.1080/01496398708068998.
[123] M.A. Hubbe, P. Tayeb, M. Joyce, P. Tyagi, M. Kehoe, K. Dimic-Misic, L. Pal, Rheology of nanocellulose-rich aqueous suspensions: A Review, BioRes. 12 (2017) 9556–9661. https://doi.org/10.15376/biores.12.4.Hubbe.
[124] M.-C. Li, Q. Wu, R.J. Moon, M.A. Hubbe, M.J. Bortner, Rheological Aspects of Cellulose Nanomaterials: Governing Factors and Emerging Applications, Advanced Materials. 33 (2021) 2006052. https://doi.org/10.1002/adma.202006052.
[125] K. Li, C.M. Clarkson, L. Wang, Y. Liu, M. Lamm, Z. Pang, Y. Zhou, J. Qian, M. Tajvidi, D.J. Gardner, H. Tekinalp, L. Hu, T. Li, A.J. Ragauskas, J.P. Youngblood, S. Ozcan, Alignment of Cellulose Nanofibers: Harnessing Nanoscale Properties to Macroscale Benefits, ACS Nano. 15 (2021) 3646–3673. https://doi.org/10.1021/acsnano.0c07613.